

**AURORAL AND MIDLATITUDE RADAR  
STUDIES: RADAR METHODS FOR IMPROVED  
DIAGNOSTICS OF THE HF-MODIFIED AND  
NATURAL IONOSPHERES**

**Frank T. Djuth  
John H. Elder  
Kenneth L. Williams**

**Geospace Research, Inc.  
550 N. Continental Boulevard, Suite 110  
El Segundo, CA 90245**

**18 March 1996**

**Final Report  
28 September 1992 through 31 January 1995**

**Approved for public release; distribution unlimited**



**PHILLIPS LABORATORY  
Directorate of Geophysics  
AIR FORCE MATERIEL COMMAND  
HANSCom AFB, MA 01731-3010**

**DTIC QUALITY INSPECTED 3**


**19961002 019**



"This technical report has been reviewed and is approved for publication"

  
\_\_\_\_\_  
KEITH M. GROVES  
Contract Manager

  
\_\_\_\_\_  
EDWARD J. BERGHORN  
Branch Chief

  
\_\_\_\_\_  
WILLIAM K. VICKERY  
Division Director

This report has been reviewed by the ESC Public Affairs Office (PA) and is releasable to the National Technical Information Service (NTIS).

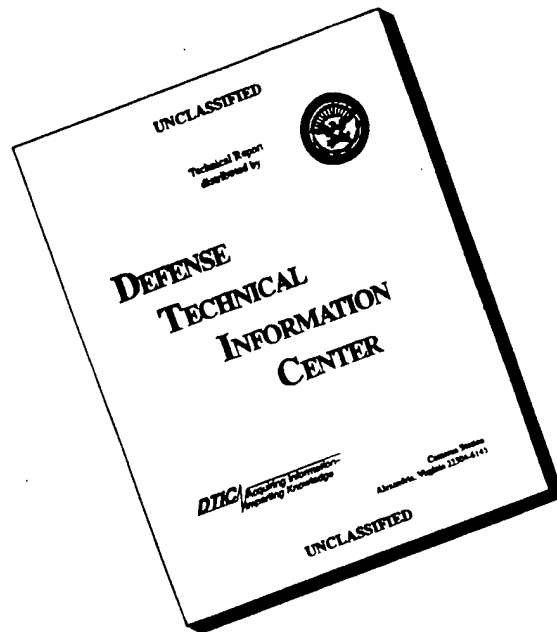
Qualified requestors may obtain additional copies from the Defense Technical Information Center (DTIC). All others should apply to the National Technical Information Service (NTIS).

If your address has changed, if you wish to be removed from the mailing list, or if the addressee is no longer employed by your organization, please notify PL/IM, 29 Randolph Road, Hanscom AFB, MA 01731-3010. This will assist us in maintaining a current mailing list.

Do not return copies of this report unless contractual obligations or notices on a specific document require that it be returned.



# DISCLAIMER NOTICE



**THIS DOCUMENT IS BEST QUALITY AVAILABLE. THE COPY FURNISHED TO DTIC CONTAINED A SIGNIFICANT NUMBER OF PAGES WHICH DO NOT REPRODUCE LEGIBLY.**



REPORT DOCUMENTATION PAGE			Form Approved OMB No. 0704-0188	
Public reporting burden for this collection of information is estimated to average 1 hour per response, including the time for reviewing instructions, searching existing data sources, gathering and maintaining the data needed, and completing and reviewing the collection of information. Send comments regarding this burden estimate or any other aspect of this collection of information, including suggestions for reducing this burden, to Washington Headquarters Services, Directorate for Information Operations and Reports, 1215 Jefferson Davis Highway, Suite 1204, Arlington, VA 22202-4302, and to the Office of Management and Budget, Paperwork Reduction Project (0704-0188), Washington, DC 20503.				
1. AGENCY USE ONLY (Leave blank)		2. REPORT DATE 18 March 1996	3. REPORT TYPE AND DATES COVERED Final Report, 28 Sep 1992 through 31 Jan 1995	
4. TITLE AND SUBTITLE Auroral and Midlatitude Radar Studies: Radar Methods for Improved Diagnostics of the HF-modified and Natural Ionospheres			5. FUNDING NUMBERS PE61102F PR 2310 TA GJ WUAA	
6. AUTHOR(S) Frank T. Djuth, John H. Elder, and Kenneth L. Williams			Contract F19628-92-C-0168	
7. PERFORMING ORGANIZATION NAME(S) AND ADDRESS(ES) Geospace Research, Inc. 550 N. Continental Boulevard, Suite 110 El Segundo, CA 90245			8. PERFORMING ORGANIZATION REPORT NUMBER GRI-BA-96-7150	
9. SPONSORING / MONITORING AGENCY NAME(S) AND ADDRESS(ES) Phillips Laboratory 29 Randolph Road Hanscom AFB, MA 01731-3010 Contract Manager: Keith M. Groves/GPIA			10. SPONSORING / MONITORING AGENCY REPORT NUMBER PL-TR-96-2070	
11. SUPPLEMENTARY NOTES				
12a. DISTRIBUTION / AVAILABILITY STATEMENT Approved for public release; distribution unlimited			12b. DISTRIBUTION CODE	
13. ABSTRACT (Maximum 200 words) This research program addresses fundamental issues related to the interaction of a high-power, high-frequency (3 - 10 MHz) radio wave with the ionosphere. Data acquired with incoherent scatter radars and a modest (50 kW) VHF radar were examined. The reported observations were made with the Arecibo HF modification facility in Puerto Rico and the Tromsø "superheater" located in Norway. Particular attention is paid to the excitation of Langmuir and ion turbulence and the development of induced ionospheric irregularities. Within 50 ms of HF beam turn on, the ionospheric plasma behaves as a smooth stratified medium. In this environment, elements of strong Langmuir turbulence are detected near the altitude where the HF frequency matches the local electron plasma frequency. The coupling between Langmuir oscillations and ionospheric perturbations is examined over both intermediate (50 ms to several seconds) and long time scales (tens of seconds and beyond) to elucidate HF energy partitioning in the plasma. An additional investigation focused on the physics of missile plumes in the lower atmosphere is also described. This can be viewed as a lower atmosphere modification experiment in which missile fuel generates a highly collisional plasma. Plume signatures were measured with a VHF radar to help verify model calculations of cross section and spectral content.				
14. SUBJECT TERMS ionospheric modification, missile plumes, high-power radio waves, ionospheric physics, VHF radar, incoherent scatter radar			15. NUMBER OF PAGES 70	
			16. PRICE CODE	
17. SECURITY CLASSIFICATION OF REPORT Unclassified	18. SECURITY CLASSIFICATION OF THIS PAGE Unclassified	19. SECURITY CLASSIFICATION OF ABSTRACT Unclassified	20. LIMITATION OF ABSTRACT SAR	



## TABLE OF CONTENTS

1. Objectives and Goals of Research Program .....	1
2. HF Ionospheric Modification Research.....	1
2.1 Introduction.....	1
2.1.1 The Arecibo Experience - A Transformation of Ideas.....	2
2.1.2 Excitation of Resonant Waves - Theoretical Developments .....	3
2.2 Observations of Langmuir Turbulence With the Arecibo Radar.....	5
2.3 Interaction and Coupling of HF-Induced Langmuir Turbulence.....	17
2.3.1 Wave-Plasma Interactions Over Intermediate Time Scales.....	20
2.3.2 Wave-Plasma Interactions at Late Times .....	23
2.4 Renewed Observations of HF-Accelerated Electrons .....	29
2.5 Summary of Arecibo Ionospheric Modification Results.....	33
2.6 Studies With the Tromsø Superheater.....	35
2.7 Summary of Tromsø Results .....	38
3. Measurements of Missile Plumes.....	38
3.1 Introduction.....	38
3.2 Lance Plume Investigation at White Sands Missile Range .....	39
3.3 Summary of Lance Missile Results.....	56
References.....	57



## **1. Objectives and Goals of Research Program**

Two tasks were performed under contract F19628-92-C-0168. The first entailed studies of the interaction of a powerful, high-frequency radio wave transmitted from the ground into the ionosphere. The overall goal was to achieve a more complete understanding of HF ionospheric modification physics. The key objectives were (1) to obtain a better understanding of microstructuring of the plasma by HF waves, (2) to explore resonant wave-plasma interactions in the ionosphere, (3) to examine the energy spectrum of HF-accelerated electrons, and (4) to investigate HF energy partitioning in the ionospheric plasma. The second task focused on the physics of rocket/missile plumes in the atmosphere. This can be viewed as a lower atmosphere modification experiment in that the plume fuel generates a highly collisional plasma. A VHF radar was deployed at White Sands Missile Range in New Mexico to probe the coherent and incoherent scatter from a Lance missile plume. The diagnostic techniques employed were not unlike those used in investigations of the HF-modified ionosphere and the natural atmosphere/ionosphere.

## **2. HF Ionospheric Modification Research**

HF ionospheric modification refers to the use of high-power, high-frequency (~2-15 MHz) radio waves to modify the earth's ionosphere. Usually, this involves the use of large ground-based facilities capable of transmitting ~0.5 to 1 MW of HF power continuously. The one-way antenna gain tends to be in the range of 17 to 23 dBi. Experimental results presented below were acquired at two such facilities, one located at Arecibo, Puerto Rico, the other at Tromsø, Norway. The frequency of the high-power waves is typically adjusted so that radio wave reflection occurs in the ionospheric region under study. Waves having either O-mode or X-mode polarization are normally transmitted. For the observations described in this section, O-mode polarization waves were used, and the high-power transmissions targeted the ionospheric F region (between 200 and 350 km altitude). The F-region modification process entails a variety of effects including the heating of the ambient electron gas, changes in bulk electron density, the formation of ionospheric irregularities, the excitation of Langmuir turbulence, and the acceleration of background thermal electrons to suprathermal energies. Competition among these various phenomena determine the partitioning of HF energy in the plasma. The overall goal of this program is to obtain a detailed understanding of the partitioning process.

### **2.1 Introduction**

There is a rich history of prior investigations in the area of ionospheric modification beginning in the early 1970's and continuing into the present. Extensive studies of HF-induced plasma turbulence and artificially-produced, field-aligned irregularities (FAIs) have been performed at Arecibo. Characteristics of the HF enhanced plasma lines (HFPLs) observed with the Arecibo 430 MHz radar are described by *Kantor [1974]*, *Carlson and Duncan [1977]*,



*Muldrew and Showen* [1977], *Showen and Kim* [1978], *Morales et al.* [1982], *Duncan and Sheerin* [1985], *Djuth* [1984], *Fejer and Sulzer*, [1984], *Djuth et al.* [1986], *Birkmayer et al.* [1986], *Isham et al.* [1987], *Muldrew* [1988], *Sulzer et al.* [1989], *Sulzer and Fejer*, [1991], *Cheung et al.* [1989], *Fejer et al.* [1989], *Thidé et al.* [1989], *Djuth et al.* [1990], *Fejer et al.* [1991], *Cheung et al.* [1992], *Isham and Hagfors* [1993], *Sulzer and Fejer* [1994], and others. Properties of AFAIs observed at Arecibo are discussed by *Frey* [1980], *Basu et al.* [1983], *Coster et al.* [1985], *Noble et al.* [1987], and *Noble and Djuth* [1990], *Stocker et al.* [1992]. Investigations of horizontally-stratified irregularities in the Arecibo F region are limited to a single study performed by *Fejer et al.* [1984]. Much theoretical work on the topic of HF-induced Langmuir turbulence was performed in the late 1960's, 1970's and 1980's [e.g., *DuBois and Goldman*, 1967; *Fejer and Kuo*, 1973; *Perkins et al.*, 1974; *Nicholson and Goldman*, 1978; *Muldrew*, 1978; *Fejer*, 1979; *Weatherall et al.*, 1982; *Sheerin et al.*, 1982; *Kuo et al.*, 1983; *Nicholson et al.*, 1984; *Payne et al.*, 1984; *Muldrew*, 1985; *Doolen et al.*, 1985; *Das et al.*, 1985; *Russel et al.*, 1986; *Kuo et al.*, 1987; *Muldrew*, 1988; *DuBois et al.*, 1988; *Fejer*, 1988; *Russel et al.*, 1988; *Payne et al.*, 1989, and others]. A general review of research activities in the field of HF ionospheric modification between 1990 and 1992 is provided by *Djuth* [1993]. More recently, the evolution of Langmuir turbulence and stimulated electromagnetic emissions were closely examined by *Thidé et al.* [1995]. The current state of our understanding of HF-induced plasma turbulence is presented below.

### **2.1.1 The Arecibo Experience - A Transformation of Well-Settled Ideas into Revolutionary New Concepts**

In the mid to late 1980's, it became clear that many physical explanations that once seemed well-settled were seriously deficient. Nowhere is this more evident than in studies of resonant Langmuir turbulence with the Arecibo 430 MHz radar. The combination of greatly improved experimental techniques together with a variety of new theoretical studies has led to changes in the way resonant interactions near the point of O-mode reflection are studied and interpreted. Over the past five years, investigations of HF-induced Langmuir wave/ion wave turbulence have yielded many interesting results that reinforce the notion that our understanding of the wave-plasma interaction is far less than complete, particularly when HF-induced irregularities are present. Previous experimental investigations at Arecibo, Puerto Rico indicate that Langmuir waves detected with the 430 MHz incoherent scatter radar occur preferentially near the point of O-mode wave reflection. This observation together with Langmuir wave spectral data acquired at Arecibo led *DuBois et al.* [1990] to argue that radar measurements of initially excited Langmuir oscillations are consistent with computer simulations of strong Langmuir turbulence (SLT) near the region of critical density. Under conditions of SLT a significant fraction of the power in the high-frequency density oscillations is contained within highly localized states termed "cavitons."



Cavitons consist of a high-frequency Langmuir field trapped in a self-consistent density depletion; they undergo cyclic nucleation, collapse, and burnout in the plasma. The theoretical study of *DuBois et al.* contained conclusions and predictions that sparked controversy and immediately triggered a new series of experimental tests. A review of recent results in this area is provided by *Djuth* [1993].

A series of controlled experiments in the nighttime F region [*Djuth et al.*, 1990; *Fejer et al.*, 1991; *Cheung et al.*, 1992; *Sulzer and Fejer*, 1994] revealed that the initial HF beam-plasma interaction was consistent with the creation of strong states of plasma turbulence [e.g., *DuBois et al.*, 1990] in the F region. At the maximum power level available at Arecibo (~80 MW ERP prior to the HF facility upgrade), the predicted characteristics of strong turbulence in a smooth, inhomogeneous plasma appear to be present for ~50 ms following HF turn-on. Although there are some skeptics and critics of the strong turbulence interpretation, no other theory yields such a comprehensive and self-consistent description of the detailed data of *Fejer et al.* [1991] and *Sulzer and Fejer* [1994].

After ~50-100 ms of HF transmissions, the nature of the wave-plasma interaction appears to undergo a permanent change of state. The current belief is that the change of state is related to the formation of HF-induced irregularities in the plasma. Over intermediate time scales of 50 ms to several seconds following HF turn-on, horizontally stratified irregularities and short-scale (3 - 6 m) field-aligned irregularities are generated in the plasma. The spectral characteristics of the Langmuir turbulence in this time domain remain basically unexplored. At late times 20-60 s after HF turn-on at high powers, large-scale (~1-5 km) "packets" of smaller-scale irregularities are excited in the plasma [e.g., *Kelley et al.*, 1995; *Djuth et al.*, 1996]. This leads to the break-up of the HFPL echo [*Djuth et al.*, 1990]. There are indications that the excitation of the irregularity packets is extremely nonlinear in nature; the physical processes involved appear to be extraordinarily interesting. Langmuir turbulence measured in this environment is observed to reside within HF-induced field-aligned structures (discussed below). In the late-time plasma environment, there is little doubt that ducted-wave propagation [*Muldrew*, 1978] plays an important role in the HFPL observations at Arecibo. The detailed physics of HF modifications over intermediate and long time scales is yet to be defined.

### **2.1.2 Excitation of Resonant Waves - Theoretical Developments**

The development of caviton theory has taken place at an astonishingly rapid pace. *DuBois et al.* [1991] extend their caviton studies to include the pumping of the plasma by high-power HF waves at subcritical electron densities. They conclude that truncated parametric decay cascades coexist with caviton collapse events in the subcritical zone below radio wave reflection. In addition, a newly-predicted feature in the ion fluctuation spectrum at zero frequency is identified and attributed to caviton collapse. These concepts are further developed in a study by *Hanssen*



[1991] and *Hanssen et al.* [1992] aimed at numerically testing the validity of the weak turbulence approximation in ionospheric modification experiments. In this investigation, results from the one-dimensional driven and damped Zakharov system of equations (ZSE) are compared with the weak turbulence approximation (WTA) derived from the same ZSE. The WTA is found to qualitatively agree with the full ZSE results in the lower portion of the resonance region for weak pump strengths. At higher pump levels the saturation spectra from the ZSE differ from the WTA cascade spectra in that the ZSE leads to a truncation in the number of parametric cascade sidebands, and the frequency intervals between cascade lines begin to fill in. In the region near HF reflection, large ensembles of localized collapse events dominate the plasma physics. No WTA exists in this region. At middle altitudes, collapse and cascade turbulence coexists, and the saturation of the parametric decay instability is facilitated by the presence of the caviton gas.

The above findings involving strong states of Langmuir turbulence in ionospheric modification experiments are strongly disputed by *Stubbe et al.* [1992a,b]. Using experimental results obtained with the Tromsø HF facility and the EISCAT UHF and VHF radars, *Stubbe et al.* show that propagating Langmuir and ion acoustic waves are an essential part of the physical description at Tromsø and that parametric decay represents a major process in the production of Langmuir turbulence. They conclude that there is no convincing evidence at Tromsø that cavitons coexist with propagating Langmuir waves. Observations of the temporal evolution of Langmuir wave spectra are presented along with HF power dependences of Langmuir wave and ion wave spectra. These data are used to argue against the need for a strong Langmuir turbulence description. In commenting on the *Stubbe et al.* [1992a] paper, *DuBois et al.* [1992] invoke the same Tromsø data base described above as supporting evidence for the existence of cavitons and their coexistence with Langmuir decay cascades. In their reply, *Stubbe et al.* [1992b] use additional theoretical arguments to question the applicability of the work of *DuBois et al.* [1990] to ionospheric modification experiments. In light of this intense controversy, H. Kohl [private communication, 1994] has recently presented early-time (relative to HF turn-on) VHF HFPL observations from EISCAT that seem to exhibit spectral features similar to those predicted by *DuBois et al.*

The space and time distribution of Langmuir turbulence is discussed in detail by *DuBois et al.* [1993a,b] with reference to observations at Arecibo and Tromsø. In this work, SLT theory, as part of a unified theory, is shown to give rise to at least four unique physical signatures in ionospheric plasmas. These include: (1) a caviton continuum plus free mode peak in the plasma line power spectrum near the reflection altitude for Arecibo conditions, (2) a truncated decay-cascade spectrum at lower altitudes, (3) a continuous spectrum underlying the decay cascade, and (4) a zero frequency feature in the ion line power spectrum directly related to caviton dynamics. Elements of signatures (1), (2), and (3) are found in the Arecibo observations. Signature (4) is in



need of verification; no appropriate 430-MHz radar data currently exists in the early time environment. (*Fejer et al.* [1991] and *Sulzer and Fejer* [1994] examined only the HFPL spectrum with good spatial and temporal resolution.) An improved model of the low-frequency ion fluctuations is outlined in a comparison between theory and experiment offered by *DuBois et al.* [1993a]. The basis of an improved model for the electron density response is described in detail by *DuBois et al.* [1994].

It is important to note that the Zakharov model equations are derived from fluid theory, and therefore do not intrinsically include kinetic effects. Nevertheless, damping operators are included phenomenologically to approximate linear Landau damping [e.g., *DuBois et al.*, 1990; *Hanssen et al.*, 1992]. As noted by *Stubbe et al.* [1992a], the inclusion of damping in this manner cannot be rigorously justified within the Zakharov model. To resolve this issue, *Helmersen and Mjølhus* [1994] developed a semikinetik model for ionospheric Langmuir turbulence. This model treats the low-frequency ion dynamics using a linearized kinetic description, while employing the high-frequency Zakharov equation to describe the electron dynamics. *Helmersen and Mjølhus* conclude the predictions of this model are in good qualitative agreement with quasi-fluid Zakharov models used in the past (described above). In addition, the oscillating two-stream instability (OTSI) threshold appears to be lowered somewhat in the semikinetik model. *Sprague and Fejer* [1995] have also studied the OTSI using one-dimensional simulations based on the Zakharov equations. They address the issue of simultaneous excitation of parametric decay cascades and the OTSI. This is motivated by the lack of a convincing explanation for the OTSI feature in the Arecibo HFPL spectrum [e.g., *Sulzer et al.*, 1984; *Sulzer et al.*, 1989; *Sulzer and Fejer*, 1994] based on previous simulations of caviton dynamics. *Sprague and Fejer* find low enough HF pump levels can support both parametric decay cascades and the OTSI feature. Inconsistencies between this work and that of *Hanssen et al.* [1992] may be caused by differences in the specification of ion damping.

## **2.2 Observations of Langmuir Turbulence With the Arecibo 430 MHz Radar and Its Evolutionary Path.**

On the basis of the data acquired at Arecibo Observatory as part of this project, we now know that several distinct stages exist in the development of the Langmuir turbulence in an initially unmodified, nighttime, *F*-region that is both smooth and stable. A smooth ionosphere is by definition free of natural spread-F irregularities; in general background perturbations of less than 0.1% rms are assumed over spatial scales extending from 10 to 1000 m. A stable ionosphere refers to the fact that layer motion is minimal (<10 m/s), and that the dynamics of geomagnetic storms are absent. Moreover, conditions suitable to the development of very large HF-induced temperatures and temperature gradients [*Djuth et al.* 1987; *Djuth*, 1989] are assumed not to be present. In addition, there is an implicit assumption that phenomena that interrupt or varies the



delivery of the HF pump wave to the F region are absent. For example, sporadic E and/or intermediate ion layers must not be intense enough to significantly impact the pump wave strength. Time varying absorption in the daytime D layer over periods of 1-10 ms following HF turn-on greatly complicate the interpretation of the experimental observations. For this reason, special attention is paid to nighttime observations. This has the added benefit of greatly reducing the Landau damping decrement of Langmuir waves because daytime photoelectrons are absent.

The general characteristics of Langmuir turbulence excited in a smooth/stable F region after sundown are repeatable provided that remnant irregularities from previous ionospheric modification transmissions do not exist in the plasma. Figure 1 illustrates a background ionosphere measured during the evening at Arecibo. The background electron density profile of Figure 1 was measured three-minutes in advance of the turn-on of the HF beam at 21:00 AST. In this case,  $f_oF_2$  is 9.4 MHz and the modification frequency is 5.1 MHz. The former corresponds to a maximum plasma density of  $1.09 \times 10^6 \text{ cm}^{-3}$ ; whereas the 5.1 MHz modification wave reflects at a "critical altitude" corresponding to an electron density of  $3.2 \times 10^6 \text{ cm}^{-3}$ . This electron density point is marked by an arrow in Figure 1. The ionosphere scale length  $H \equiv n_o / [dn_e(z)/dz]$  is measured to be  $29.2 \pm 1.2 \text{ km}$  near the critical altitude, where  $n_e(z)$  is electron density as a function of altitude  $z$ , and  $n_o$  is the electron density at the altitude of interest. During the observation period of Figure 1,  $T_e = T_i = 943 \pm 4 \text{ K}$ , where  $T_e$  and  $T_i$  are the electron and ion temperature respectively. These measurements were made near the critical altitude using standard incoherent scatter ion-line analyses.

High-resolution measurements of Langmuir wave and ion wave power versus altitude are presented in Figure 2. The observational format is similar to that of *Djuth et al.* [1990], but the spatial resolution is approximately 4 times better. The Arecibo 430 MHz radar was operated in a "short pulse" mode; a  $0.5 \mu\text{s}$  pulse was transmitted within an interpulse period of  $730 \mu\text{s}$ . The receivers at the two plasma line channels ( $430 \text{ MHz} \pm f_{\text{HF}}$ ) and ion line channel (430 MHz) each had a bandwidth of 2 MHz. All three receiver channels were simultaneously monitored. The data streams were oversampled to facilitate interpolation over spatial scales less than 75 m (the resolution dictated by the  $0.5 \mu\text{s}$  pulse). All data were sampled at range gates separated by  $0.125 \mu\text{s}$ , yielding a sample spacing of 18.75 m. For the measurements, the 430 MHz radar beam was pointed toward the center of the HF modification volume in the F region. The zenith angle and azimuth of the radar beam were  $3.5^\circ$  and  $33^\circ$ , respectively. No HF transmissions were made for 12 min prior to turn-on of the HF beam in Figure 2. The HF frequency was set to 5.1 MHz, and approximately 80 MW effective radiated power was transmitted. The HF beam was turned on for the one-minute transmission of Figure 2 and then turned off in preparation for the next "cold" turn-on of the HF beam.



May 3, 1990 2106:50 - 2107:01 AST

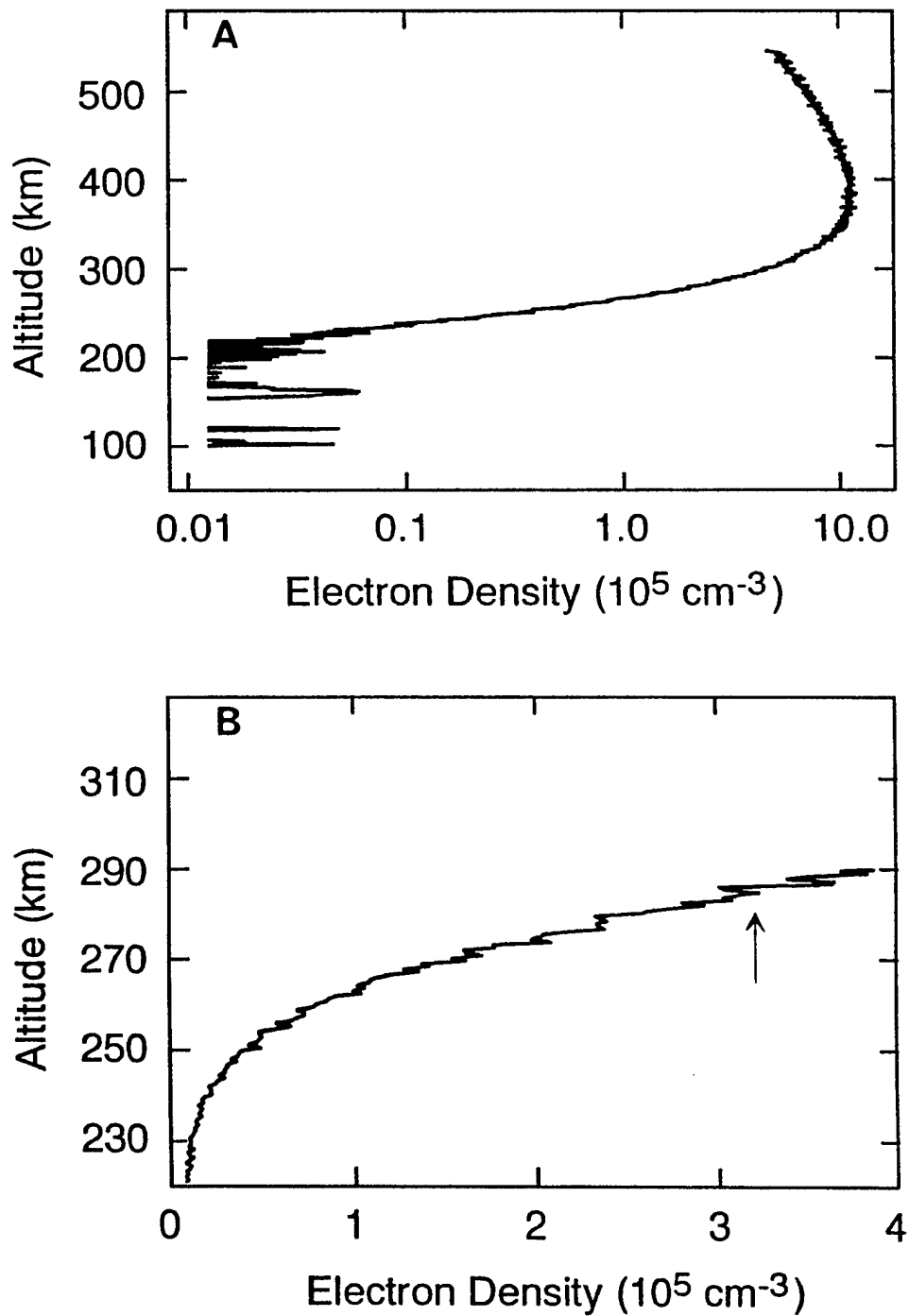


Figure 1. Background electron density profile measured prior to HF beam turn-on at 2110:00 AST (Panel A), and expanded view of bottomside F-region gradient (Panel B).



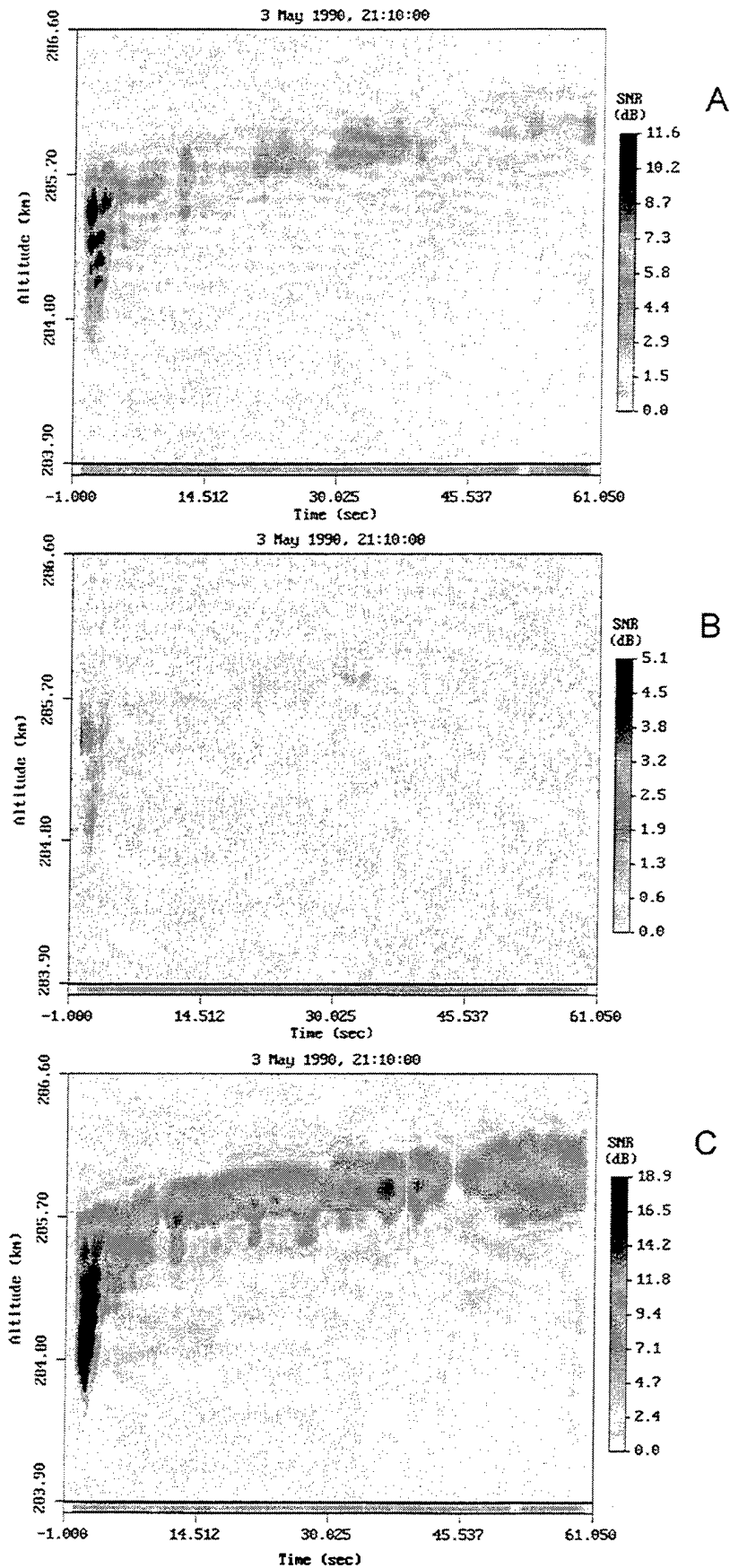


Figure 2. Temporal development of the HF-enhanced upshifted plasma line (Panel A), the enhanced ion line (Panel B), and the enhanced downshifted line (Panel C) in a cold background ionosphere.



In Figure 2, the strongest HF-enhanced plasma line (HFPL) and HF-enhanced ion-line (HFIL) echoes occur at the maxima of the HF standing pattern in the plasma. This is discussed in greater detail below. The strong scatter initially evident at the highest altitudes is located near the first maximum of the HF standing wave pattern. Over time scales of several seconds, echoes are evident near other maxima of the standing wave pattern at lower heights. The downward extension of the echo in altitude and its retreat back to higher altitudes is part of the "overshoot process." The time history of the overshoot was originally examined by *Showen and Kim* [1978]; an altitude-resolved view of the overshoot was first provided by *Djuth et al.* [1990]. After the overshoot, echoes of Figure 2 are generally restricted to the first two maxima of the HF standing wave pattern for the remainder of the 1-min transmission (i.e., for the next  $\sim 57$  s). At late times (20 s to 90 s) after a cold HF turn-on at a high power level (80 MW ERP), the HFPL echo breaks up as larger scale (1-5 km) packets of irregularities develop. Initial conditions in the natural plasma determine the exact onset time of the breakup. The beginning of the breakup process is evident in Figure 2 near the end of the 60-s transmission period at the downshifted HFPL. Notice how the weak echo below reflection begins to extend downward in altitude. A better view of the breakup is provided in *Djuth et al.* [1990]; the focus of the current investigation is on the phenomenology of the induced turbulence prior the breakup of the echo. Small gaps in the HFPL echoes evident near 39 and 44 s relative time are caused by the brief loss of transmissions from half of the HF antenna array. During these periods, antenna arcing triggers a detection circuit which automatically shuts down part of the antenna array, and the transmitted ERP is reduced by a factor of 4.

Except for the exact time delay of the HFPL breakup, the development of the induced turbulence illustrated in Figure 2 is typical of all other measurements made at Arecibo in a cold background ionosphere under nighttime conditions. However, the absolute power of the HFPL can vary by a few dB from one 1-min HF transmission to the next. The exact cause of this relatively small variation is not known, but it may be related to variations in the output power of the HF transmitter and/or subtle changes in the background plasma. Notice that during the overshoot process (first  $\sim 3$  s following HF turn-on) the strongest echoes at the downshifted HFPL are lower in height than those at the upshifted HFPL. This consistent feature of the cold turn-on morphology. It is interesting to note that this altitude asymmetry is the reverse of what would be expected if Langmuir oscillations propagated freely up and down the interaction region. In the case of freely propagating waves in a smooth plasma, the strength of the upshifted HFPL would tend to increase with decreasing height, whereas the downshifted HFPL would be strongest near the first maximum in the standing wave pattern. In Figure 2, strong ion-line backscatter is observed only for a brief ( $\leq 300$  ms) period following HF turn-on. HFIL echoes tend to be strongest near the first maximum of the standing wave pattern. However, the HFIL participates in



the overshoot process as is evident in the downward extension of the weakened HFIL echo, and its retreat to the first standing wave maximum.

In Figure 3, the first  $\sim 5.6$  s of observations following HF turn-on are presented on an expanded temporal scale. This data segment highlights the overshoot period and clearly reveals the presence of horizontal stratifications in the HFPL data. Much weaker stratifications are also discernible in the HFIL backscatter. In these observations, the first detection of HFPL echoes occurs  $\sim 2$ -6 ms after HF turn-on rather than within 2 ms in similar measurements reported by Djuth *et al.* [1990]. The reason for this lies in the trade-off between altitude resolution and system sensitivity. Both measurements were made using receivers having bandpasses of 2 MHz. However, the earlier measurements employed radar pulses that were 1.5  $\mu$ s in length rather than 0.5  $\mu$ s. With very short pulses, the Arecibo radar never develops its full peak power output. Taking into account the 1-MHz bandpass of the Arecibo 430 MHz transmitter, we estimate that for the current observations the system sensitivity is at least a factor of three worse than in the case of Djuth *et al.* [1990]. The measurements presented here have limited temporal integration that is not sufficient to overcome the adverse impacts of reduced transmitter power when signals are weak. Other more sensitive measurements made by integrating coded long-pulse data [e.g., Sulzer and Fejer, 1994] indicate that the HFPL echo becomes visible within 1 ms of turn-on in a cold background ionosphere.

Figure 4 shows an "altitude slice" of the observations presented in Figure 3 for a short temporal integration period (36.5 ms) beginning 2.30 s after HF turn-on. In this figure, simultaneous measurements at the upshifted and downshifted HFPL are plotted along with the theoretically calculated standing wave pattern of the modifying HF wave assuming no absorption of the pump wave in the plasma. As noted above, in the nighttime *F*-region the assumption of low absorption for a  $f_{\text{HF}} = 5.1$  MHz pump wave is a very good one. The standing wave pattern was calculated for the Arecibo geomagnetic field geometry using an accurate approximation to the full wave solution [Lundborg and Thidé, 1985, 1986; Thidé and Lundborg, 1986]. This pattern was fit to the downshifted HFPL observations allowing the scale length  $H$  and the critical altitude (where  $f_{\text{cp}} = f_{\text{HF}}$ ) to vary as free parameters. The scale length determines the absolute separation between maxima in the standing wave pattern, but the relative separation is not strongly dependent on  $H$ . In this particular example, the deduced value of  $H$  is  $28.9 \pm 0.8$  km. This compares well with the estimate  $29.2 \pm 1.2$  km obtained from the incoherent scatter electron density profile of Figure 1. However, it is noteworthy that  $H$  is more accurately estimated with 36.5 ms of HFPL data than with 11 s of incoherent scatter observations!

Overall, the peaks in HFPL backscatter conform to the maxima in the standing wave pattern. The exact match is rather striking. Because of the limited altitude resolution of the measurements ( $\sim 75$  m), the minima do not approach the zero power level. This would be



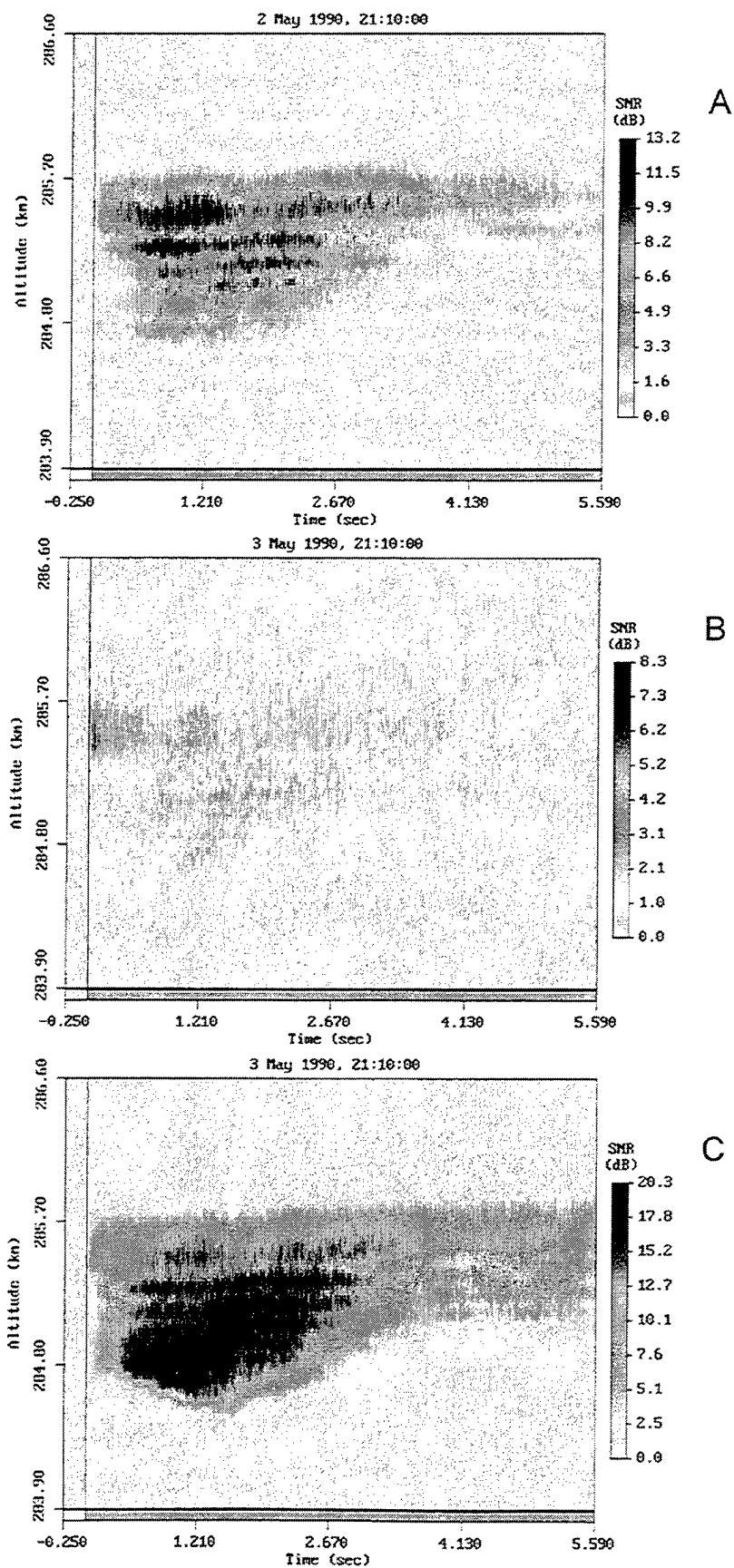


Figure 3. A more detailed view of the first 5.6 s of modifications shown in Figure 2. This data segment highlights the transient downward extension of the Arecibo radar echoes after HF turn-on.



May 3, 1990

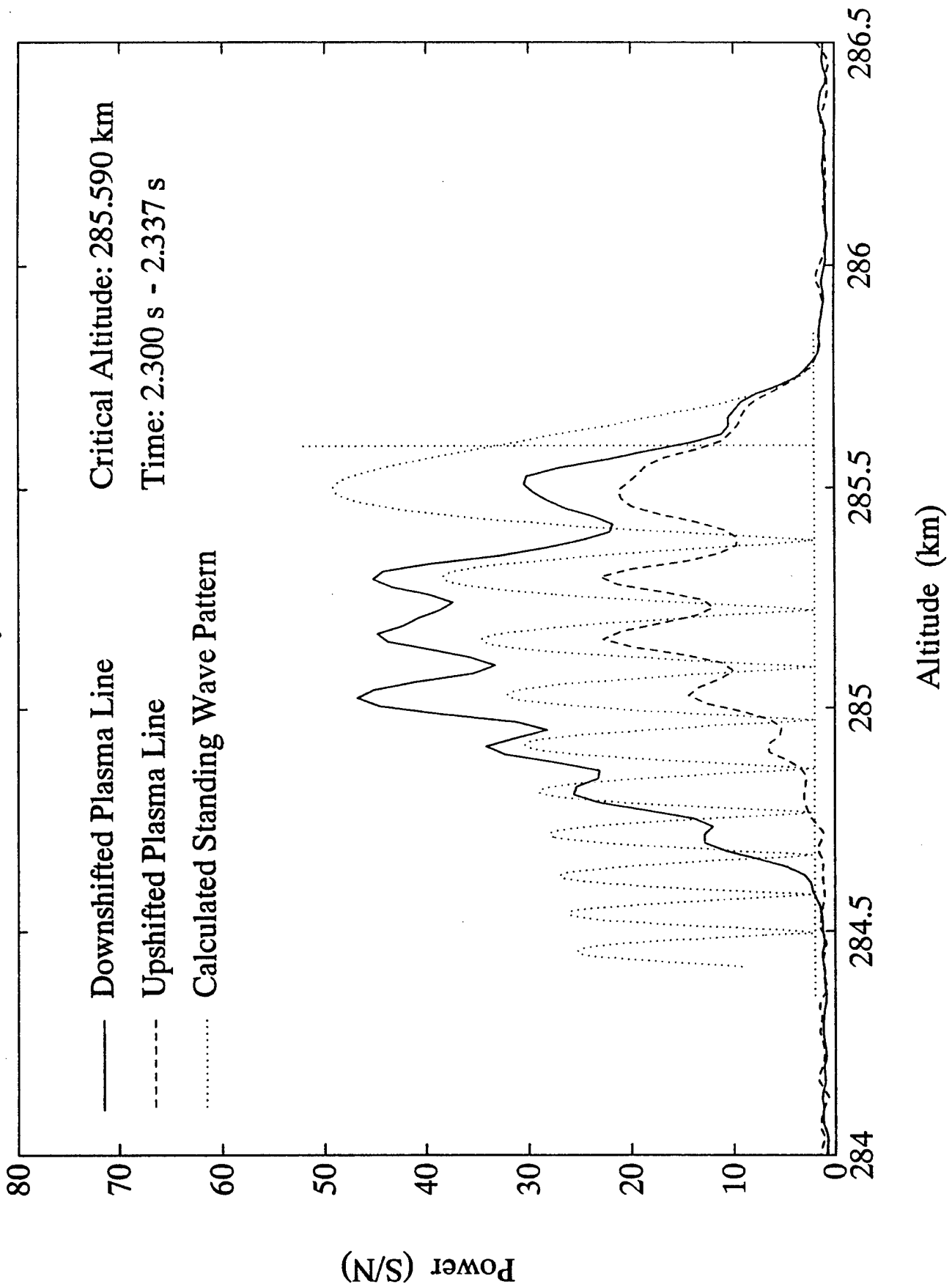


Figure 4. Comparison between the altitude profiles of HFPL echoes and the theoretical standing wave pattern.



expected if very little collisional or anomalous absorption were present. Notice that in the region of HF wave evanescence above the critical altitude, there is a distinctive bump in upshifted/downshifted HFPL power. This bump is commonly observed in the data.

In Figure 5, four altitude slices are presented to illustrate the early time evolution of the radar echoes after HF turn-on. Within the first 37 ms of HF turn-on, the upshifted/downshifted HFPL and the HFIL are strongly excited at the first maximum of the HF standing wave pattern. (From Figure 4, one finds that the first maximum is near 285.5 km.) In addition, very weak HFPL excitation is present near 284.7 km. This is the altitude at which frequency matching conditions are satisfied for weakly driven parametric instabilities. The matching condition can be expressed as

$$\omega_r^2 = \omega_{ep}^2 + \sin^2 \theta \omega_{ec}^2 + \frac{3k^2 \kappa T_e}{m_e} \approx \omega_{HF}^2, \quad (1)$$

where  $\omega_r$  is Langmuir wave frequency,  $\omega_{ep}$  and  $\omega_{ec}$  are the electron plasma frequency and electron cyclotron frequency, respectively,  $\theta$  is the angle between the radar line-of-sight and the geomagnetic field,  $k$  is radar wavenumber,  $T_e$  is electron temperature,  $m_e$  is electron mass, and  $\kappa$  is Boltzmann's constant. Spectral observations made at the matching height are reported by *Fejer et al.* [1991] and *Sulzer and Fejer* [1994]. Overall these spectra are either of the "below threshold" type [Fejer and Sulzer, 1984] or those attributable to a weakly excited parametric decay instability [e.g. Fejer and Kuo, 1973; Djuth et al., 1986]. The "below threshold" spectrum is the result of radio wave scattering off of Debye-shielded ion-acoustic waves. Thus the HFPL spectrum has the same shape as the natural ion-line spectrum. Weakly excited parametric instability spectra contain a slightly elevated decay line component at  $430 \text{ MHz} \pm (f_{HF} - f_{ia})$  and often exhibit a very low-level parametric decay cascade [e.g., *Fejer and Kuo*, 1973]. After 37 ms of HF transmissions, the HFPL echoes quickly spread to lower altitudes, but the detected HFILs are still narrowly confined to the first maximum of the standing wave pattern.

The development of the HFPL line echo over times scales of several seconds is illustrated in Figure 6. HFIL scatter is presented only in the upper left hand panel because strong enhancements are restricted to times less than  $\sim 300$  ms. The top right panel shows that the downshifted HFPL scatter reaches as low as the eighth maxima in the standing pattern. Following the overshoot the HFPL echo collapses to the region near HF reflection. After  $\sim 5$  s of continuous HF transmissions, the HFPL echo is confined to the first, and sometimes first and second maxima, of the standing wave pattern. When the HFPL echo breaks up at later times, the signature of the standing wave pattern on the HFPL echo vanishes.

Results from the 1-min HF transmission made prior to that of Figure 2 are shown in Figure 7. In this case, the HF beam had been turned off for 10 min to insure that the turn-on occurred in



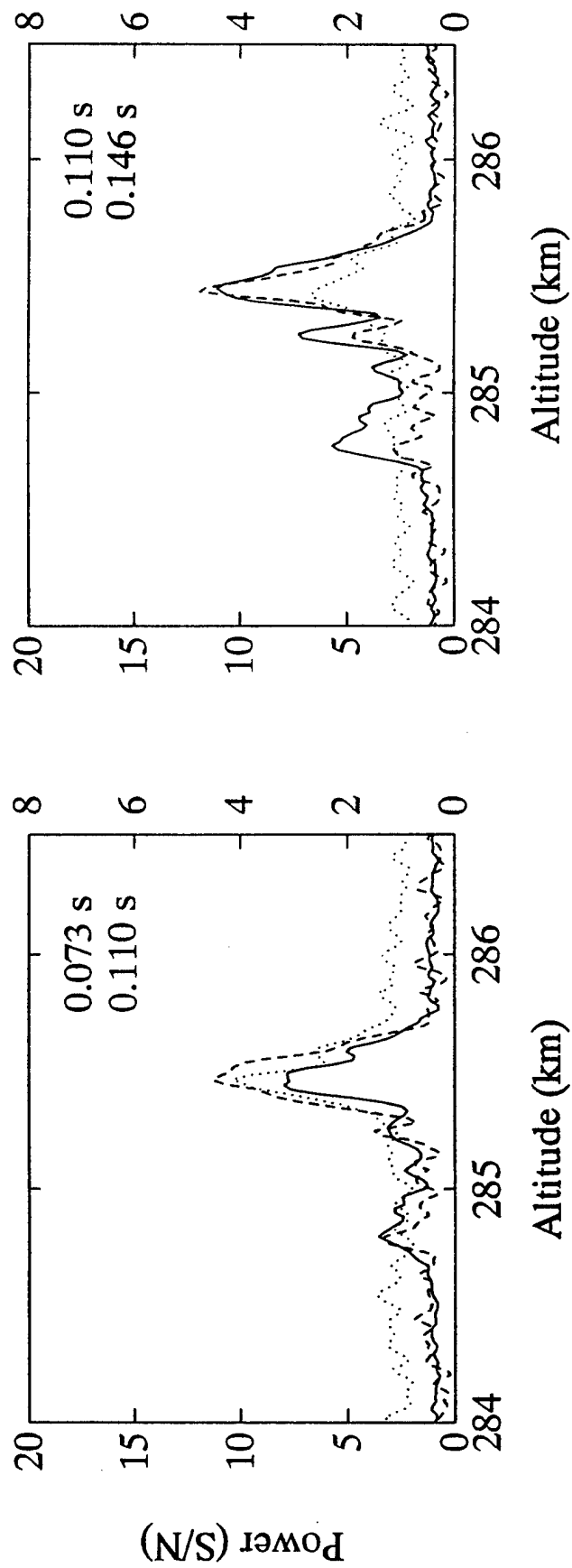
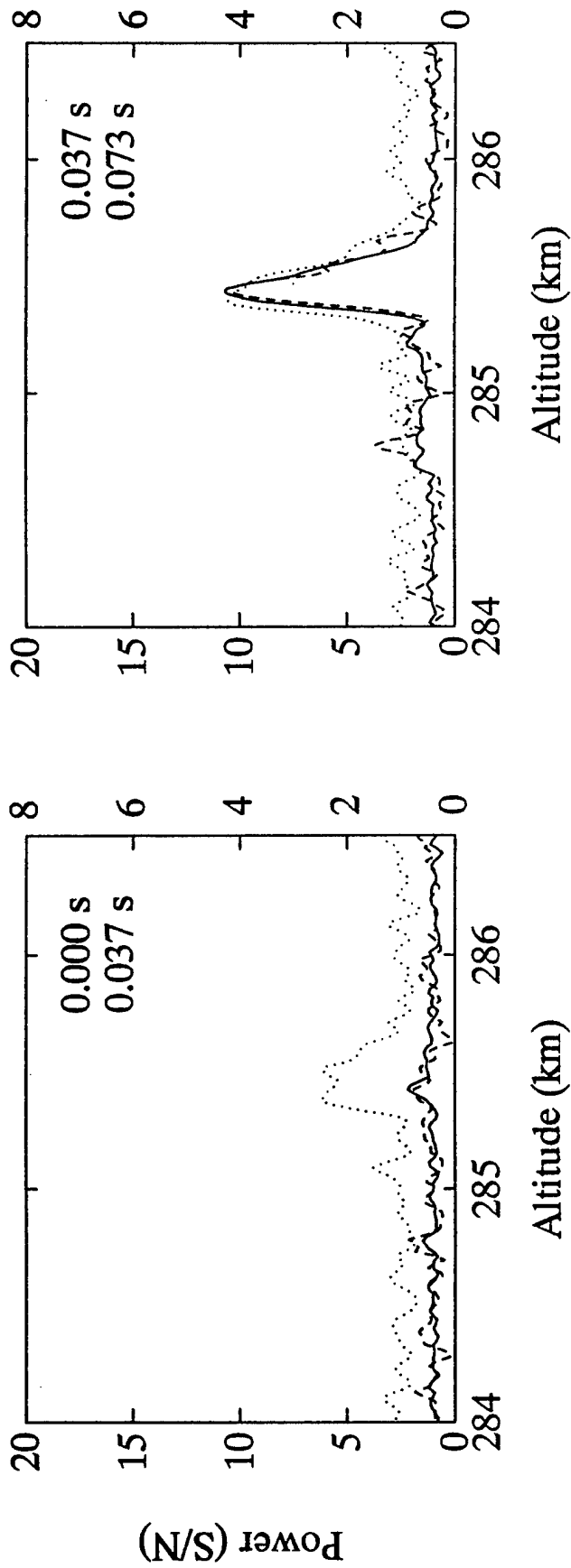


Figure 5. Early time development of HFPL and HFIL backscatter. The scale at left applies to the upshifted (dashed line) and downshifted (solid line) HFPL; the scale at right applies the HFIL (dotted line).



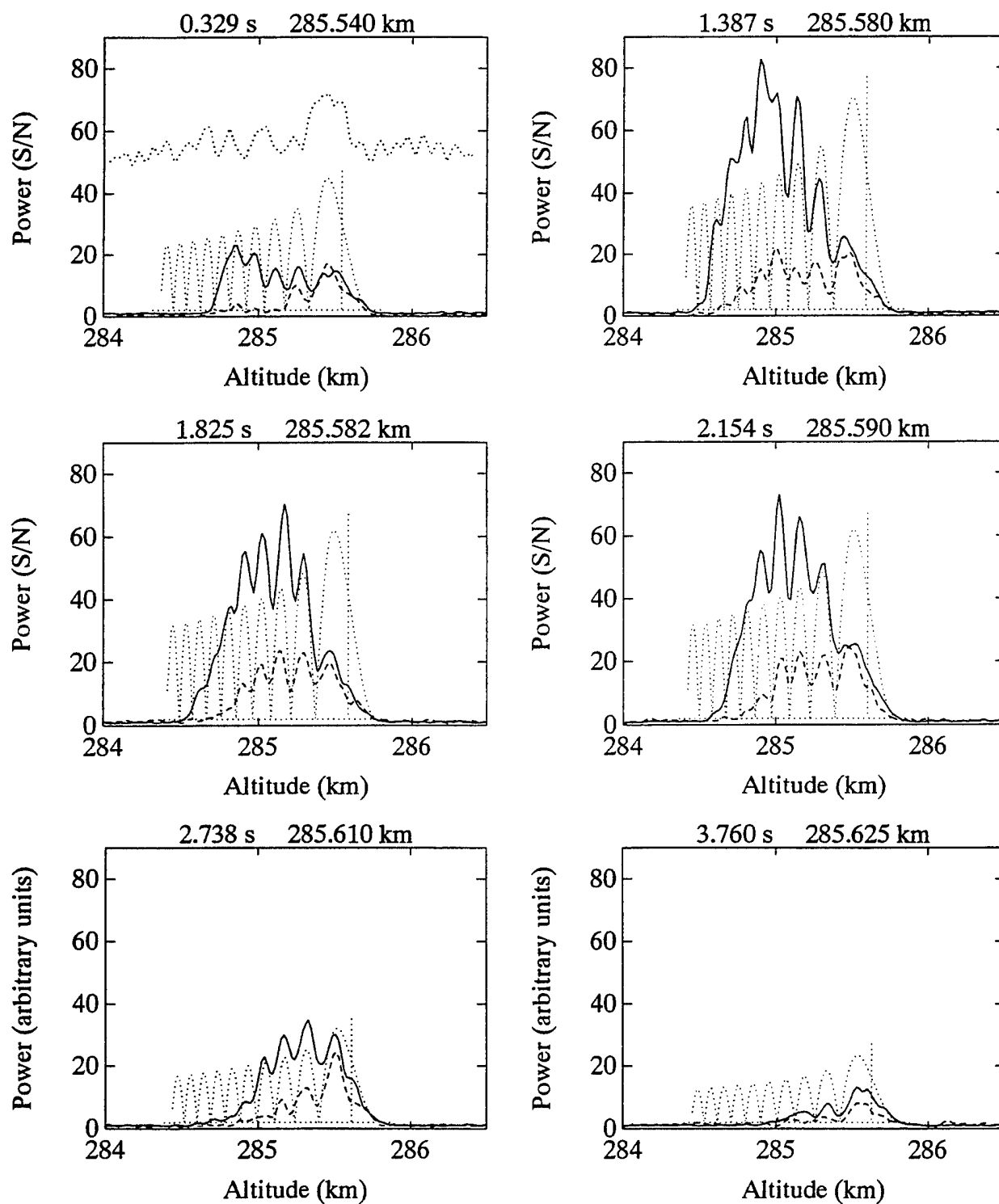


Figure 6. Development of HFPL backscatter over time scales of seconds.



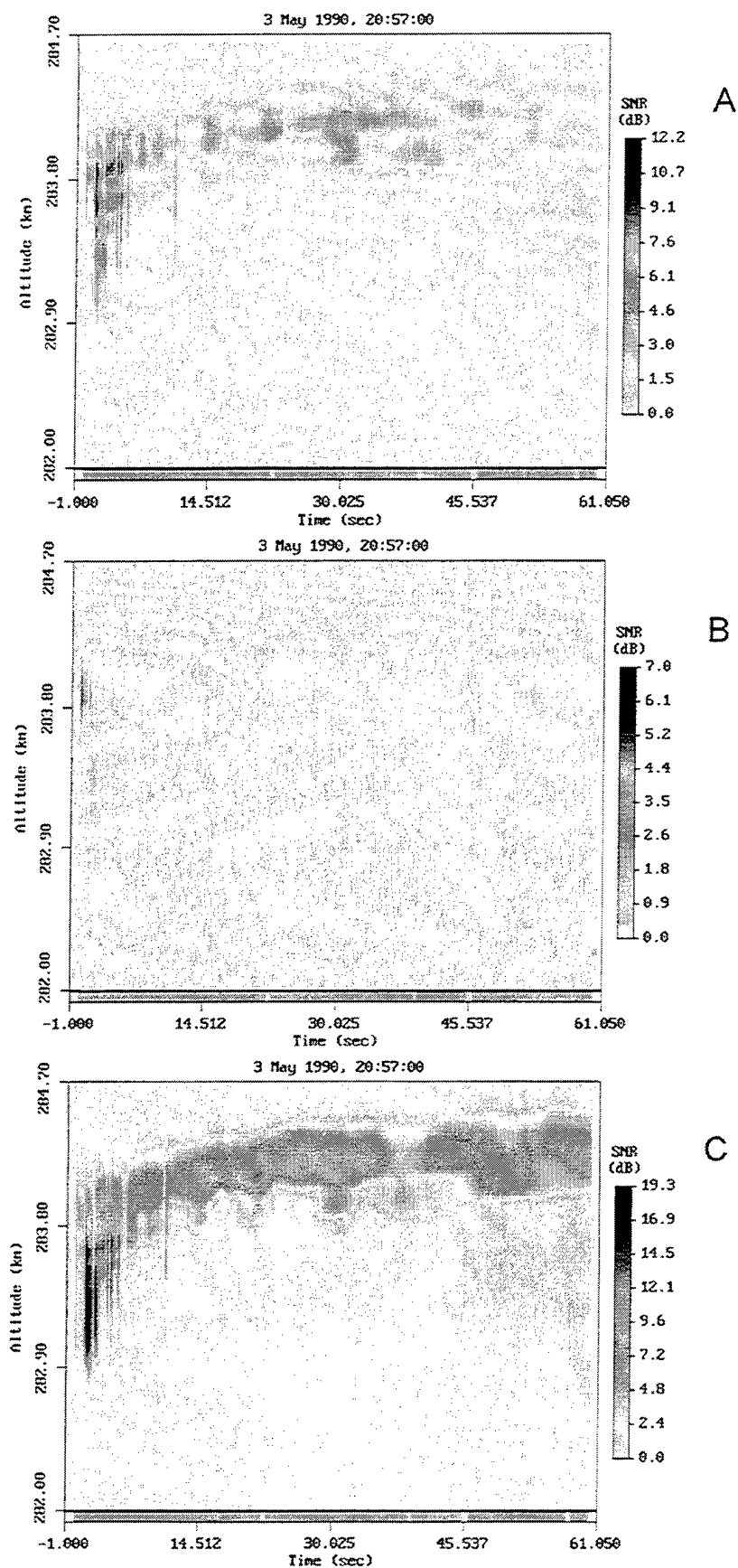


Figure 7. Temporal development of the HF-enhanced upshifted plasma line (Panel A), the enhanced ion line (Panel B), and the enhanced downshifted line (Panel C) in a cold background ionosphere. Unscheduled factor-of-four reductions in HF power density are evident in these observations.



a cold background plasma. This observation is somewhat unique because of the manner in which half of the HF transmitter array arced and was shut down during the overshoot period. These observations are presented on an expanded temporal scale in Figure 8. As noted above, abrupt changes in HFPL and HFIL power are caused by the sudden reduction/increase in HF ERP by a factor of 4. The basic outline of the overshoot process evident in Figure 3 is also found in Figure 8. However, note that HF power changes during the overshoot (first 3 s following HF turn on) uniformly decrease or increase the echo amplitudes at all altitudes. After the cold-start overshoot is complete, the switching of the HF power level from low to high (3.7 s, 4.2 s, and 4.9 s after turn-on) creates a downward extension of the echo which quickly retreats back to the "normal" echo location at higher altitudes. This is characteristic of the overshoot phenomenon in a plasma "preconditioned" by a past history of HF transmissions. On the basis of the current observations, it would appear that the minimum preconditioning period is the time required for the overshoot to take place in a cold ionospheric plasma ( $\sim 2.5$  s in Figure 8).

During the observations discussed above, the ionospherically-reflected HF modifying wave was monitored at Arecibo Observatory. The amplitude of the received signal is plotted in Figure 9 for the HF transmissions of Figure 2. The two notches apparent at 39 s and 44 s are caused by the shut-down of half of the HF antenna as noted earlier. Overall, the variation of signal amplitude with time is rather unremarkable. This is consistent with previous Arecibo experiments conducted by *Fejer et al.* [1989]. In that study, little anomalous absorption of the HF pump wave was detectable over time scales ranging from milliseconds to two seconds with  $f_{\text{HF}} = 5.3$  MHz. The observed fading periods in Figure 9 (several seconds) are expected for any HF signal (strong or very weak) reflecting in the F region. Arecibo observations in this area contrast markedly with the temporal history of HF reflected power measured at the HF facility near Tromsø, Norway [*Fejer and Kopka*, 1981] and at the SURA facility located near Nizhny Novgorod, Russia [e.g., *Frolov et al.*, 1996]. At these facilities, anomalous absorption of the HF pump wave is evident in the measurements. Absorption is produced by the excitation of microinstabilities at early times (a few ms) after HF turn-on and by the generation of artificial geomagnetic field-aligned irregularities over time scales of seconds.

### **2.3 Interaction and Coupling of HF-Induced Langmuir Turbulence with HF-Excited Electron Density Irregularities.**

The excitation of HF-induced irregularities alters propagational paths of Langmuir oscillations. In so doing, the irregularities allow the Arecibo 430 MHz radar to view wave-plasma interactions that are not initially driven along the line-of-sight of the radar. This is in sharp contrast to processes that occur within the first 50 ms of HF turn-on. In this case a smooth, stratified, background plasma exists, and it can be assumed that the wave-plasma interaction is strictly along the radar line-of-sight.



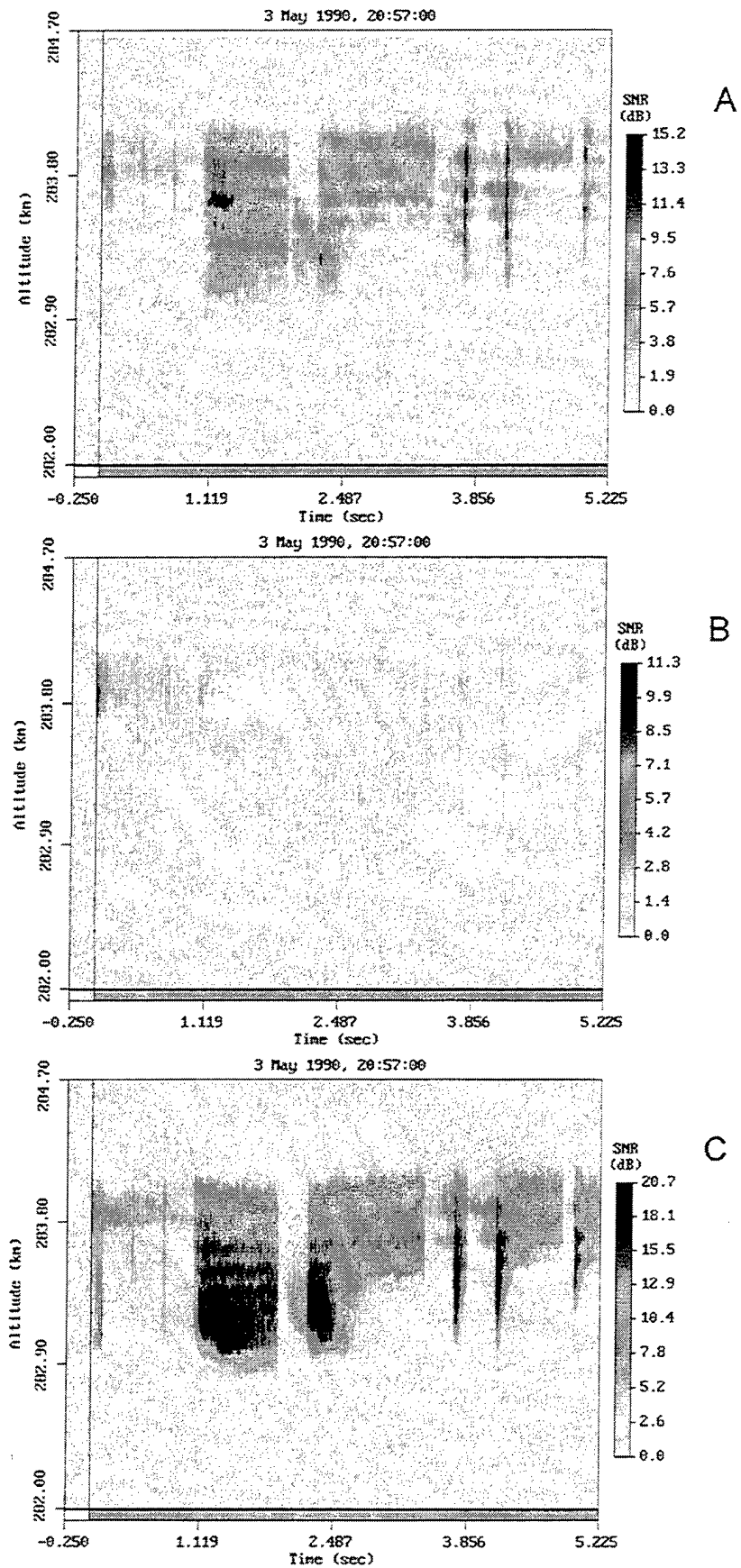


Figure 8. A more detailed view of the first 5.2 s of modifications shown in Figure 6. This data segment illustrates the response of the plasma to step-wise changes in HF power near HF turn-on.



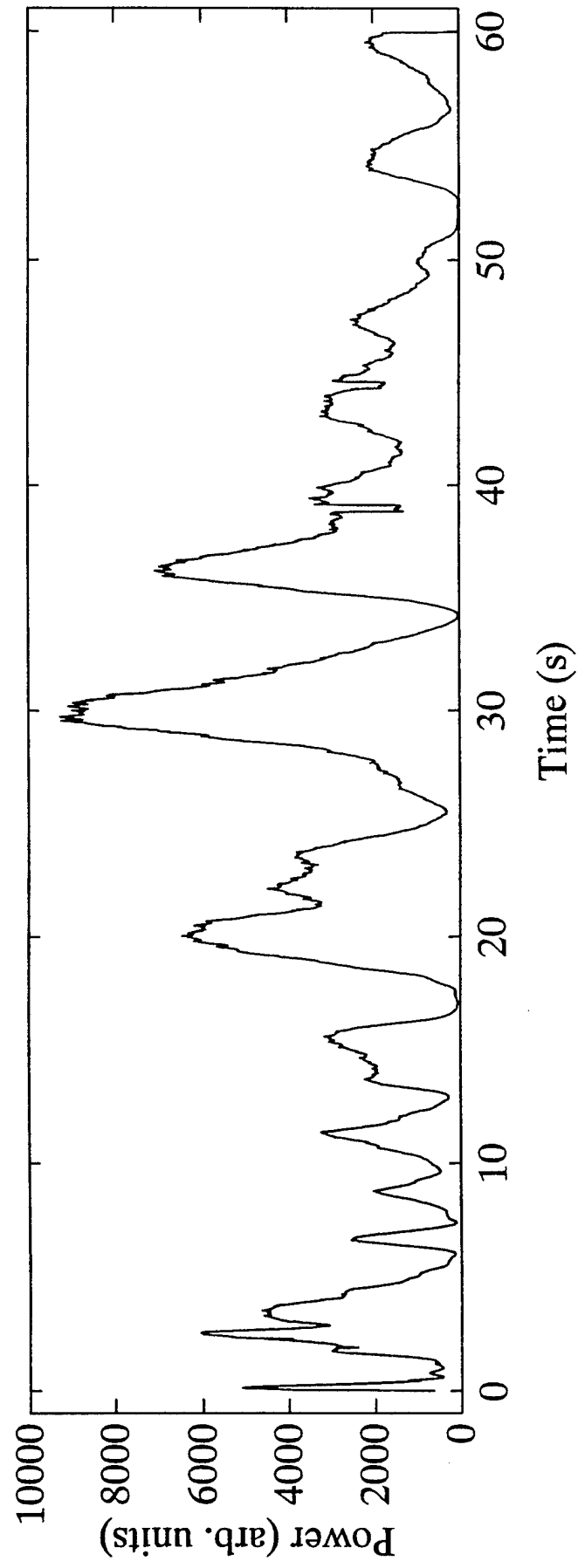


Figure 9. Power of the ionospherically-reflected HF wave for a one-minute modification period beginning at 2100:00 on 3 May 1990.



Langmuir turbulence initially excited in the plasma may also aid in the production of horizontally stratified irregularities and short-scale artificial field aligned irregularities (AFAIs). In one suggested scenario [Noble and Djuth, 1990], ponderomotively driven instabilities could greatly influence the early time development of AFAIs by producing "seed" irregularities that initiate nonlinear growth at the upper hybrid resonance. Moreover, the spatially-averaged ponderomotive force of the Langmuir turbulence follows the standing wave pattern of the pump wave and could drive the observed horizontally-stratified irregularities directly [Fejer *et al.*, 1984]. However, recent plasma simulations addressing this issue [D. F. DuBois, private communication, 1995] seem to indicate that this is not easily accomplished given the ERP of the Arecibo HF facility.

The role played by Langmuir turbulence in the production of large-scale ( $\sim 1$  km) packets of irregularities in the late time modification environment is not currently known. However, one can safely assume that the Langmuir turbulence is ducted in the associated field-aligned irregularities [e.g., Muldrew, 1978].

As part of this project, a limited amount of data were acquired that allow interactions between Langmuir turbulence and HF-induced irregularities to be investigated. In the following two sections, the coupling process is examined for interactions that develop over intermediate time scales (50 ms to several seconds) and over long time scales (20 s to several minutes).

### 2.3.1 Wave-Plasma Interactions Over Intermediate Time Scales

Of the two known types of irregularities that develop over time scales of 50 ms to several seconds (horizontally-stratified irregularities and short-scale AFAIs), only the AFAIs were investigated experimentally as part of this program. These measurements were made during the NASA-CRRES *El Coqui* rocket campaign of July 1992. During AFAI observing periods of greatest interest here, the Arecibo 430 MHz radar was dedicated to another experiment. As a result no supporting HFPL data obtained with the Arecibo radar is available.

AFAI data were acquired with a 50 MHz radar deployed on the island of Antigua. The 50 MHz antenna consisted of four rows of 26 half-wave dipoles. The vertical and horizontal two-way beamwidths were  $\sim 10^\circ$  and  $\sim 2^\circ$ , respectively. Because of the well-known aspect sensitivity of FAI scatter [e.g., Noble and Djuth, 1990], the radar was pointed perpendicular to geomagnetic field lines in the Arecibo *F* region to optimize system sensitivity. The radar beam was set at an elevation angle of  $\sim 21^\circ$  and was directed toward the ionospheric location of peak HF power density at 250 km altitude. Because of the CRRES rocket campaign, the Arecibo HF beam was tilted  $12^\circ$  from vertical in the direction of geographic north. This tilt is well within the Spitzer angle ( $15.7^\circ$ ) calculated for  $f_{\text{HF}} = 5.1$  MHz and the geomagnetic field geometry at Arecibo. At 250 km altitude, the HF beam was centered  $\sim 50$  km off the north shore of Puerto Rico. The 50 MHz radar radiated approximately 40 kW peak power. During the observations, the interpulse



period (IPP) was set to 6 ms, and the pulse width was 6.67  $\mu$ s. The latter corresponds to a range resolution of 1.0 km.

Figure 10a illustrates the development of 3-m AFAIs in a "cold" background ionosphere. Prior to HF turn-on at 0 s relative time, the Arecibo HF beam had been turned off for 8 min. The Arecibo HF frequency was set to 5.1 MHz, and approximately 60 MW ERP was transmitted for a one-minute interval. The range extent of the 50 MHz radar echo is consistent with the estimated east-west width of the Arecibo HF beam. In this particular case, there appears to be secondary peaks in scattering cross section on either side of the central peak. The reason for this is not well understood. The overall echo strength builds over time scales of 5 s, then diminishes over the remaining 55 s of the modification period. There is a hint of similar behavior in AFAI data acquired by *Coster et al.* [1985] during experiments conducted in 1981. However, these AFAI measurements were not made in an initially cold background ionosphere. The temporal behavior exhibited in Figure 10a needs to be tested for consistency in future experiments.

One important aspect of these observations is the relatively short period of time required to detect 3-m AFAI after HF turn-on in a cold ionosphere. In Figure 10b, the observations of Figure 10a are shown on an expanded temporal scale. The first radar echoes emerge above the noise background within 200 ms of HF beam turn-on. This time (200 ms) represents an upper limit on the time period required to generate significant HF-induced electron density perturbations in the plasma. The time period is not inconsistent with the inferred 50 ms transition time from a smooth ionospheric plasma present at HF turn-on to a plasma altered by induced irregularities. The 50 ms time scale is based on changes in the spectral signature of HFPL echoes [e.g., Sulzer and Fejer, 1994].

In other tests conducted with the Antigua radar, it was found that AFAI scatter can be detected after a cold turn-on of the HF beam at only 4 MW ERP. These measurements were made on July 8, 1992. The HF beam was turned off for 18 min prior to the turn-on at 4 MW ERP. This detection threshold is somewhat less than the value of 12.8 MW reported by Noble and Djuth [1990]. The discrepancy arises in part because of the greater sensitivity of the Antigua radar to AFAIs brought about by its reduced range to the modified volume. The Antigua radar range to the center of the HF beam was  $\sim 625$  km versus  $\sim 730$  km for Guadeloupe. The (range)<sup>-4</sup> dependence of backscatter power gives rise to a factor of  $\sim 2$  improvement in radar sensitivity at Antigua. In addition, a better aspect geometry may have also contributed to increased sensitivity at Antigua.

It should be noted that the 4 MW ERP detection threshold is so low as to rule out AFAI production caused solely by the thermal parametric instability [e.g., Grach et al., 1977, 1978a,b; Das and Fejer, 1979]. A comparison of theoretical thresholds is provided in *Noble et al.* [1987]. *Noble and Djuth* [1990] show that the detection threshold for AFAIs is close to that of the



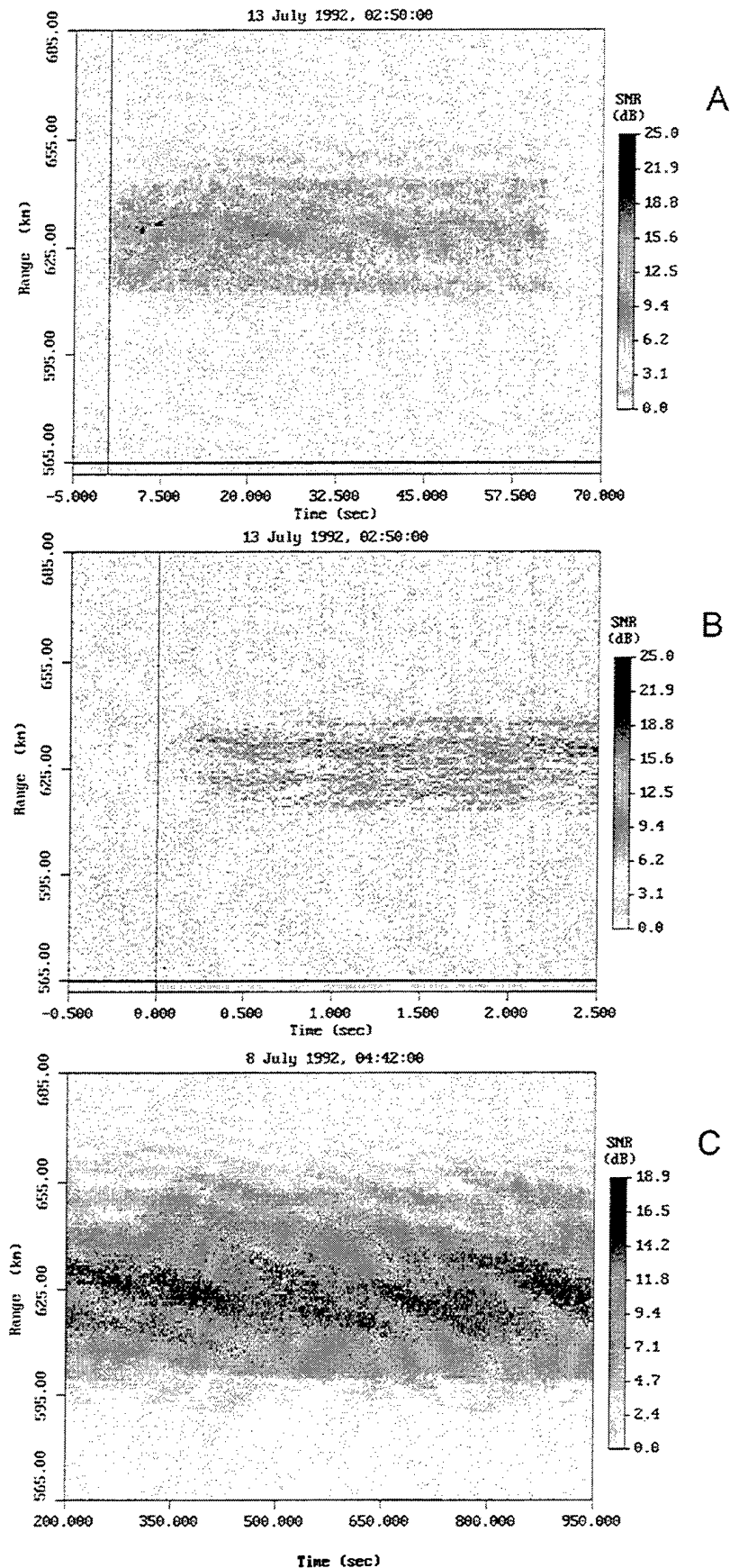


Figure 10. Temporal development of 3-m AFAIs in a cold background ionosphere (Panel A), expanded view of Panel A at HF turn-on (Panel B), and 3-m AFAIs in the late-time environment (Panel C).



Arecibo HFPL. This suggests a different scenario for AFAI generation. Intense Langmuir oscillations produced by strong turbulence and/or parametric decay processes invariably lead to the formation of small-scale electron density perturbations. These irregularities can subsequently be reinforced by Langmuir wave self-focusing in the plasma. Field-aligned irregularities initially driven near the region of HF reflections could subsequently penetrate into the region of the upper hybrid resonance and trigger so-called resonance instabilities [e.g., *Vas'kov and Gurevich, 1975, 1977; Inhester et al., 1981; Inhester, 1982*]. Thus, ionospheric irregularities initially driven by intense Langmuir oscillations at higher heights could provide "seed" irregularities for other processes that may subsequently dominate the development of AFAIs (including the thermal parametric instability). Memory of the seed irregularities that trigger the resonant processes is of course lost in the plasma. On the other hand, AFAIs that are strongly driven near the upper hybrid resonance level will diffuse up and down geomagnetic field lines. If these irregularities penetrate to heights near HF reflection, they will greatly impact wave propagation in the plasma and may alter the production of Langmuir turbulence.

### 2.3.2 Wave-Plasma Interactions at Late Times in the Modification Process

The late-time (e.g., few minutes after HF turn-on) large-scale modification environment is populated by a discrete number of kilometer-scale field-aligned structures. Each structure contains a packet of filamentary irregularities having spatial scales across the geomagnetic field  $\mathbf{B}$  of 3-17 m; the separation between individual filaments is approximately 15 m [*Kelly et al., 1995*]. Evidence of such packets of filamentary irregularities at Arecibo is embedded in the Rayleigh fading statistics of 50 MHz FAI backscatter reported by *Coster et al. [1985]*. The Rayleigh fading is brought about by the presence of a limited number of scattering centers within a radar range cell. In the case of *Coster et al. [1985]*, each range cell was 12 km wide. On the basis of these observations, one can estimate that there are typically several tens of such scattering centers in the Arecibo HF beam.

Data acquired with the Antigua 50 MHz radar in the late time environment are shown in Figure 10c. As noted above these data were acquired with 1-km range resolution. The tilted structures in the range versus time versus intensity (RTI) plot are caused by the movement of large scattering regions across the HF beam. Individual scattering centers cannot be resolved in RTI plots of this nature because the wavefront of the 50 MHz beam extends across the entire HF-modified volume (roughly the size of the HF beam). The radial speed of a scattering region in Figure 10c can be estimated from the change in range of a scattering zone with time. This yields speeds of the order of 40 m/s, which is consistent with the radial drift speed of the background ionosphere deduced from simultaneous observations with the Arecibo 430 MHz radar. Additional comparisons of this nature are required to confirm that AFAI drift speed is always tied to the  $\mathbf{E} \times \mathbf{B}$  drift of the background ionosphere, where  $\mathbf{E}$  is the ambient electric field.



If one scans the Arecibo 430 MHz radar beam across the HF-modified volume at very late times (i.e., several minutes after HF turn-on), one finds that the Langmuir turbulence resides within field-aligned packets of irregularities. Figure 11a shows power measured at the downshifted HFPL as the Arecibo radar beam scans across the modified region. In this case, continuous HF transmissions were made beginning 10 min prior to the observations shown. During this observation, the frequency of the HF transmissions was 5.1 MHz and ~80 MW effective radiated power was transmitted.

The radar beam was positioned at a zenith angle of  $3.5^\circ$ ; the azimuth sweep started at  $163^\circ$  (19:59:45 AST), moved through center of the HF beam at 270 km altitude ( $33^\circ$  azimuth) at 20:05:30 AST, and arrived at  $270^\circ$  azimuth at 20:10:25 AST. Beginning at  $163^\circ$  azimuth, the 430 MHz radar scans across the southeast quadrant of the HF beam on its northward path through the center of the HF beam ( $33^\circ$  azimuth). Thereafter, the radar line-of-sight moves nearly east-west across the northwest quadrant of the HF beam. After reaching the geographic north position ( $0^\circ$  azimuth) at 20:07:00 AST, the beam moves west-southwest as it scans towards  $270^\circ$  azimuth.

From the scanning results one can conclude that the HF-modified ionospheric volume did not precisely match the expected position of the HF beam in a static ionosphere. For the measured electron density gradient near the point HF reflection (Figure 1), the beam should be centered almost directly above the HF facility. However, it appears that the center of the HF beam in the ionosphere and associated ionospheric modifications were located approximately 10 km southwest of the nominal center position in a static ionosphere. Movements of the HF beam in the Arecibo ionosphere have been previously noted. CCD optical images of HF-induced airglow [ $O(2^1D)$  6300 Å] have been used to determine the location and spatial extent of the region of HF-accelerated electrons, and in so doing establish the exact location of the HF beam in the sky [e.g., *Bernhardt et al.*, 1988]. These prior measurements were made under nighttime winter conditions at solar minimum. In this situation an imbalance in electron energy thermal dissipation occurs, which gives rise to large electron temperature enhancements and corresponding electron density depletions [*Djuth et al.* 1987; *Newman et al.*, 1988; *Djuth*, 1989]. Electron thermal pressures within the HF beam often produce an electron density depletion comparable in size to the HF beam. This leads to refractive self-focusing of the HF beam [*Bernhardt et al.*, 1988]. The HF beam subsequently moves across the sky at the  $\mathbf{E} \times \mathbf{B}$  drift speed of the background plasma. When the ionosphere is no longer able to refractively capture the HF beam, the HF beam snaps back to its original vertical position. Optical measurements have not been successful in tracking the Arecibo HF beam under solar maximum conditions appropriate for the current radar measurements. The Arecibo HF facility currently has an effective radiated power that is too low (~80 MW) to produce substantial airglow emission at solar maximum. (This situation is expected to improve with the completion of a facility upgrade at Arecibo.) However, Arecibo radar



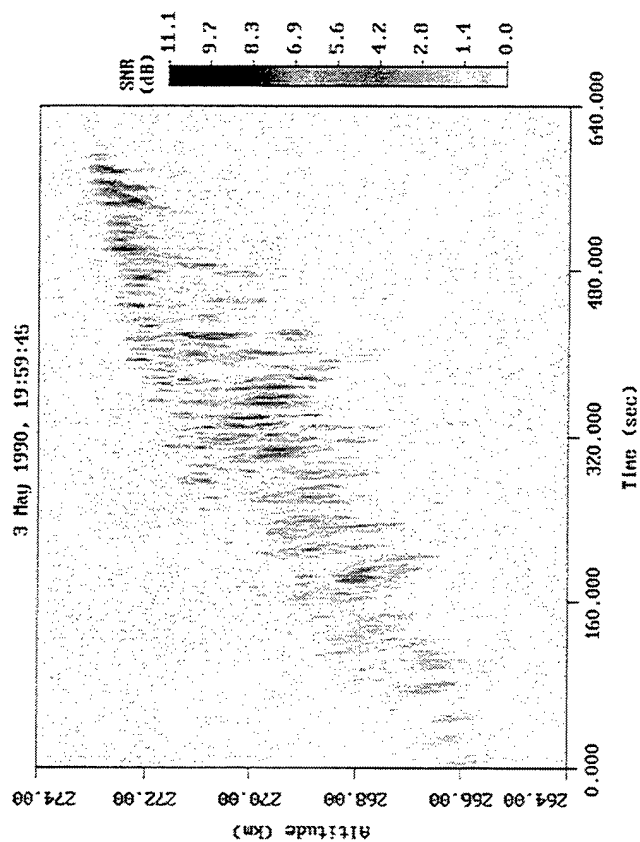


Figure 11a. HFPL power measured at the downshifted plasma line as the 430 MHz beam scans across the HF-modified ionospheric volume.

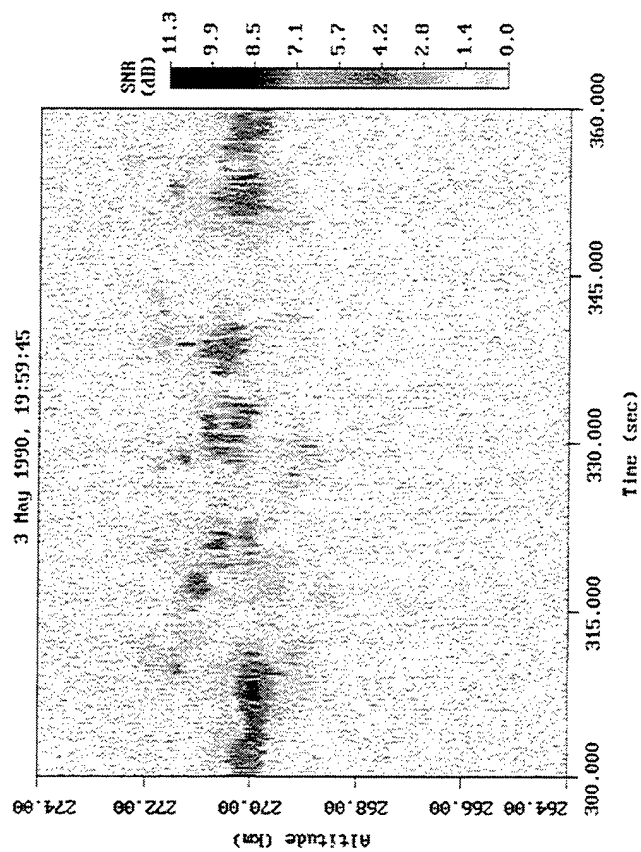


Figure 11b. Temporal expansion of the echoes in Figure 11a near the center of the modified ionospheric volume.



measurements of HF-accelerated electrons at solar maximum indicate that HF beam movements also occur in the solar maximum plasma [K. M. Groves, private communication, 1994]. Thus, the radar measurements described above appear to be consistent with the notion that HF beam movements occur under both solar minimum and solar maximum conditions.

In Figure 11a, the increase in average plasma line altitude with time is caused by the natural movement of the ionosphere upwards. Note, however, that regions of HFPL scatter are highly structured. The detected Langmuir turbulence is believed to reside in large-scale ( $\sim 1$  km) "packets" of geomagnetic field-aligned irregularities. These irregularity packets are clearly evident in the rocket observations reported by *Kelley et al.* [1995]. Langmuir wave propagation in geomagnetic field-aligned ducts [e.g., *Muldrew*, 1978, 1985] plays a key role in observations of this nature. This allows HFPL backscatter to be detected over an extended altitude interval (2-3 km). Given the measured scale length  $H=29.2$  km near the point of HF reflection, perturbations with a maximum variation of  $\sim 10\%$  relative to the background profile would produce the observed 3-km spread in the HFPL. This value is similar to the 8% maximum perturbation reported by *Djuth et al.* [1995] in experiments involving a stationary radar beam and compares well with 8-9% perturbations measured with rocket-borne instruments [*Kelley et al.*, 1995]. Essentially, the Langmuir turbulence "paints" the field-aligned structures in which it resides. The slight tilts in the vertical filaments (particularly near the edges of Figure 11a) are thought to be caused by the alignment of the echoes with the geomagnetic field.

Figure 11b shows an expanded view of the Langmuir turbulence as the 430 MHz radar beam passes near the center of the HF modified volume. The "clouds" of highly structured backscatter are not unlike those reported by *Djuth et al.* [1990, 1995]. In a cold unmodified ionosphere, the HFPL echo breaks up and exhibits layered altitude structure after 20-60 s of high-power (80 MW ERP) HF transmissions. This is the initiation of the filamentation instability. Packets of field-aligned irregularities are believed to represent the saturated state of the filamentation instability. This final state is thought to occur over time scales of several minutes following the turn-on of the HF beam in a cold background plasma.

In Figures 12 and 13, simultaneously recorded HFPL and HFIL power spectra are displayed versus altitude. These data were acquired with the coded long-pulse technique [*Sulzer*, 1986]. The ordinate corresponds to spectral power plotted on a linear scale. Independent spectral measurements are presented every 150 m in altitude. Two column pairs are shown for each resonant line (i.e., upshifted/downshifted plasma line and ion line). Altitudes indicated for the ion line observations at center also apply to each of the two plasma lines. The data of Figures 12 and 13 were obtained in the natural F region just prior to the CRRES AA-2 chemical release [*Djuth et al.*, 1995]. Plate 2 of *Djuth et al.* [1995] clearly shows that the F-region was heavily structured by the HF beam prior to the rocket launch. Standard incoherent scatter radar measurements were



# Altitude-Resolved HFPL and HFIL Spectra in a Heavily Conditioned Ionospheric Plasma (Upper Altitude Segment). Observation Period: 05:03:12 - 05:03:18 AST on July 12, 1992.

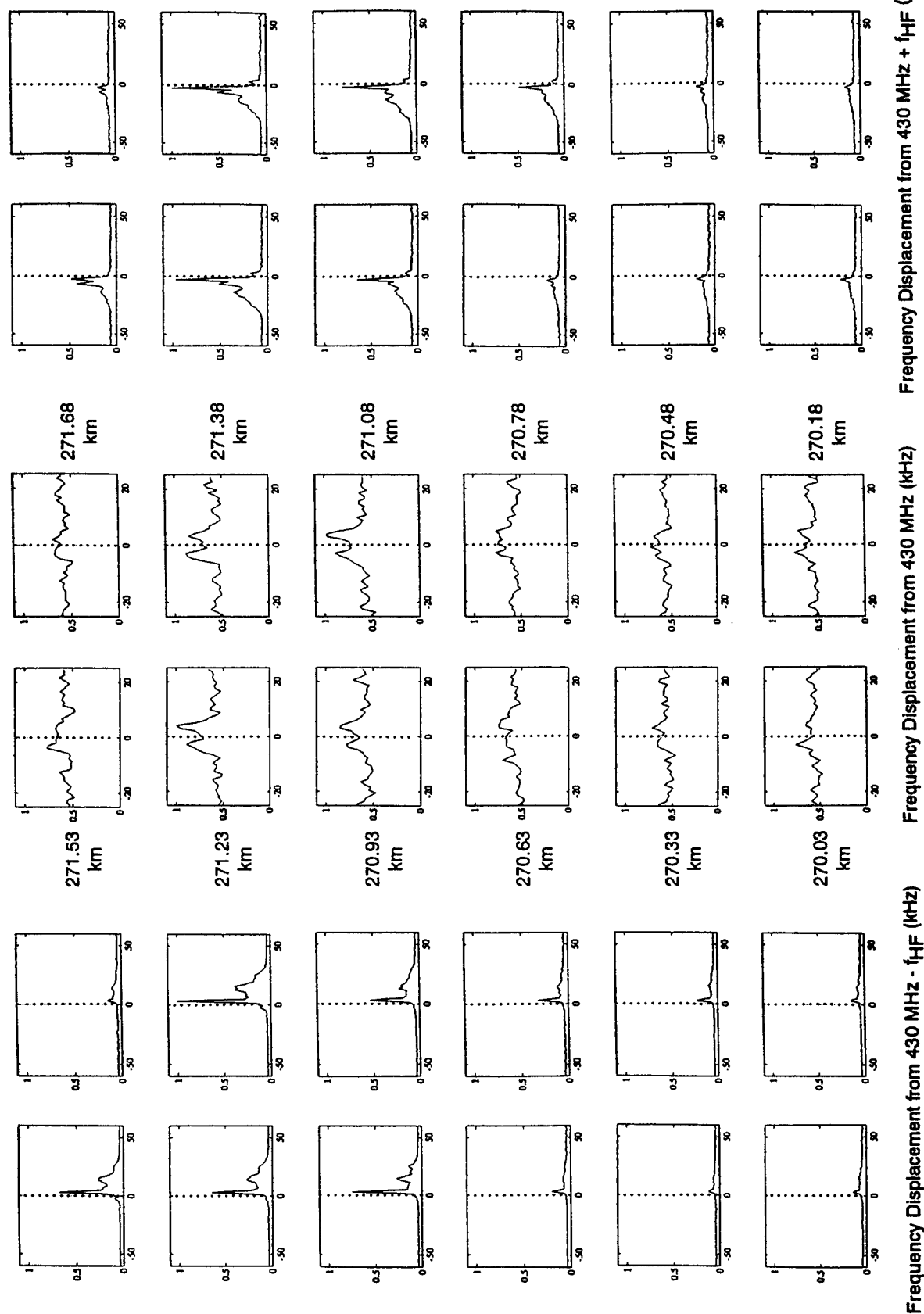
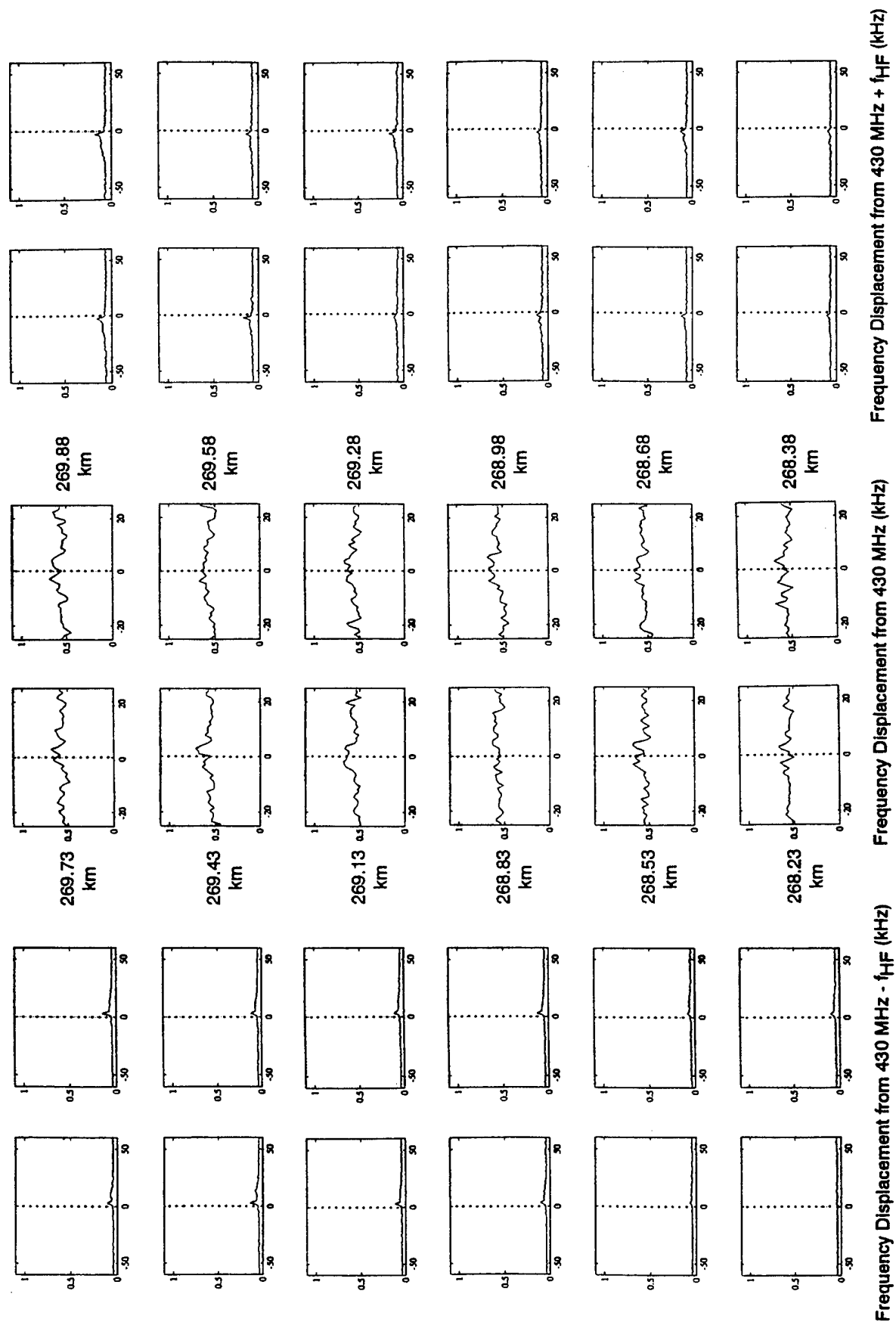


Figure 12



# **Altitude-Resolved HFPL and HFIL Spectra in a Heavily Conditioned Ionospheric Plasma (Lower Altitude Segment). Observation Period: 05:03:12 - 05:03:18 AST on July 12, 1992.**



**Figure 13**



used to establish ionospheric scale length  $H = 40$  km. The observed echo spread of 3.6 km is consistent with the presence of HF-induced electron density perturbations of the order of 8%. Simultaneous AFAI measurements made with the Antigua 50 MHz radar indicated the presence of strongly excited AFAIs. The observed radar echoes were not unlike those illustrated in Figure 10c.

The spectra of Figures 12 and 13 resemble those expected for a parametric decay process. Dominant decay line peaks and cascade sidebands are evident in both the upshifted and downshifted HFPL spectra. In addition, HFIL enhancements are visible at altitudes where the HFPL is the strongest (i.e., at altitudes between 271.23 and 271.68 km). These spectra exhibit enhanced sidebands offset from the 430 MHz radar frequency by  $f_{ia} \sim 4$  kHz, where  $f_{ia}$  is the ion-acoustic frequency in the plasma. Thus, in heavily conditioned ionospheric plasmas containing ducts, the plasma turbulence contains the signature of parametric decay processes. This is in stark contrast to measurements made within  $\sim 50$  ms of HF turn-on. In this situation, all key spectral features predicted by strong turbulence theory are evident in the Arecibo observations [Fejer *et al.*, 1991; Sulzer and Fejer, 1994]. This implies that the excitation process is affected by the presence of AFAI, or that our view of the microinstability process is restricted at early times by the smoothness of the plasma. As ionospheric ducts develop, waves excited at small angles relative to  $\mathbf{B}$  propagate into the radar field-of-view [Muldrew, 1978, 1979, 1985]. Additional studies are needed to cover the critical transition period between 50 ms and  $\sim 1$  s after HF turn-on. It is believed that a change in plasma state occurs in this time frame, and this change should be reflected in the HFPL spectra. Overall, it is important to remember that the initial HFPL observations at Arecibo Observatory [e.g., Kantor, 1974] were all made in a highly preconditioned plasma. These observations were not altitude-resolved, but the altitude-integrated spectral return appeared amenable to interpretations involving parametric decay instabilities. The current altitude-resolved measurements emphasize this point.

#### **2.4 Renewed Observations of HF-Accelerated Suprathermal Electrons**

Despite many years of study, the physical process responsible for the acceleration of electrons to suprathermal energies (2-20 eV) by HF-excited waves remains poorly understood. In part, this is because our knowledge of Langmuir turbulence production is still rather incomplete. At present, it appears that elements of caviton collapse events predicted by strong turbulence theory dominate the early time reflection layer physics. At subcritical plasma densities, the presence of a "caviton gas" facilitates the parametric instability saturation process [e.g., Nicholson and Goldman, 1978; Gurevich *et al.*, 1985; DuBois *et al.*, 1991; Cheung *et al.*, 1992; DuBois *et al.*, 1993a,b]. Under any circumstance, one expects suprathermal electrons to be produced in the presence of collapsing cavitons [Nicholson and Goldman, 1978; Vas'kov, 1983; Gurevich *et al.*, 1985; DuBois *et al.*, 1993a,b]. Moreover, even if cavitons were not produced, one might still



expect the Langmuir turbulence to accelerate electrons to suprathermal energies as a result of the "bootstrap" process of *Weinstock and Bezzerides* [1974], resonance broadening [*Weinstock*, 1975], interactions at the upper hybrid resonance [*Grach et al.*, 1984], or a variety of other stochastic processes [e.g., *Bulanov et al.*, 1990].

Studies of suprathermal electrons accelerated by HF-induced instabilities have been made in the past at Arecibo using non-resonantly enhanced plasma lines as a diagnostic [e.g., *Carlson et al.*, 1982; *Fejer and Sulzer*, 1987, *Fejer*, 1988]. Arecibo radar measurements of plasma lines enhanced by suprathermal electrons are much more sensitive to low-level electron fluxes than, for example, optical observations of induced airglow. Past observations have shown that suprathermal electrons are present in the late-time modification environment [*Carlson et al.*, 1982] and that there is a transient plasma response to the turn-on of the HF beam [*Fejer and Sulzer*, 1987, *Fejer*, 1988].

The linkage between Langmuir oscillation excitation and electron acceleration places huge demands on the experimental investigation because extremely good temporal resolution ( $\sim 50$ -100 ms) must be achieved for the suprathermal electron measurements. As noted above, at late times ( $> 50$  - 100 ms after HF turn-on) the experimental observations do not closely match theoretical predictions for a smooth inhomogeneous plasma. Clearly, this stage of the modification process is being influenced by the formation of field-aligned and horizontally-aligned irregularities, which are not incorporated into existing turbulence theory. Plasma redistribution across and along geomagnetic field lines most likely has a significant impact on the development of the Langmuir turbulence (and the associated energetic electron fluxes). On the basis of past observations, it is well-known that suprathermal electrons are routinely excited even in the late-time environment at Arecibo. However, relatively high HF power levels ( $\sim 80$  MW ERP) are required for significant electron fluxes.

Extremely good temporal resolution is not possible with optical diagnostics because the effective temporal resolution is set by the lifetime of excited states in neutral species (e.g., typically tens of seconds for  $O(^1D)$ ). Our real hope in this area lies in the application of the coded long-pulse radar technique to plasma lines enhanced by suprathermal electrons. It is by far the most sensitive diagnostic for detecting suprathermal electrons. In our observing strategy, optical diagnostics still play a crucial role in establishing absolute fluxes in several narrow electron energy bands and are required to spatially map out the region of excitation. This mapping is important for proper interpretation of the radar results. Moreover, the effective electron temperature of the suprathermal electron tail can be estimated from intensity ratios of various emissions from atomic oxygen (e.g.,  $O(^2D)$  6300 Å,  $O(^2S)$  5577 Å,  $O(^3P)$  7774 Å measurements) [*Vas'kov and Milikh*, 1983]. With the inclusion of electron energy loss processes, the effective excitation energy of each of these lines is  $\sim 3.5$  eV,  $\sim 6$  eV, and  $\sim 11$ -12 eV, respectively. Finally, infrared



emissions from molecular oxygen can be used to examine low energy electrons that are not measurable with the Arecibo 430 MHz radar. In particular, emissions at 12,700 Å and 15,800 Å provide important information about changes in electron fluxes at energies near 0.98 eV and 1.58 eV, respectively.

In future experiments, the principal diagnostics should include the Arecibo 430 MHz radar, a CCD optical imager and/or an infrared imager. During these experiments, all of the optical emissions discussed above should be monitored. The coded long-pulse technique would be used to make high range/temporal resolution measurements of plasma lines enhanced by suprathermal electrons in the nighttime F region. In the past, limited studies of this nature have been conducted at Arecibo Observatory by F. T. Djuth (Geospace Research, Inc.) and K. M. Groves (Phillips Laboratory, Hanscom Air Force Base). These observations were made during the so-called NASA/CRRES rocket campaign conducted in July 1992. Spectral measurements of plasma lines enhanced by HF-accelerated electrons are shown in Figure 14. The data integration period is ~20 s. HF-induced enhancements occur within the two dashed lines. Continuous HF transmissions at 5.1 MHz were used to modify the ionosphere. Only small segments of the plasma line spectrum containing enhancements are shown in the figure (from ~ 430 MHz - 6.05 MHz to 430 MHz - 7.00 MHz). The experimentally measured spectra extend from 430 MHz - 3 MHz to 430 MHz - 8 MHz. Notice that the enhancements from suprathermal electrons occur near the peak of the F region. The region of resonant plasma line enhancements was located at a lower height (~295 km altitude). Accelerated electrons travel from the resonance region through the topside ionosphere. Because the geomagnetic dip angle at Arecibo is ~49°, the altitude slice shown in Figure 14 maps across the HF beam at the resonance height in roughly a one-to-one fashion. At Arecibo, one typically points the radar geomagnetic south of the resonance region to measure HF-accelerated electrons moving up magnetic field lines into the topside ionosphere. It is also possible to monitor accelerated electrons moving downwards in altitudes; in this case the radar is pointed geomagnetic north of the resonance region.

In Figure 14, the location of the plasma line peak is an indicator of plasma frequency in the background ionosphere, whereas signal amplitudes provide information about the flux of suprathermal electrons in the energy range 14-15 eV. This energy coverage is dependent upon the background electron density profile. Preliminary results from this limited set of observations indicate that localized regions of electron acceleration exist within the HF beam and that the electron flux periodically varies over time scales of 60-90 s (when continuous HF transmissions are used). With the Arecibo radar, spatial features are readily observed across the geomagnetic meridian plane mapped up from the region of resonant excitation. Various spatial cuts across the heated ionospheric volume can be obtained by repositioning the radar beam in azimuth. Our limited observations indicate that electrons are accelerated to energies near 15 eV within 1 s of HF



Plasma Line Spectra Enhanced by HF-Produced Suprathermal Electrons  
13 July 1992, 04:30:00 AST

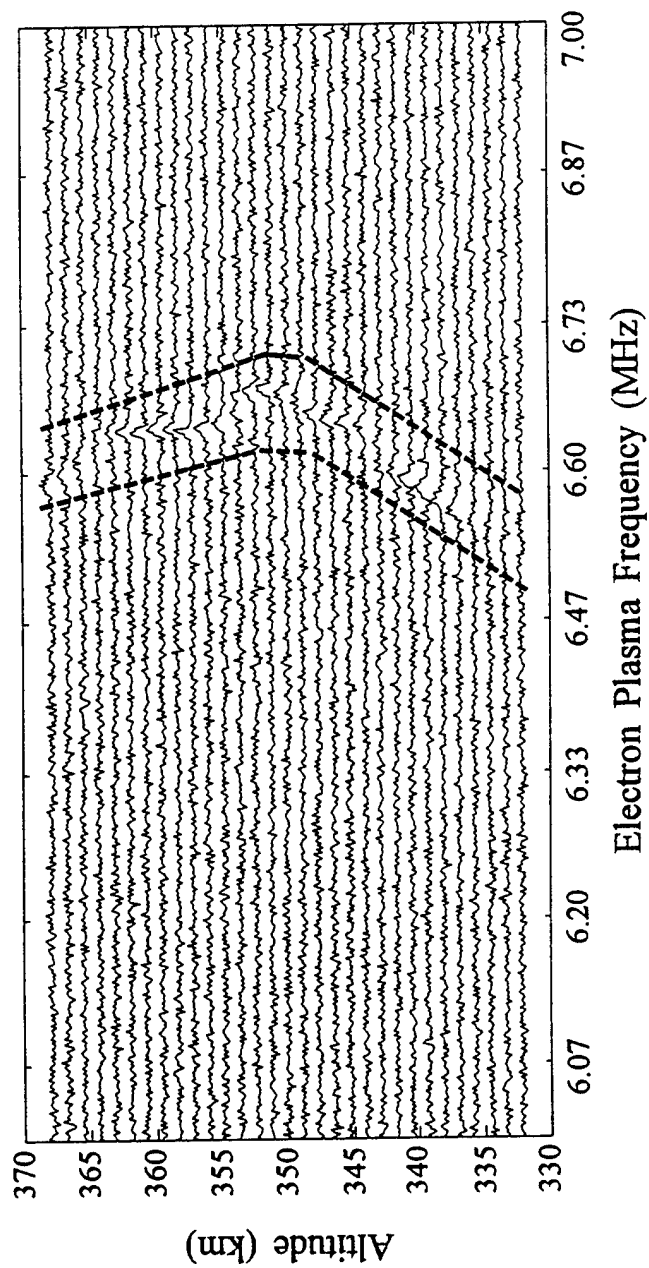


Figure 14



beam turn-on. Additional studies of this nature are needed both in the "cold" unmodified ionospheric plasma and in plasmas preconditioned by a past history of HF operations [see e.g., *Djuth et al.*, 1990].

## 2.5 Summary of Arecibo Ionospheric Modification Results.

The measurements presented above illustrate three distinct time scales associated with the ionospheric modification process. In general, the observed backscatter power from Langmuir oscillations and ion waves during the first 50 ms after HF turn-on in a cold background plasma is consistent with the creation of strong states of plasma turbulence near the critical point in the plasma. During this period, HFPLs detected with the Arecibo 430 MHz radar are strongly excited at the first maximum of the HF standing wave pattern in the plasma. As expected, much weaker HFPLs are observed at the altitude where the frequency matching condition is satisfied for weakly driven parametric instabilities. Moderate HFIL scatter is present at early times near the first maximum of the HF standing wave pattern. Much weaker HFIL echoes are observed near standing wave maxima at lower altitudes. The space and time distribution of Langmuir turbulence described by *DuBois et al.* [1993a,b] predicts a strong "zero frequency" feature in the HFIL spectrum that is directly related to caviton dynamics. While spectral measurements of this nature have yet to be made, the fact that the strongest HFILs occur near the first standing wave maximum is promising from the perspective of caviton theory. Previous HFPL spectral measurements made in the early time environment at Arecibo [*Fejer et al.*, 1991; *Sulzer and Fejer*, 1994] indicate that the signatures of caviton collapse are present near the first maximum of the standing wave pattern.

As indicated in Figure 4, Langmuir turbulence is detected at Arecibo in the region of HF evanescence above the critical point in the plasma. This is a region where the caviton gas is predicted to exhibit spatial and temporal correlations [*DuBois et al.*, 1990; *DuBois, D. F.*, private communication, 1995]. In this region, the caviton model predicts that there should be a dominant zero frequency peak in the ion line spectrum. Most noteworthy is the fact the HFPL spectrum is expected to contain distinctive peaks similar to a parametric decay cascade. However, the physical process responsible for the cascade sidebands arises from "lattice structure" within the plasma and is not related to the parametric decay instability. Physically, the parametric decay instability cannot be excited above the critical altitude, and even at the first or second maxima in the standing wave pattern the instability threshold is too high and/or the growth rate is too slow for the process to be consequential at Arecibo.

After ~50-100 ms of HF transmissions, the HF-modified plasma appears to undergo a permanent change of state. The current belief is that the change of state is related to the formation of HF-induced irregularities in the plasma. Over intermediate time scales of 50 ms to several seconds following HF turn-on, horizontally stratified irregularities and short-scale (3 - 6 m) field-



aligned irregularities are generated in the plasma. The spectral characteristics of the Langmuir turbulence have not yet been explored in this time domain. However, as shown in Figures 12 and 13, ducted propagation of parametric decay waves appears to dominate the late time environment. The decay line spectra noted by *Fejer et al.*, [1991] and *Sulzer and Fejer* [1994] at high HF duty cycles are probably related to the formation of large scale electron density structures in the plasma.

Langmuir turbulence excited in a cold plasma over time scales of 100 ms to several seconds tends to conform to the standing wave pattern of the reflected HF pump wave (Figures 2-4). As part of the "overshoot" process the HFPL backscatter at 430 MHz extends downward in altitude approaching the region of the upper hybrid resonance. After several seconds a retreat to higher altitudes near HF reflection ensues. Thereafter, strong HFPL echoes are confined to the first and second maxima of the standing wave pattern. This continues until the HFPL echo breaks up because of the formation of large-scale plasma structures. No viable explanations currently exist for this behavior. However, because the HF standing wave pattern, as mirrored in HFPL backscatter, persists unaltered over time scales of tens of seconds, one can conclude that irregularities formed in the plasma over these time scales do not greatly disrupt the propagation of the pump wave.

Important changes in the plasma state are revealed in Figure 8. In this case, it is observed that the transient response of the plasma to HF pulsing changes after a few seconds of transmissions in a cold background plasma. This may be related to the excitation of short-scale AFAIs in the plasma or the formation of horizontally stratified irregularities. Whatever the cause, the plasma response is permanently altered until conditions of a smooth background plasma return.

In a cold plasma, it takes only a few hundred milliseconds before scatter from short-scale (3-6 m) AFAI is detected (Figure 10). This sets an upper limit on the time required for induced plasma inhomogeneities to develop following HF turn-on. Indeed, Arecibo HFPL observations indicate that the actual time scale may be closer to 50 ms.

At late times 20-60 s after HF turn-on at high powers, large-scale (~1-5 km) "packets" of smaller-scale irregularities begin to form in the plasma [e.g., *Kelley et al.*, 1995; *Djuth et al.*, 1996]. This leads to the break-up of the HFPL echo [*Djuth et al.*, 1990]. The filamentary irregularities probably evolve into a final saturated state within 5 minutes of full-power illumination (80 MW ERP) by the HF beam. In this regard, nighttime conditions are assumed to prevail making HF absorptive losses en route to the F-region (e.g. D-region absorption) negligible. There are indications that the excitation of the irregularity packets is extremely nonlinear in nature. Limited tests at Arecibo indicate that they are probably not excited at 20 MW ERP, but are strongly excited at 80 MW. The breakup of the HFPL in response to the formation of large-scale structures is often quite rapid giving rise to speculation that the final saturated state evolves quickly. Additional experimental tests at Arecibo are required to clarify these issues.



The presence of large-scale induced structures are evident in measurements of 3-m AFAI backscatter. Regions of enhanced scatter (scattering centers) occupy the HF-modified volume. The scattering centers appear to move at the same speed and in the same direction as the  $\mathbf{E} \times \mathbf{B}$  background ionospheric drift.

Langmuir turbulence measured in this late-time environment appears to reside in HF-induced field-aligned structures (Figure 11). In this environment, there is little doubt that ducted-wave propagation [Muldrew, 1978] plays an important role in the HFPL observations at Arecibo (Figures 12 and 13). The Langmuir turbulence appears to "paint" the large-scale structures and may serve as a useful diagnostic for monitoring the late-time plasma state. The presence of highly evolved packets of irregularities may greatly impact HF energy coupling to the plasma. This in turn could alter the development of microinstabilities and related electron acceleration processes. It is clear that our knowledge of HF modifications at intermediate and late times is incomplete and that in many cases the detailed plasma physics has yet to be defined.

Because the Arecibo HF facility underwent an upgrade following the CRRES rocket campaign in summer 1992, only a limited radar data set is currently available for studies of HF-accelerated electrons. Initial tests with the high-resolution coded long-pulse technique indicates that regions of electron acceleration dynamically change in the late time modification environment. This can arise if electrons are accelerated within discrete large scale structures of the type described above. In future experiments the evolution of the suprathermal electron spectrum will be measured in an initially cold background plasma. The present study verifies that the radar technique used is very powerful. It is sensitive to extremely low fluxes of suprathermal electrons and provides a method for monitoring accelerated electrons across the HF beam.

## 2.6 Studies with the Tromsø Superheater

As part of this project a limited investigation of the HF modification physics at auroral latitudes was performed. This study made use of a pre-existing data set acquired with the Tromsø upgraded HF facility (so-called superheater) in November 1990. The principal plasma diagnostics were the European Incoherent Scatter (EISCAT) UHF (933 MHz) and VHF (224 MHz) radars. A brief description of the principal results is presented below; more detailed explanations are found in *Djuth et al.* [1994].

The most remarkable feature of the Tromsø HFPL observations is a dramatic decrease in the height of the HF-induced turbulence at the highest powers available with the Tromsø superheater. The HF power level required for this to occur appears to be between ~270 and 540 MW ERP; the exact value is dependent on radio wave losses in the ionospheric *D* region. Because the time interval of the altitude decline (tens of seconds) matches expected time constants for the growth/decay of HF-induced electron temperature enhancements, it is appropriate to examine physical processes linked to elevated electron temperatures.



The altitude interval at which enhanced Langmuir oscillations and ion waves are detected with the EISCAT radars is dependent on radar frequency (i.e., measured plasma wavenumber), the altitude profile of electron density, and electron temperature. Linear parametric decay instability theory [e.g., *Perkins et al.*, 1974; *Fejer*, 1978, *Stubbe et al.*, 1992a] employs resonant frequency matching conditions together with the Bohm-Gross dispersion relationship to establish the excitation altitude. With the caviton physics described by *DuBois et al.* [1990], emphasis is placed on the critical layer ( $f_{HF}=f_{ep}$ , where  $f_{ep}$  is the electron plasma frequency) as a region of strong excitation; *DuBois et al.* [1991] suggest that parametric decay cascades coexist and interact with a caviton gas throughout most of the turbulence region. With either of the above approaches, the altitude of plasma line excitation is determined primarily by the electron density profile. The zone of excitation extends from the region of HF wave reflection downwards to altitudes where resonant Langmuir waves having large wavenumbers are heavily Landau damped. The width of this region is approximately 0.1 H, where H is the ionospheric scale length. For scale lengths appropriate for the observations presented above, the total excitation region is 3-4 km wide. The Bragg condition establishes the plasma wavenumber detected by a radar operating at a frequency,  $f_r$ . This wavenumber together with electron temperature and H determines the height of the radar backscatter. By applying the results of linear parametric instability theory to a smoothly stratified F layer, one obtains the following expression for the location of the Langmuir and ion waves

$$\Delta h = \frac{12 \kappa T_e f_r^2 H}{m_e c^2 (f_{HF})^2} , \quad (2)$$

where  $\Delta h$  is distance below the critical point,  $T_e$  is electron temperature,  $m_e$  is electron mass,  $\kappa$  is Boltzmann's constant, and  $c$  is the speed of light. Moreover, as discussed by *Stubbe et al.* [1992], it is also possible to obtain ion wave backscatter at a higher height because of ion nonlinear Landau damping cascades. This height is given by

$$\Delta h = \frac{3 \kappa T_e f_r^2 H}{m_e c^2 (f_{HF})^2} . \quad (3)$$

The observations reveal an altitude difference in the backscatter detected with the VHF and UHF radars at HF turn-on. The VHF ion line and plasma line echoes are located at greater altitudes than the UHF returns. This is consistent with the predictions of (2). In addition, strong UHF ion lines are seen at higher altitudes where the UHF plasma line is either very weak or totally absent. Ion waves produced by nonlinear Landau damping cascades may contribute to the ion line



echoes at higher heights as indicated by (3). From (2), it is clear that the height of the resonantly excited turbulence can decrease because of large increases in  $T_e$  and/or  $H$ . A large increase in  $T_e$  would lower the excitation height, but the magnitude of the height change should be radar frequency dependent. HFPL measurements show that this is not the case. Echoes simultaneously measured with the VHF and UHF radars descend in altitude by approximately the same amount (3 km). Similar arguments can be made with respect to increases in  $H$  for a critical surface that is fixed in altitude.

A more viable explanation is that the altitude decline is brought about by changes in the electron density profile that lower the height of the critical layer. This could occur if plasma were forced downwards from the region of radio wave reflection or if significant amounts of plasma were pushed upwards from lower altitudes. However, if thermal forcing is invoked, it is difficult to understand how a great deal of plasma can be redistributed over spatial scales of 3 km, given our current understanding of electron thermal gradients in the HF-modified volume and their spatial derivative along geomagnetic field lines. Thermal conduction tends to smooth out the HF-enhanced electron temperature profile [e.g., Mantas *et al.*, 1981] making significant plasma transport difficult to achieve and maintain over relatively small spatial scales. However, electron-temperature dependent changes in plasma recombination rates may allow the critical layer to move downwards. In particular, in the lower portion of the  $F$  region (below ~220 km altitude) increased  $T_e$  will decrease the dissociative recombination rate of molecular ions [e.g., Kolesnik, 1982]. This rate is inversely proportional to  $T_e$ . Thus, the background electron density is expected to increase in response to electron temperature enhancements. This could lead to a lowering of the critical layer over thermal time scales, which is consistent with the observations. Additional studies are needed to test this hypothesis. In particular, the altitude decrease should be absent when the modifying HF wave reflects at altitudes greater than ~250 km where fewer molecular ions are present. The current data base consists of many observations made under conditions of relatively low radio wave absorption in the  $D$ -region, but the range of HF reflection heights is limited to altitudes between 200 and 230 km. The change in the altitude of the resonantly excited waves is a nonlinear function of transmitted HF power. This may indicate that an instability threshold has been exceeded in the  $F$  region giving rise to an additional heat source in the plasma.

Although we have focused on thermal effects in the plasma, we cannot rule out the possibility that other physical processes may be responsible for the dramatic decline in the altitude of the induced plasma turbulence. Additional experimental observations focusing on changes in background plasma parameters during the HF heating period would greatly facilitate interpretation of the present results.



## 2.7 Summary of Tromsø Results

Langmuir/ion turbulence excited with the upgraded high-power (1.2 GW effective radiated power) HF heating facility at Tromsø, Norway was measured with the EISCAT VHF and UHF incoherent scatter radars. In this initial work, we focused on the altitudinal development of the turbulence observed at the highest HF power levels available. Quite remarkably, the observed plasma turbulence plunges downwards in altitude over time scales of tens of seconds following HF beam turn-on; the bottom altitude is generally reached after about 30 seconds. This phenomenon has a well-defined HF power threshold. It is most likely caused by changes in the electron density profile brought about by HF heating of the electron gas. If this is the case, then the heat source must be nonlinearly dependent on HF power. Overall, the characteristics of the Tromsø turbulence are quite distinctive when compared to similar high-resolution measurements made at Arecibo Observatory, Puerto Rico. After HF transmissions have been made for tens of seconds at Tromsø, billowing altitude structures are often seen in sharp contrast to layers of turbulence observed at Arecibo. A detailed discussion of this work is provided in *Djuth et al.* [1994]

## 3. Measurements of Missile Plumes

The missile plume and the rocket acceleration curve provide important information for sensing the launch phase of a theater ballistic missile. For effective target acquisition it is necessary to determine the radar cross section and spectral characteristics of the plume backscatter and assess this in reference to the signature of the missile body.

### 3.1 Introduction

Prior to the present study, only one limited measurement of this nature had been made. In the present project, a more complete data set was secured using the HF Active Auroral Research Program (HAARP) 49.92 MHz VHF radar. Particular emphasis was placed on monitoring the plume signature from liftoff through engine cutoff in the upper atmosphere. This information was used to test several existing models describing the plume chemistry, verify computer simulation capabilities, and identify problems/deficiencies in the model results.

Because of the absence of a comprehensive data base, it is difficult to fully characterize the plume physics. Currently, it is believed that the highest velocity gases are generated close to the missile. These gases are shielded from most radar diagnostics because of the surrounding overdense plasma. Beyond the plasma critical surface there exists a large turbulent region containing partially ionized plasma. Most radars that operate in the VHF to UHF range detect incoherent backscatter from this part of the plume.

Complex numerical codes designed to simulate the plume composition, temperature/velocity and plasma content generally consist of three elements. The first addresses the combustion, thermodynamics, and fluid dynamics of gases at the rocket motor and nozzle. In



effect, these reactions generate the source plasma that initializes the latter two stages of the code. The second calculational element addresses issues related to the outer plume velocity field, mixing layer combustion and growth, and chemical reactions in the ionized, collisional plasma. Finally, the interaction of an electromagnetic wave with the plume is calculated taking into account incoherent scattering from the hot randomly moving electrons in the highly collisional plume. Coherent backscatter from turbulent structures moving with the missile is not fully taken into account in most models. The important end items produced by the codes are the absolute radar cross section of the plume and its corresponding Doppler spectrum.

### **3.2 Lance Plume Investigation at White Sands Missile Range**

In February 1993, the scope of this project was altered to include radar field support and radar data analyses for VHF (49.92 MHz) radar studies at White Sands Missile Range, New Mexico. The experiments at White Sands were aimed at determining the radar signature of missile plumes. Particular attention was focused on collecting data during the initial launch blast and the succeeding boost phase. Such measurements provide valuable inputs for models of the scattering phenomenology.

A field site survey was conducted at the White Sands Missile Range to establish a radar location that was shielded from clutter arising from the local San Andres Mountains. This was accomplished by nestling the radar in Sweetwater Canyon. The height of the radar site was 1710 m MSL and the altitude of the RAMS launch facility was at 1320 m MSL. With this arrangement, the range to the launch pad was 9.3 km, and the elevation angle was  $-2.5^\circ$ . The radar field-of-view to the RAMS launch site was unobstructed. However, the radar line-of-sight to RAMS was only  $\sim 15$  m above a ridge (1630 m MSL) 1.5 km away. The transmitted signal therefore encountered diffraction/multipath en route to the launch site. However, wave propagation analyses indicated that a modest amount of beam focusing occurred at the launch site. Thus, the ridge was expected to slightly improve radar sensitivity at the launch site.

Two field campaigns were conducted at White Sands Missile range in an effort to monitor a single launch of a Lance missile (GM-52C). The Lance is a liquid-fueled, scud-like missile. It served as a target for the Loral Vought Systems' Extended Range Interceptor (ERINT). The actual launch occurred during the second campaign. From the perspective of the overall Lance/ERINT program, the Lance missile was only a target. Operationally, plume radar measurements were secondary to the principal objective of the launch. The first campaign started on March 25, 1993 and extended through April 9, 1993. Because of difficulties with the ERINT intercept vehicle, the first planned launch scheduled for April 8 was delayed. Consequently, no plume data were acquired during the first campaign. Nevertheless, the first campaign provided a test bed for the optimization of radar operations and served to validate the projected VHF radar sensitivity.



The first campaign established the overall radar system configuration. The radar antenna consisted of an array of four six-element yagi antennas. The yagi antennas were purchased from DX Engineering; Model 6DX-6 was optimized for operations at 49.92 MHz. Two yagis each were mounted on two 60-foot poles. The separation between each yagi element within the symmetric 2 x 2 array was 1.5 radar wavelengths  $\lambda$ , where  $\lambda = \sim 6$  m. Antenna cabling consisted of four balun (one for each yagi), two quarter-wave impedance transformers, and two grounding stubs connected to a single grounding rod. The antenna configuration is illustrated in Figure 15. This antenna system had a peak gain of  $\sim 21$  dBi.

The HAARP 49.92 MHz radar was conservatively operated at 25 kW peak power. An uncoded radar pulse 10  $\mu$ s in duration was employed yielding a range resolution of 1.5 km. The interpulse period (IPP) was set to a relatively large value (1.2 ms) to avoid aliased clutter from the Sacramento Mountains ( $\sim 60$ -90 km downrange) and airplane echoes arising from commercial traffic out of El Paso Airport. As a result the full bandwidth for pulse-to-pulse spectral analyses was 833 Hz. The complex (in-phase and quadrature) radar receiver channels each had a bandwidth of  $\sim 100$  kHz, thereby producing a 200 kHz bandpass at baseband. Typically, the backscatter from 256 pulses was used to perform an FFT spectral analyses. The FFT integration period was  $\sim 0.3$  s, and the associated Doppler resolution was  $\sim 10$  m/s.

The principal data acquisition system was the 16-bit Stimulated Electromagnetic Emissions processor built by Geospace Research, Inc. for the HAARP project. Radar receiver voltages were continuously digitized at the rate of one complex voltage pair every 8  $\mu$ s. Absolute time was recorded along with the one pulse per second "tick" from a time code generator. This time code generator was synchronized with the White Sands phase-locked time standard through a hardwired IRIG-B connection. Thus, absolute time was known to 8  $\mu$ s resolution. For backup purposes, all radar data were recorded on analog tape and on two additional 8-bit radar processors.

During the first campaign the measurement sensitivity was established, and a calibration study for establishing absolute radar cross section was initiated. In the White Sands tests, the radar system sensitivity was determined by the stability of the clutter background. Although this clutter contribution was greatly reduced at radar ranges of interest for the measurements, strong clutter was nevertheless present in the data. This is the inevitable situation when a radar beam is directed at a launch complex and the surrounding terrain. Figure 16 shows mean radar clutter versus range and the residual after mean clutter subtraction. The residual clutter is quite small for measurements of this type. The clutter subtraction can never be perfect because the clutter amplitude changes slightly from pulse to pulse owing to variations in radio phase paths to "hard targets." These variations are caused by fluctuations in the refractive index of air. Because of the dryness of the air at White Sands, phase path changes are small. As a result, the contribution of



# Yagi Antenna Array Deployed For Missile Plume Investigation

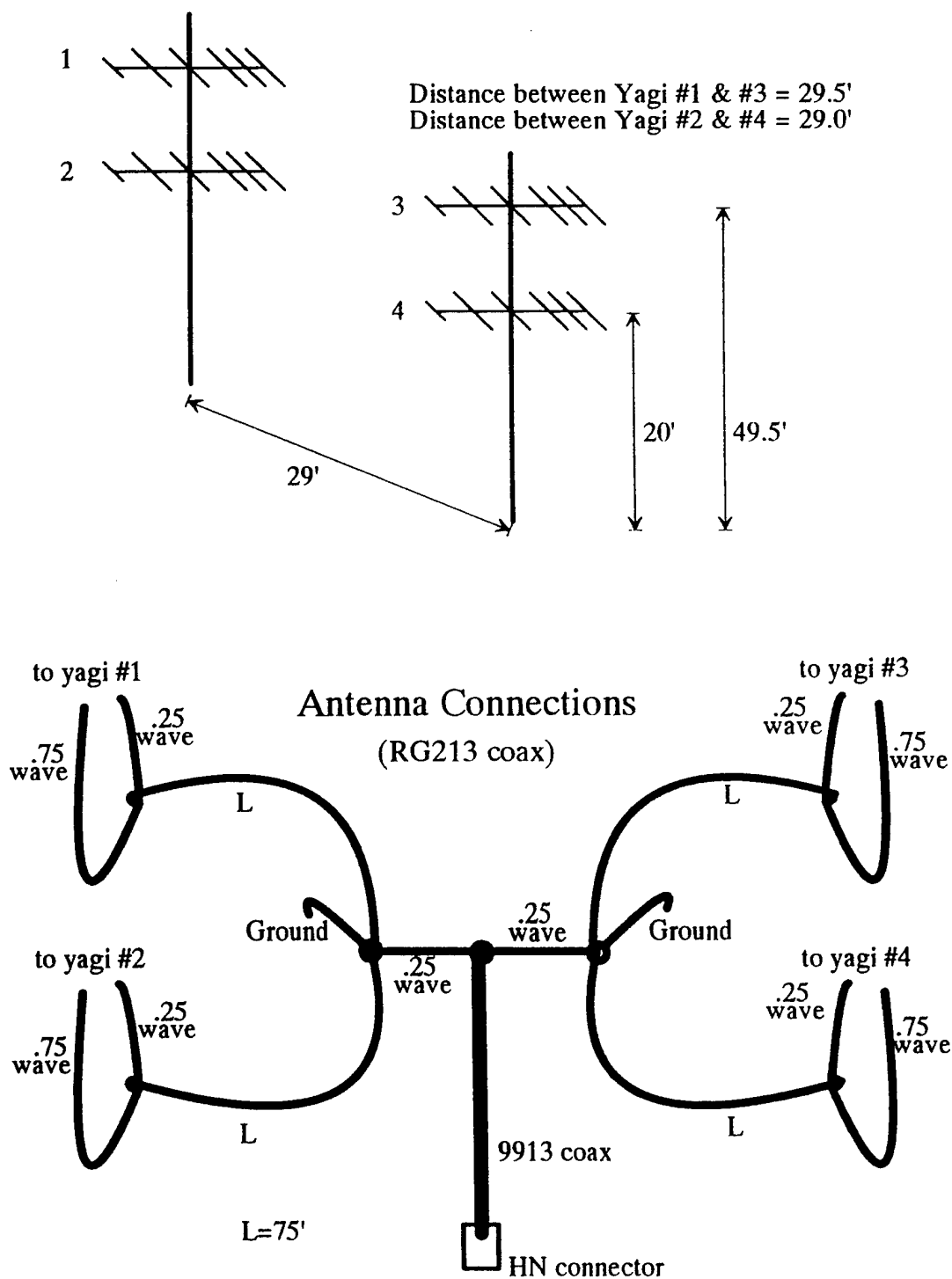


Figure 15



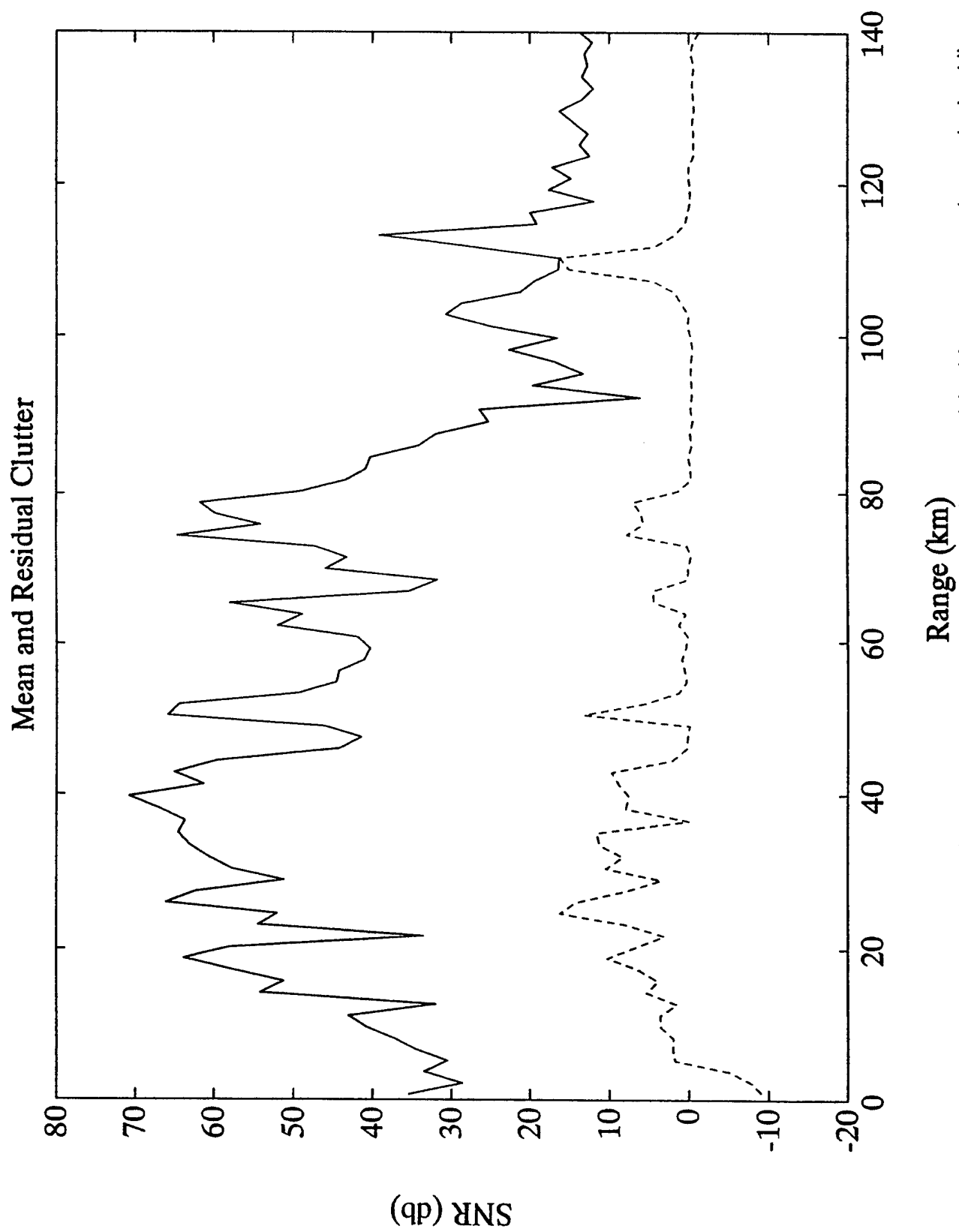


Figure 16. The mean clutter is shown as a continuous line; the clutter residual is represented as a dashed line.



atmospheric fluctuations to the residual clutter is rather small. Clutter variations caused by pulse-to-pulse fluctuations in transmitted radar power were found to be extremely small (roughly -9 dB SNR in Figure 16). Note that at the range to the launch pad (9.3 km) the residual clutter is particularly low.

Two-meter diameter jimspheres (metallic-coated balloons) were used to calibrate the radar for absolute cross section. At 49.92 MHz the cross section of the jimsphere is  $11.3 \text{ m}^2$ . This is a relatively large cross section yielding significant (30-50 dB) signal-to-noise ratios near the launch complex. Three jimsphere releases were executed during the first campaign. One such release is illustrated in Figure 17. In this display, time is reference to the balloon release, and backscatter power is expressed as signal-to-noise ratio (dB). The results of Figure 17 were acquired at the range to the missile launch pad (9.3 km). Two views of the data on different temporal scales are provided. The jimspheres are independently tracked with an S-band radar, so their absolute positions are known throughout the calibration period. The ascent rate of a jimsphere is approximately 1000-1100 ft/min. The calibration balloons were routinely tracked to 20,000 ft over a period of ~20 min.

Calibration measurements were also made with an airplane operated by MIT/Lincoln Laboratories to map out the radar beam in azimuth and elevation angle. The Lincoln Lab measurements provided relative power data across the beam. These observations indicated that there was a peak in the antenna pattern at  $\sim 1.7^\circ$  elevation angle along the azimuthal radar line-of-sight to the RAM launch facility, or about 2000 ft above the launch area. The elevation angle of the launch pad as observed from the radar site was  $-2.5^\circ$ . From the jimsphere calibrations, it became clear that there was a major antenna lobe approximately 200 ft above the launch area, or at a  $-2.1^\circ$  elevation angle. This is consistent with the results of several low passes over the launch site with the Lincoln Laboratory airplane. Azimuth maps of the radar beam made with the plane revealed that the main azimuthal lobe was directed at the launch site as expected, but that there was also a second azimuthal lobe having 1-2 dB less gain  $\sim 28^\circ$  east of the launch site. This second lobe did not materially affect the radar measurements.

Analyses of the jimsphere results indicated that the theoretically predicted antenna pattern was reasonably accurate. Modest (6 dB) fading was on occasion observed as the jimsphere rose through the first and second antenna lobes in elevation angle. These two lobes are evident in Figure 17 at 11.5 s and 90 s relative to the balloon release. This is attributed to multi-path interference from unspecified scatterers within the radar range cell. A closer look at the signal characteristics is provided in Figure 18. In this display, signal power is shown on an expanded temporal scale (top panel) and the quadrature, or imaginary, voltage component of the baseband signal is plotted in the lower panel. Frequency modulation in the (radial) Doppler shift of the balloon echo is evident in the lower plot. The modulation cycle appears to be locked to the fading



Jimsphere Release for Radar Calibration: 7 April 1993, 10:00 MST

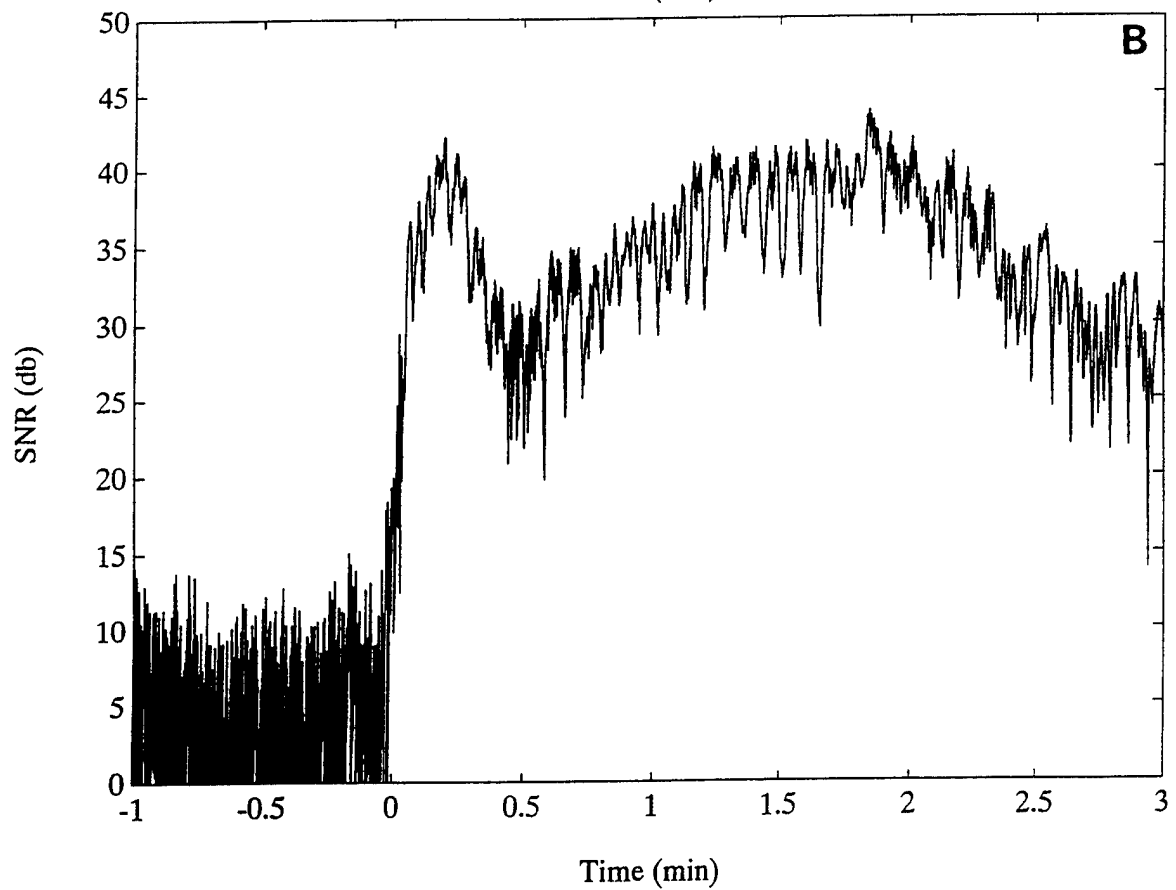
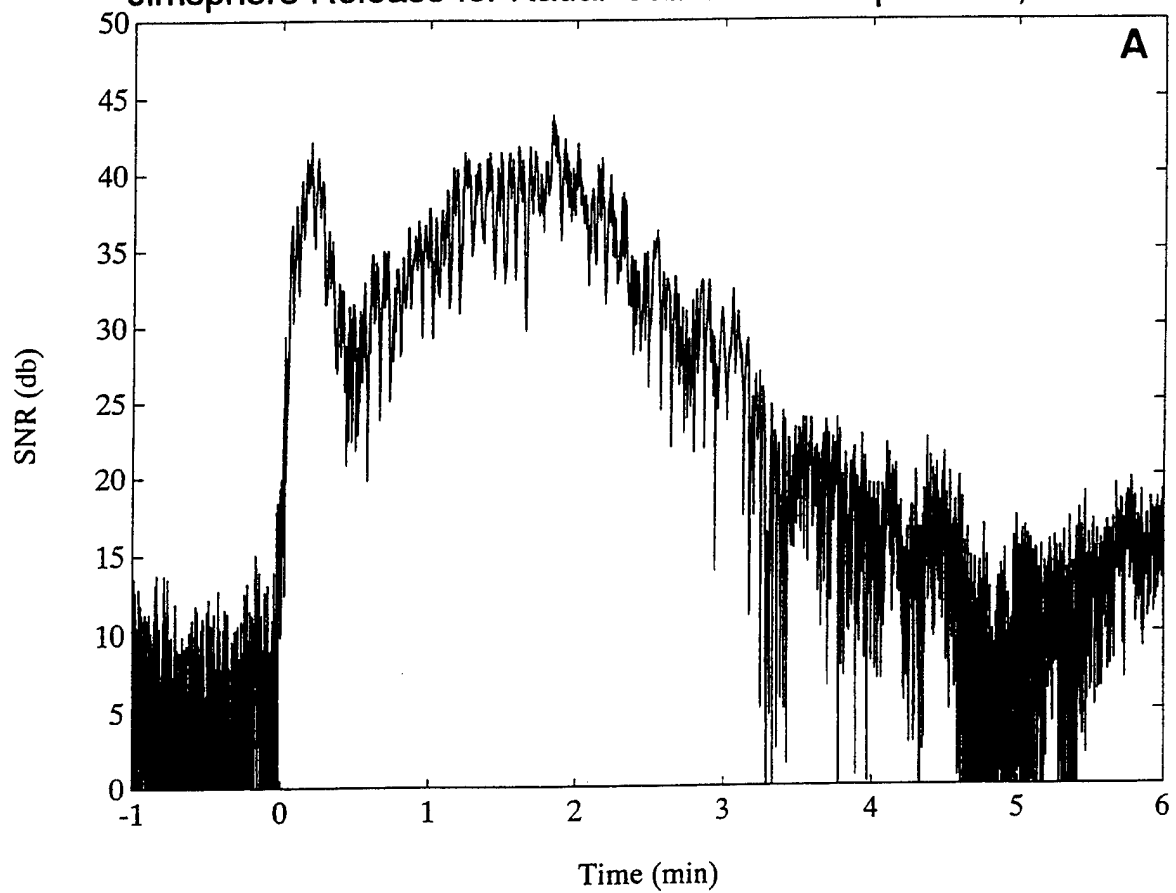


Figure 17



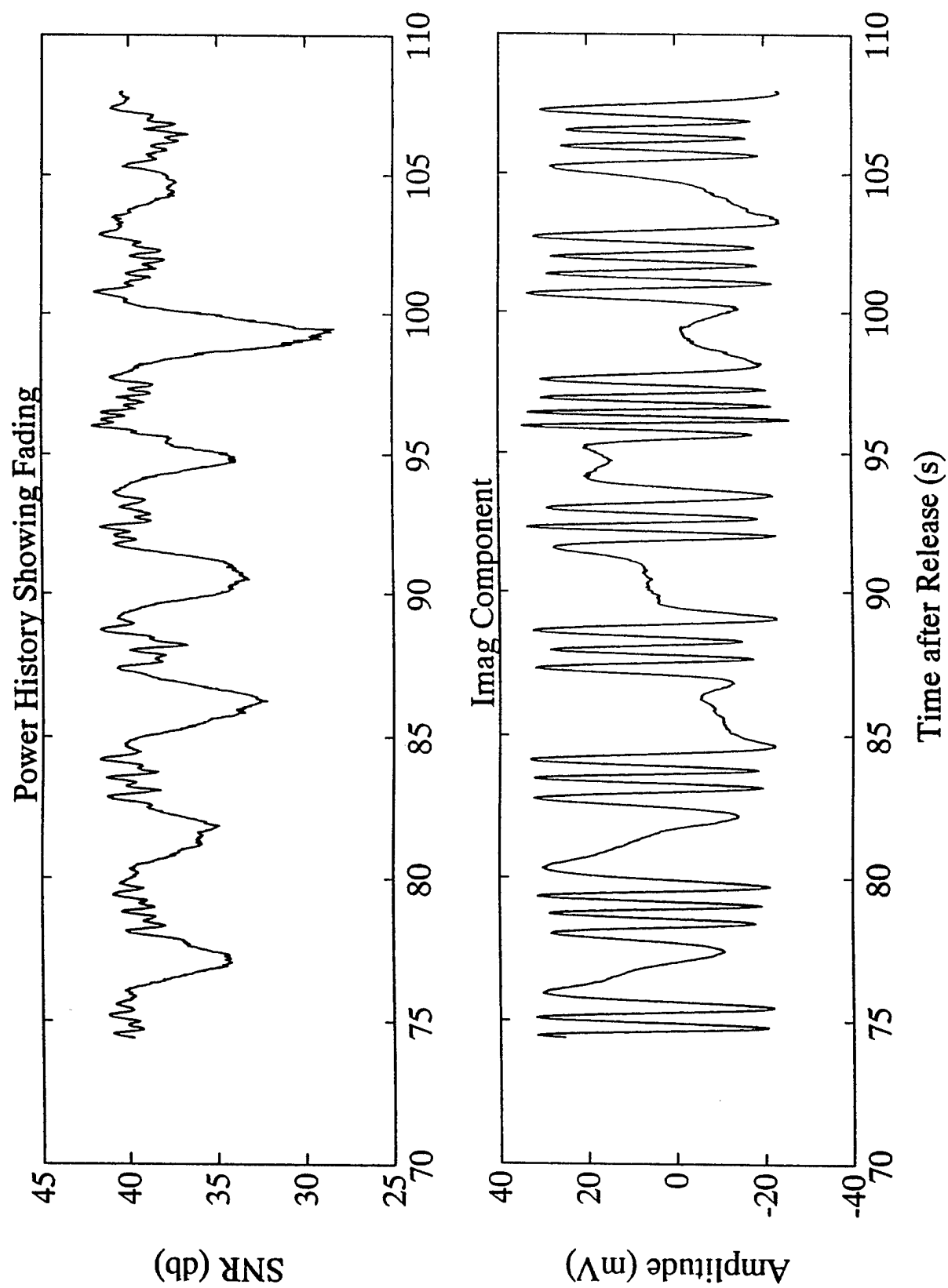


Figure 18. Correlation between jimsphere amplitude fading and the frequency of the imaginary voltage component.



period. The frequency modulation phenomenon may be attributable to irregular horizontal balloon motions brought about by vortex shedding of air surrounding the balloon. However, the reason why the amplitude fading is locked to the frequency modulation is not well understood.

Commercial aircraft traffic out of El Paso Airport was used to verify radar performance with respect to a rapidly moving hard target. The top panel of Figure 19 shows the backscatter power from an airplane expressed as a signal-to-noise ratio versus time. The phase history of the echo is provided in the center panel. At the bottom, the spectral signature of the plane is presented. Notice that the frequency spectrum is "clean" in the sense that modulation products are absent.

After the first campaign, several new launch dates were supplied to the plume radar participants on rather short notice. This gave rise to several aborted attempts to re-deploy the VHF radar. The first aborted attempt occurred during the period of April 21, 1993 through April 22, 1993; the second attempt took place April 29, 1993 through April 30, 1993. In each case, equipment and personnel were sent out to White Sands Missile Range.

The second field campaign occurred during the period June 1, 1993 through June 10, 1993. During this deployment, the VHF radar system was optimized for Lance plume detection. Moreover, an aggressive calibration program was initiated that included ten jimsphere balloon releases and a complete system temperature analysis. This campaign culminated with the launch of the Lance missile at 09:42:48 MST on June 8, 1993.

An overview of the rocket and plume spectra versus time is presented in Figure 20. Time is referenced to the launch of the Lance missile, and signal strength is expressed as a signal-to-noise ratio in dB. Spectra were calculated using pulse-to-pulse FFT analyses of 256 consecutive radar pulses. A four-term Blackman-Harris window was used with the FFT. The aliased bandwidth of the spectra is 833.3 Hz, and each Fourier cell is 3.25 Hz in width. This corresponds to a Doppler spread of  $\sim 10$  m/s. In Figure 20a, data acquired at the launch range of 9.3 km are presented. The dark streak that moves downward with time is the echo of the Lance missile. Weak broadband signals observed near 1.0 s and 2.9 s are caused by the Lance plume. During these periods, the missile was passing through the first and second antenna lobes in elevation angle, respectively. The weak plume echoes have a positive Doppler shift relative to the missile because the plume gases are flowing outwards toward the radar. An expanded view of these observations is presented in Figure 20b. Finally, Figure 20c shows similar data acquired in the adjacent range cell (10.5 km). Notice the curve in the Lance Doppler history near 5 s relative time. This is caused by deceleration of the Lance missile at the main engine cutoff.

The spectrum of the Lance vehicle and plume recorded near 1.0 s after launch is shown in Figure 21. The data segment covers the period 1.03 -1.34 s, which contains one of two plume



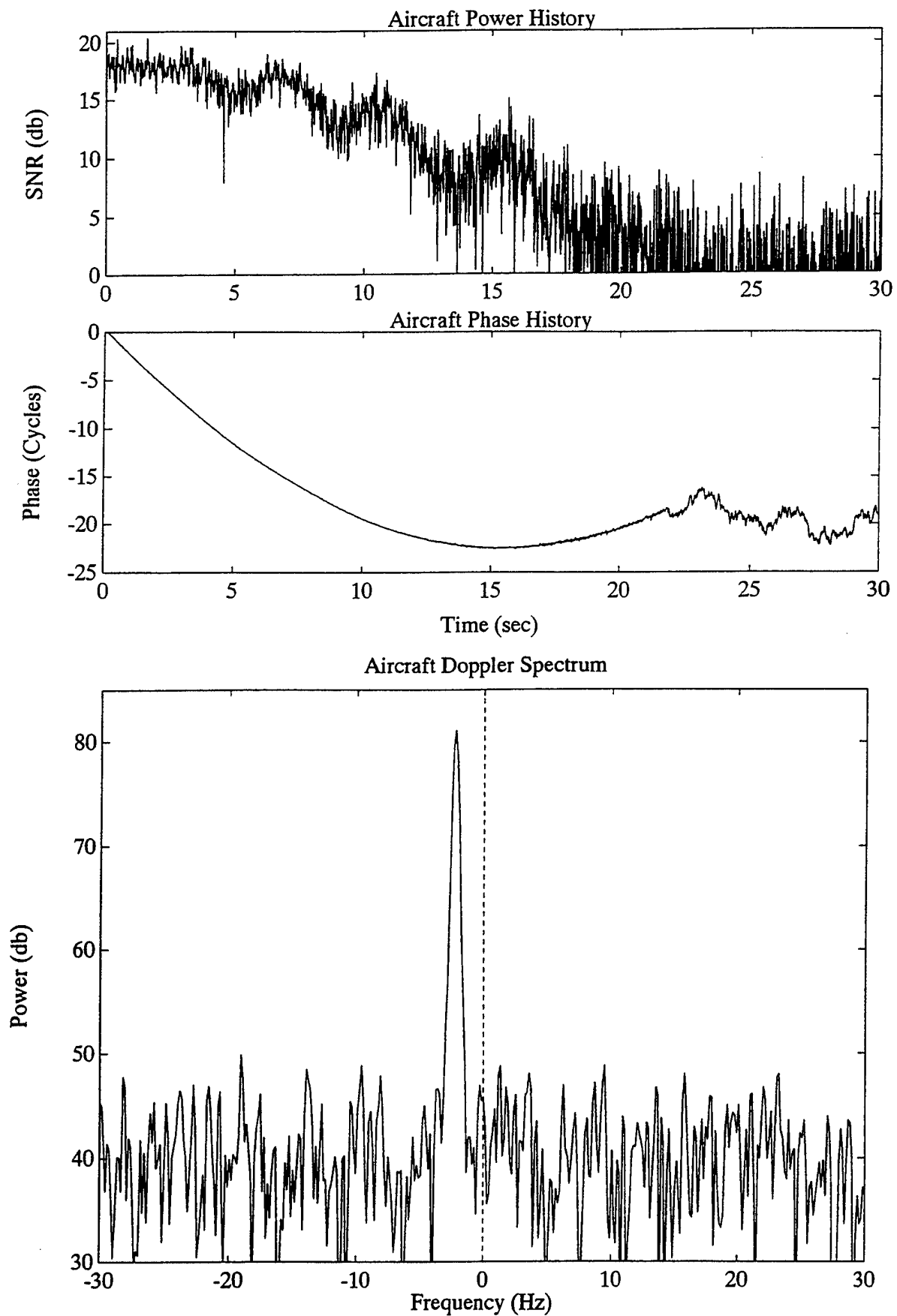


Figure 19. Commercial aircraft monitored with the VHF radar.



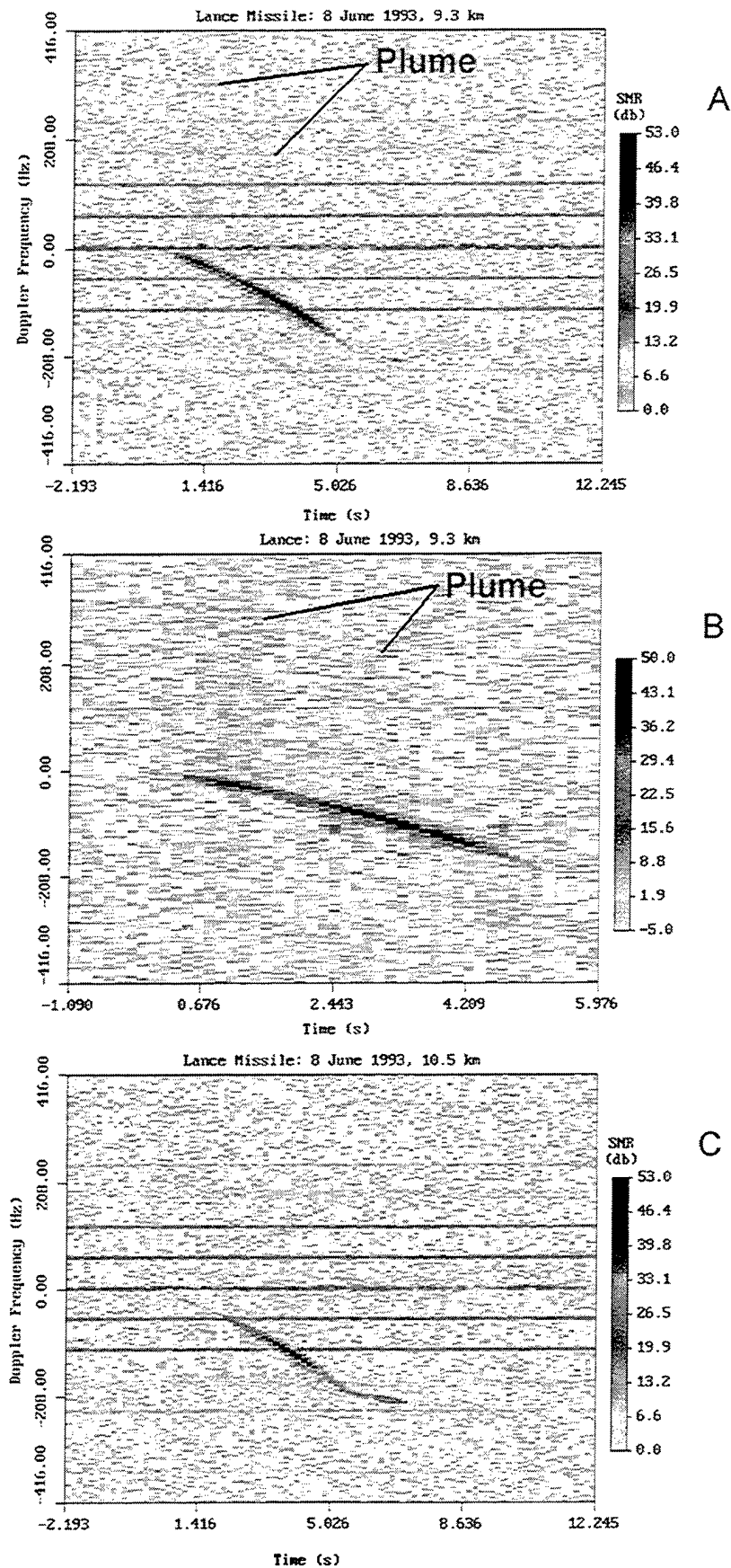


Figure 20. Radar signature of the Lance missile body and plume at 9.3 km range (Panel A), expanded view of Panel A highlighting plume echoes (Panel B), and data acquired at 10.5 km range (Panel C).



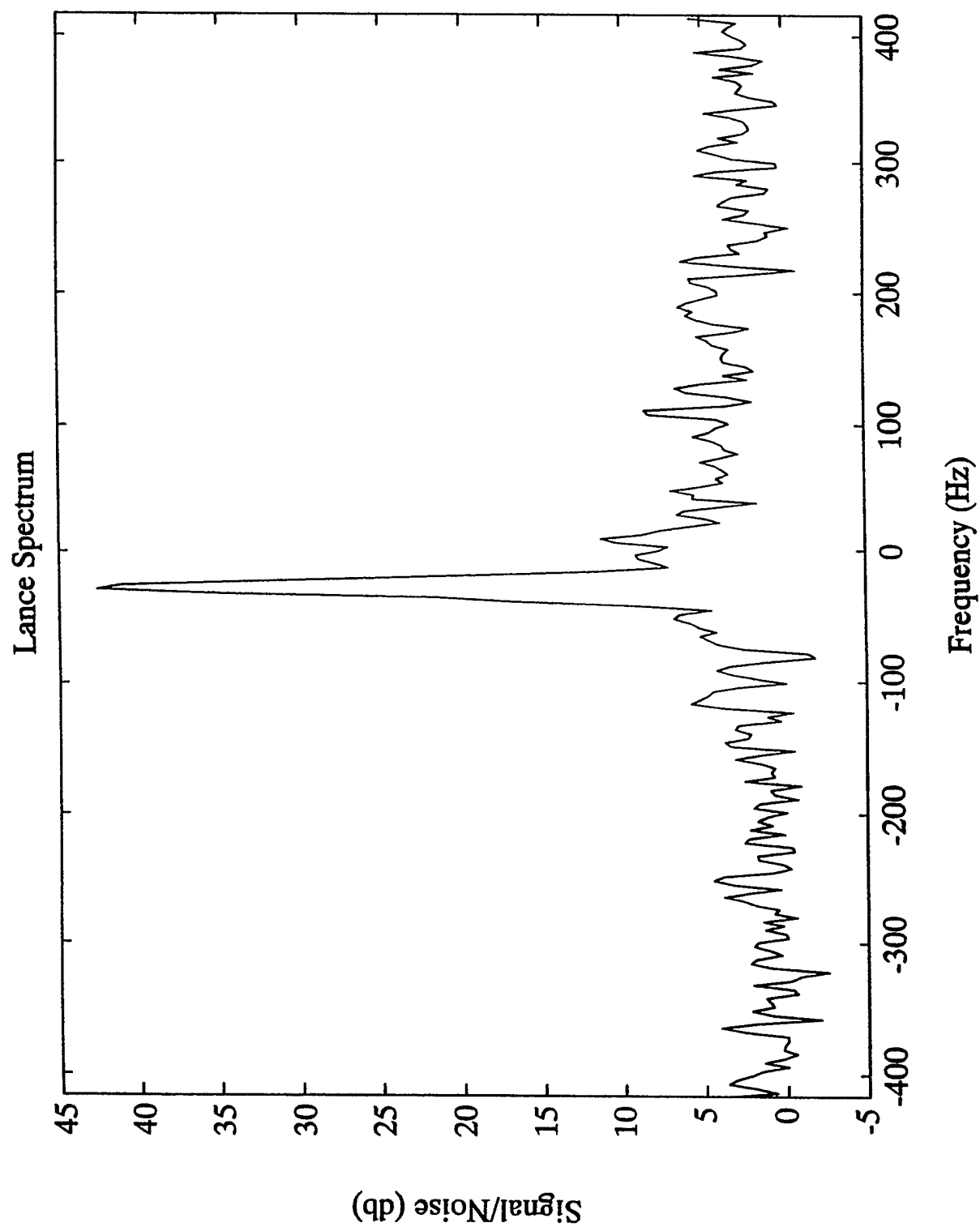


Figure 21. Spectrum containing backscatter from Lance missile and broadband plume measured ~1 s after launch.



echoes. The figure shows that the anticipated broadband plume signature is approximately 42 dB smaller than the coherent backscatter from the Lance vehicle at the time of observation.

Wideband Doppler spectra were processed during the period when the Lance missile was in the field-of-view of the radar for a period of ~12 s following the launch. During this period the Lance missile crossed several radar range gates, and appropriate measures had to be taken to ensure that the temporal history of the total cross section was adequately represented. Particular attention was paid to the weighting of backscatter power when the missile crossed from one range cell to the next. Range cells were crossed near 4.2, 5.5 s and 8 s after the launch. The plume backscatter was most prominent during the periods 0.6-1.8 s and 2.4-3.9 s after launch as the missile crossed the two main elevation lobes of the radar beam. These observations yielded plume echoes that were 42-45 dB smaller than the cross section of the Lance vehicle. Weaker backscatter signals from the plume were also detected during the first 0.5 seconds following launch.

There was speculation by many of the investigators that enhanced echoes from specular backscatter may arise because of the plume. Such echoes are usually indistinguishable in the time/frequency domain from backscatter from the missile body itself. To determine whether such an effect exists, the flight of the missile was followed through the transition point of main engine cutoff and sustainer engine initiation. There is a substantial decrease in the size of the missile plume at this transition. The strategy was to look for abrupt changes in the backscatter cross section at this event.

The main engine cutoff time could be accurately established from the data because the radial Doppler velocity of the target is continuously tracked, and a deceleration curve is generated by engine cutoff. Figure 22 illustrates the radial velocity curve determined from the VHF radar and from independent range measurements. The continuous line represents the VHF radar observations; the shaded region indicates the maximum error bars of the measurements. These error bars are determined by the distribution of the Lance echo across multiple FFT cells. The dashed line in Figure 22 is a plot of radial velocity determined by White Sands tracking radars. Overall, there is very good agreement between the two measurements of radial velocity. Notice the break in the velocity curve near 5.3 s after liftoff. This corresponds to the time of main engine cutoff. The deceleration of the vehicle at this time is clearly evident in the data.

A plot of (range)<sup>4</sup>-corrected backscatter power from the Lance is provided in Figure 23. In the top panel, power is plotted versus time after liftoff, whereas in the lower panel time has been converted to elevation angle to the target. The peaks in the antenna pattern near -2° and +2° elevation are reflected in these plots. Superimposed on the antenna pattern are large changes in the vehicle cross section as the missile pitches and rolls in flight. The dotted vertical line in the upper panels indicates the time of main engine shutdown. Unfortunately, this shut down occurred



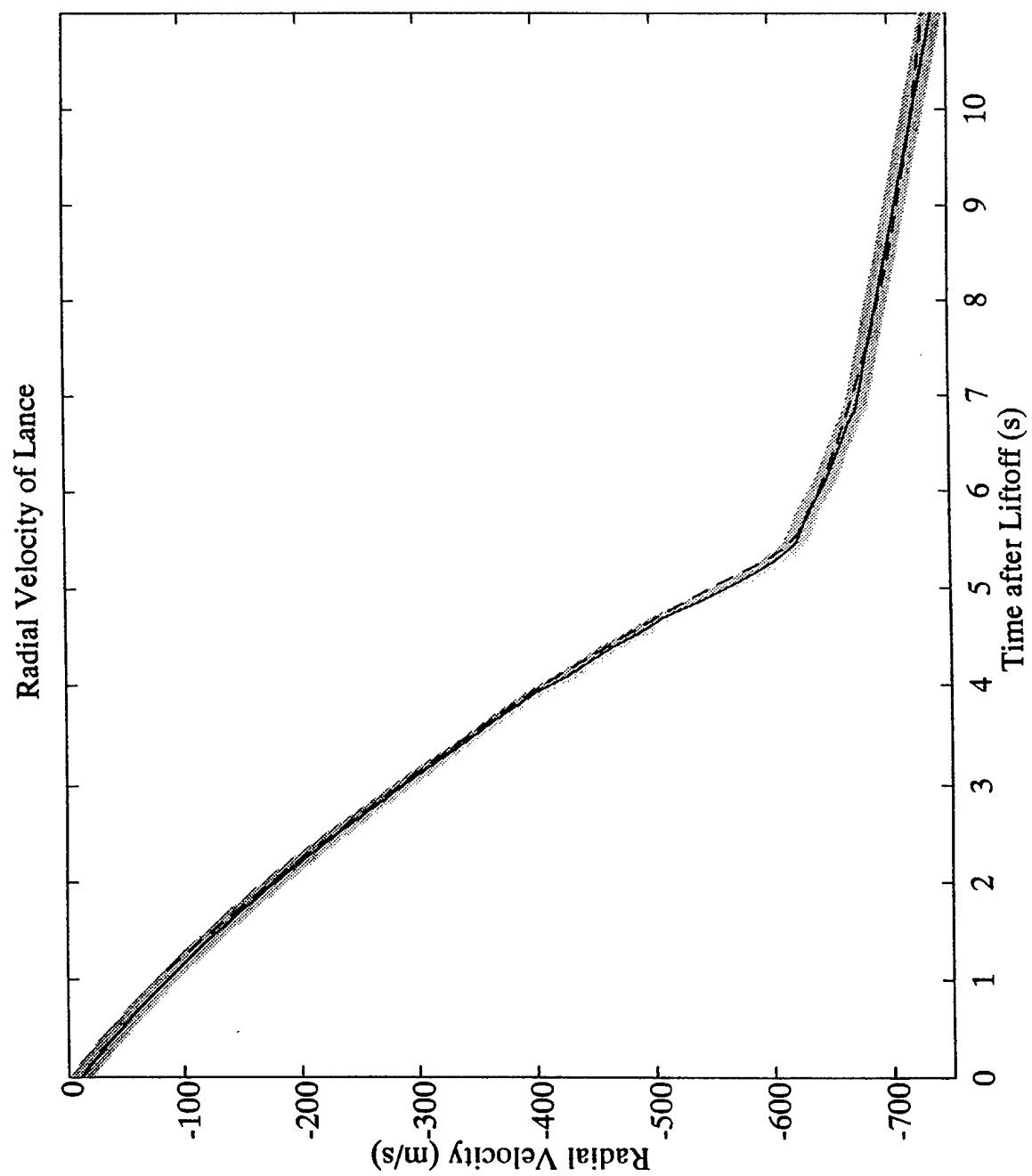
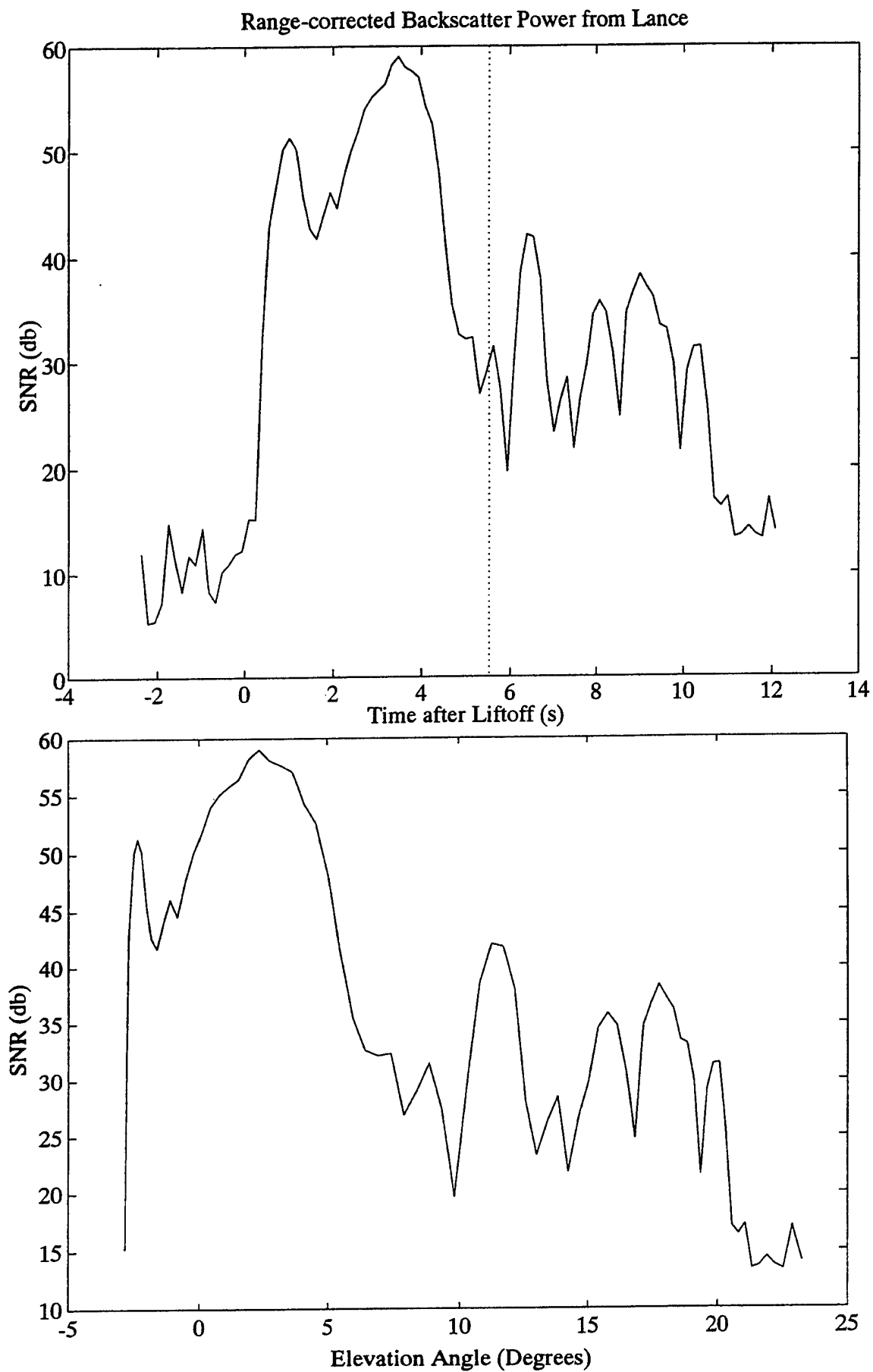


Figure 22





**Figure 23**



while the Lance was in a null of the antenna pattern, and the corresponding results are somewhat ambiguous. It is difficult to separate out changes in Lance cross section brought about by changes in vehicle orientation and antenna pattern from a reduction in cross section brought about by absence of a specular return from the plume. It would appear that the plume does not contribute a large specular component to the backscatter return.

It was suggested that there might be a plume-induced change in the missile cross section at early times when there is a change in aspect angle of the missile. Because the observed dip in radar backscatter near 2 s after launch was somewhat less than that predicted, additional attention was paid to understanding the changes in absolute cross section versus time after launch. At this point in the flight, the radar antenna pattern itself makes the largest contribution to the temporal profile of radar backscatter. Consequently, uncertainties in this profile are limited by our knowledge of the antenna pattern. Comparisons between the Lance backscatter versus elevation angle and the measured antenna pattern indicate that the upper limit on changes in aspect-sensitive backscatter from the plume is 1-2 dB.

An assessment of absolute plume cross section required that jimsphere balloon data be carefully analyzed to separate out the balloon contribution from the ground clutter. Both frequency-domain and time-domain analyses were developed for this purpose. Consistency was achieved between these two analysis approaches, giving us confidence that the ground clutter problem had been properly addressed. Data from the four best jimsphere launches containing minimal amounts of time-varying clutter were selected for this study. Temporal profiles of radar backscatter from these jimspheres are presented in Figure 24. Time is referenced to the release of the jimsphere. All measurements shown were made at a range of 9.3 km. All balloon observations contain double humped scattering profiles consistent with the above discussions of the elevation lobes in the antenna pattern. In addition, the backscatter in panels A and D exhibit periodic fading at a level of about 6 dB. This is similar to the effect discussed in connection with Figures 17 and 18. Notice that the observations of panel C were made just 90 min before those of Panel D, yet there is no sign of periodic fading in panel C. This behavior adds to the curious nature of this phenomenon.

Although the flight paths of the jimspheres in Figure 24 varied somewhat from one release to the next, the paths did not change enough to warrant the large variations in radar signal-to-noise ratio (SNR) evident in the four panels. Indeed, the measured backscatter power from the jimsphere could vary by as much as two orders of magnitude in balloon flights that took similar (but not identical) ascent routes. In several instances, the backscatter power varied 10-20 dB among two jimspheres released 90 minutes apart. The data in panels C and D illustrate this effect. Only recently have we come to realize that the jimspheres used in this calibration exercise (and others) were quite old. The metallic coating on the jimspheres was degrading by varying amounts



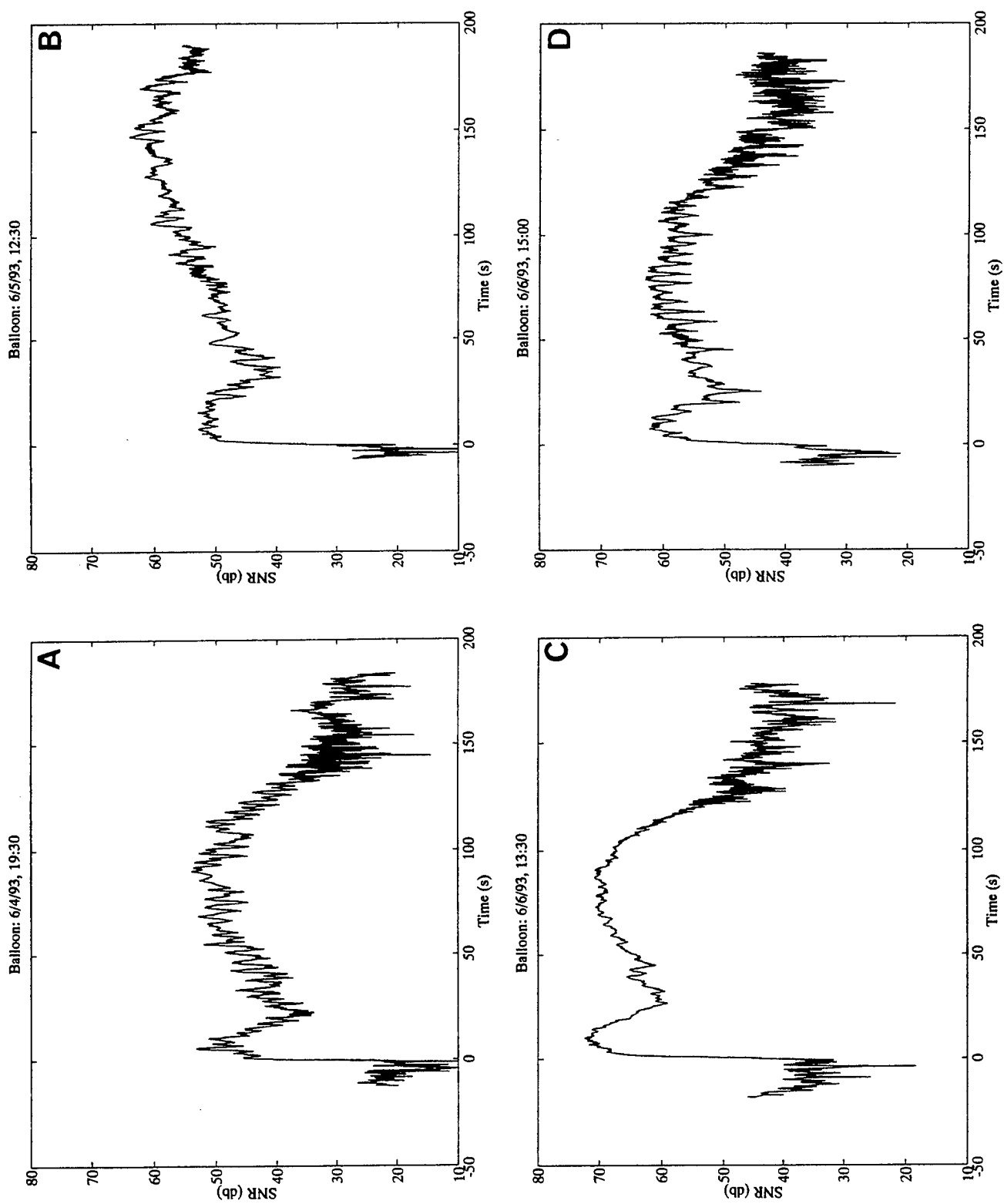


Figure 24. Temporal profiles of radar backscatter from four jimsphere releases during the second Lance campaign.



on different balloons. This reduces the balloon cross section, and probably accounts for the variations in SNR in Figure 24. In light of this, data from panel C were selected for calibration purposes. This jimsphere release had the largest SNR, and therefore it is assumed that the metallic coating on the balloon was more or less intact.

One can solve the radar equation for target cross section, where the target is the jimsphere of Figure 24c. This yields

$$\sigma = \frac{\text{SNR} (4\pi)^3 R^4 L A (\kappa T B)}{G^2 \lambda^2 P_t}, \quad (4)$$

where  $\sigma$  is cross section ( $\text{m}^2$ ), SNR is signal-to-noise ratio,  $R$  is range,  $L$  is the two-way transmission loss,  $A$  is the noise aliasing factor,  $\kappa$  is Boltzmann's constant,  $T$  is system temperature,  $B$  is the bandwidth of the FFT cell,  $G$  is antenna gain,  $\lambda$  is radar wavelength, and  $P_t$  is peak transmitter power. For SNR=71.5 dB (measured at the first peak in Figure 24c),  $R=9.3$  km (known),  $L=4$  dB (measured),  $A=300$  (measured),  $T=12,000$  K (measured),  $B=1.63$  Hz (known),  $G=18.1$  dBi (deduced),  $\lambda=6.01$  m (known), and  $P_t=25$  kW (estimated), one obtains a cross section for a 2-m sphere of 10.5 dBsm. In effect (4) can be solved for the product of  $(G^2 \times P_t)$ . We have estimated  $P_t=25$  kW based on measurements with a directional coupler, leaving  $G$  as the only deduced parameter.

Using the above parameters, one can readily solve for the total Lance hard target/coherent plume scatter cross section. At the time of the first wideband plume echo ( $t=1.0$  s) the missile was passing through the first antenna lobe in elevation angle ( $\sim 200$  ft above the launch site). The measured SNR was 51 dB (Figure 23). This corresponds to the first peak in the jimsphere calibration data. One obtains  $\sigma = -10.0$  dBsm for the hard Lance cross section. The second plume echo occurred while the missile was crossing the second antenna lobe in elevation angle ( $t=2.9$  s). On the basis of the Lincoln Laboratory airplane calibration data, we assume that the antenna gain is 3 dB greater than the value calculated for the first lobe ( $G=21.1$  instead of 18.1) and observe that the Lance SNR = 58 dB. This yields  $\sigma = -9.0$  dBsm. The deduced value of  $\sigma$  at  $t=1.0$  s is close to the model prediction of Scientific Applications International Corporation (SAIC), -7.5 dBsm; at  $t=2.9$  s the SAIC model value is -10.5 dBsm, which again is in reasonable agreement with the deduced value. Differences between model values and deduced cross sections are attributable to uncertainties in the radar antenna pattern and perhaps to slight differences between the expected and actual orientation of the Lance missile.

The radar parameters discussed above can be applied to the broadband plume echoes to provide estimates of absolute plume cross section. One obtains  $\sigma = -53$  dBsm per 3.25 Hz frequency cell at  $t=1.0$  s, and  $\sigma = -54$  dBsm per 3.25 Hz frequency cell at  $t=2.9$  s. The integrated broadband cross sections at  $t=1.0$  s and  $t=2.9$  s are roughly -32 and -33 dBsm, respectively. This



is approximately two orders of magnitude smaller than model predictions prior to the Lance experiment.

### **3.3 Summary of Lance Missile Results**

VHF (49.92 MHz) radar observations of a Lance missile plume reveal a very weak broadband plume echo having a cross section of approximately -53 dBsm per 3.25 Hz (10 m/s Doppler) frequency cell, or a frequency integrated cross section of approximately -32 dBsm. Plume signals were observed only as the Lance missile passed through the two main antenna lobes near the ground. The radar experiment provided a single viewing angle to the plume at a fixed polarization (linear, horizontal). A specular return from the plume was not decisively detected, but the experiment was not optimum for such measurements. During the key test period when main engine cutoff occurred, the Lance missile was entering an antenna null. Thus, additional observations are required to resolve this issue.

In future tests, multi-frequency observations across the band 50 MHz to 2 GHz are highly desirable. Additionally, measurements of the full wave polarization matrix and observations at a variety of different aspect angles relative to the plume would greatly facilitate comparisons with model results.



## BIBLIOGRAPHY

- Basu, S., S. Basu, S. Ganguly, and W. E. Gordon, Coordinated study of subkilometer and 3-m irregularities in the F region generated by high power HF heating at Arecibo, *J. Geophys. Res.*, **88**, 9217-9225, 1983.
- Bernhardt, P. A., L. M. Duncan, and C. A. Tepley, Artificial airglow excited by high-power radio waves, *Science*, **242**, 1022-1027, 1988.
- Birkmayer, W., T. Hagfors, and W. Kofman, Small-scale plasma-depletions in Arecibo high-frequency modification experiments, *Phys. Rev. Lett.*, **57**, 1008-1011, 1986.
- Birkmayer, W. T., and T. Hagfors, Observational technique and parameter estimation in plasma line spectrum observations of the ionosphere by chirped I.S. radar, *J. Atmos. Terr. Phys.*, **48**, 1009-1019, 1986.
- Birkmayer, W. T., T. Hagfors, and M. P. Sulzer, A new method for accurate ionospheric electron density measurements by incoherent scatter radar, *J. Geophys. Res.*, **89**, 6841-6849, 1984.
- Bulanov, S. V., L. M. Kovrizhnykh, and A. S. Sakharov, *Regular Mechanisms of Electron and Ion Acceleration in the Interaction of Strong Electromagnetic Waves with a Plasma*, Science Reports, 186, Elsevier Science Publishers B. V. (North-Holland), Amsterdam, The Netherlands, 1-51, 1990.
- Burinskaya, T. M., and A. S. Volokitin, Nonlinear dynamics of thermal modulation instability, *Physica D Amsterdam*, **2**, 117-125, 1981.
- Carlson, H. C., and L. M. Duncan, HF excited instabilities in space plasmas, *Radio Sci.*, **12**, 1001-1013, 1977.
- Carlson, H. C., W. E. Gordon, and R. L. Showen, High frequency induced enhancements of the incoherent scatter spectrum at Arecibo, *J. Geophys. Res.*, **77**, 12142-1250, 1972.
- Carlson, H. C., V. B. Wickwar, and G. P. Mantas, Observations of fluxes of suprathermal electrons accelerated by HF excited instabilities, *J. Atm. Terr. Phys.*, **44**, 1089-1100, 1982.
- Cheung, P. Y., A. Y. Wong, T. Tanikawa, J. Santoru, D. F. DuBois, H. A. Rose, and D. Russell, Short time scale evidence for strong Langmuir turbulence during heating of the ionosphere, *Phys. Rev. Lett.*, **62**, 2676-2679, 1989.
- Cheung, P. Y., D. F. DuBois, T. Fukuchi, K. Kawan, H. A. Rose, D. Russel, T. Tanikawa, and A. Y. Wong, Investigation of strong Langmuir turbulence in ionospheric modification, *J. Geophys. Res.*, **97**, 10575-10600, 1992.
- Coster, A. J., F. T. Djuth, R. J. Jost, and W. E. Gordon, The temporal evolution of three-meter striations in the modified ionosphere, *J. Geophys. Res.*, **90**, 2807-2818, 1985.
- Das, A. C., and J. A. Fejer, Resonance instability of small-scale field aligned irregularities, *J. Geophys. Res.*, **84**, 6701-6704, 1979.
- Das, A. C., J. A. Fejer, and N. J. Martinic, Three-dimensional saturation spectrum of the parametric decay instability, *Radio Sci.*, **20**, 813-818, 1985.



- Djuth, F. T., HF-enhanced plasma lines in the lower ionosphere, *Radio Sci.*, **19**, 383-394, 1984.
- Djuth, F. T., HF-induced radar backscatter, *J. Atmos. Terr. Phys.*, **47**, 1225-1243, 1985.
- Djuth, F. T., Response of the Arecibo ionosphere to large HF-induced electron temperature enhancements, *Adv. Space Res.*, **9**, (5)123-(5)131, 1989.
- Djuth, F. T., Nonlinear resonance effects produced in the *F* region by high-power radio waves, *The Review of Radio Science 1990-1992*, ed. W. R. Stone, Oxford University Press, Chapter 29, 601-610, 1993.
- Djuth, F. T., C. A. Gonzales, and H. M. Ierkic, Temporal evolution of the HF-enhanced plasma line in the Arecibo *F* region, *J. Geophys. Res.*, **91**, 12089-12107, 1986.
- Djuth, F. T., B. Thidé, H. M. Ierkic, and M. P. Sulzer, Large *F*-region electron-temperature enhancements generated by high-power HF radio waves, *Geophys. Res. Lett.*, **14**, 953-956, 1987a.
- Djuth, F. T., R. J. Jost, H. M. Ierkic, M. P. Sulzer, and S. T. Noble, Observations of HF-enhanced ion waves in the ionosphere, *Geophys. Res. Lett.*, **14**, 194-197, 1987b.
- Djuth, F. T., Response of the Arecibo ionosphere to large HF-induced electron temperature enhancements, *Adv. Space Res.*, **9**, (5)123-(5)131, 1989.
- Djuth, F. T., M. P. Sulzer, and J. H. Elder, High resolution observations of HF-induced plasma waves in the ionosphere, *Geophys. Res. Lett.*, **17**, 1893-1896, 1990.
- Djuth, F. T., M. P. Sulzer, and J. H. Elder, Application of the Coded Long Pulse Technique to Plasma Line Studies of the Ionosphere, *Geophys. Res. Lett.*, **21**, 2725-2728, 1994a.
- Djuth, F. T., P. Stubbe, M. P. Sulzer, H. Kohl, M. T. Rietveld, and J. H. Elder, Altitude characteristics of plasma turbulence excited with the Tromsø superheater, *J. Geophys. Res.*, **99**, 333-339, 1994b.
- Djuth, F. T., M. P. Sulzer, J. H. Elder, and K. M. Groves, The CRRES AA 2 release: HF wave-plasma interactions in a dense  $\text{Ba}^+$  cloud, *J. Geophys. Res.*, **100**, 17347-17366, 1995.
- Djuth, F. T., M. P. Sulzer, and J. H. Elder, Langmuir oscillations and the standing wave pattern at Arecibo, *J. Geophys. Res.*, submitted, 1996.
- Doolen, G. D., D. F. DuBois, and H. A. Rose, Nucleation of cavitons in strong Langmuir turbulence, *Phys. Rev. Lett.*, **54**, 804-807, 1985.
- DuBois, D. F., and M. V. Goldman, Parametrically excited plasma fluctuations, *Phys. Rev.*, **164**, 207-222, 1967.
- DuBois, D. F., H. A. Rose, and D. Russell, Power spectra of fluctuations in strong Langmuir turbulence, *Phys. Rev. Lett.*, **61**, 2209-2212, 1988.
- DuBois, D. F., H. A. Rose, and D. Russell, Excitation of strong Langmuir turbulence in plasmas near critical density: application to HF heating of the ionosphere, *J. Geophys. Res.*, **95**, 21221-21272, 1990.
- DuBois, D. F., A. Hanssen, and H. A. Rose, Comment on "Langmuir Turbulence and Ionospheric Modification" by P. Stubbe, H. Kohl, and M. T. Rietveld, *J. Geophys. Res.*, **97**, 15059-15066, 1992.



- DuBois, D. F., H. A. Rose, and D. Russell, Coexistence of parametric decay cascades and caviton collapse at subcritical densities, *Phys. Rev. Lett.*, **66**, 1970-1973, 1991.
- DuBois, D. F., A. Hanssen, H. A. Rose, and D. Russell, Space and time distribution of HF excited Langmuir turbulence in the ionosphere: comparison of theory and experiment, *J. Geophys. Res.*, **98**, 17543-17567, 1993a.
- DuBois, D. F., A. Hansen, H. A. Rose, and D. Russell, Excitation of strong Langmuir turbulence in the ionosphere: comparison of theory and observations, *Phys. Fluids*, **5**, 2616-2622, 1993b.
- DuBois, D. F., D. Russel, and H. A. Rose, Reduced description of strong Langmuir Turbulence from kinetic theory, *Phys. Plasmas*, **2**, 76, 1994.
- Duncan, L. M., and R. A. Behnke, Observations of self-focusing electromagnetic waves in the ionosphere, *Phys. Rev. Lett.*, **41**, 998-1001, 1978.
- Duncan, L. M., and J. P. Sheerin, High-resolution studies of the HF ionospheric modification interaction region, *J. Geophys. Res.*, **90**, 8371-8376, 1985.
- Duncan, L. M., J. P. Sheerin, and R. A. Behnke, Observations of ionospheric cavities generated by high-power radio waves, *Phys. Rev. Lett.*, **61**, 239-242, 1988.
- Dysthe, K. B., E. Mjølhus, H. L. Pécseli, and K. Rypdal, Thermal cavitons, *Physica Scr.*, **T2/2**, 548-559, 1982.
- Dysthe, K. B., E. Mjølhus, H. L. Pécseli, and K. Rypdal, A thermal oscillating two-stream instability, *Phys. Fluids*, **26**, 146-157, 1983.
- Erukhimov, L. M., S. A. Metelev, N. A. Mityakov, and V. L. Frolov, Hysteresis effect in the artificial excitation of inhomogeneities in the ionospheric plasma, *Radiophysics*, **21**, 1738-1741, 1978.
- Farley, D. T., C. LaHoz, and B. G. Fejer, Studies of the self-focusing instability at Arecibo, *J. Geophys. Res.*, **88**, 2093-2102, 1983.
- Fejer, J. A., Ionospheric modification and parametric instabilities, *Rev. Geophys.*, **17**, 135-153, 1979.
- Fejer, J. A., Physical processes of ionospheric heating experiments, *Adv. Space Res.*, **8**, (1)261-(1)270, 1988.
- Fejer, J. A., and Y. Kuo, Structure in the nonlinear saturation spectrum of parametric instabilities, *Phys. Fluids*, **16**, 1490-1496, 1973.
- Fejer, J. A., and H. Kopka, The effect of plasma instabilities on the ionospherically reflected wave from a high-power transmitter, *J. Geophys. Res.*, **86**, 5746 - 5750, 1981.
- Fejer, J. A., and M. P. Sulzer, The HF-induced plasma line below threshold, *Radio Sci.*, **19**, 675-682, 1984.
- Fejer, J. A., and M. P. Sulzer, Observations of suprathermal electron fluxes during ionospheric modification experiments, *J. Geophys. Res.*, **92**, 3441-3444, 1987.



- Fejer, J. A., F. T. Djuth, and C. A. Gonzales, Bragg backscatter from plasma inhomogeneities due to a powerful ionospherically reflected radio wave, *J. Geophys. Res.*, **89**, 9145-9147, 1984.
- Fejer, J. A., F. T. Djuth, H. M. Ierkic, and M. P. Sulzer, Simultaneous observations of the enhanced plasma line and the reflected HF wave at Arecibo, *J. Atm. Terr. Phys.*, **51**, 721-725, 1989.
- Fejer, J. A., M. P. Sulzer, and F. T. Djuth, Height dependence of the observed spectrum of radar backscatter from HF-induced ionospheric Langmuir turbulence, *J. Geophys. Res.*, **96**, 15,985-16,008, 1991.
- Fialer, P. A., Field-aligned scattering from a heated region of the ionosphere-Observations at HF and VHF, *Radio Sci.*, **9**, 923-940, 1974.
- Frey, A., Artificially produced field-aligned short-scale striations, M. S. thesis, Rice University, Houston, Texas, 1980.
- Frey, A., The observation of HF-enhanced plasma waves with the EISCAT/UHF-radar in the presence of strong Landau damping, *Geophys. Res. Lett.*, **13**, 438 - 441, 1986.
- Frey, A., and W. E. Gordon, HF produced ionospheric electron density irregularities diagnosed by UHF radio star scintillations, *J. Atm. Terr. Phys.*, **44**, 1101-1111, 1982.
- Frolov, V. L., L. M. Erukhimov, S. A. Metelev, and E. N. Sergeev, Temporal behavior of artificial small-scale ionospheric irregularities: Review of experimental results, *J. Atm. Terr. Phys.*, in press, 1996.
- Gordon, W. E., R. Showen, and H. C. Carlson, Ionospheric heating at Arecibo: first tests, *J. Geophys. Res.*, **76**, 7801-7813, 1971.
- Grach, S. M., A. N. Karashtin, N. A. Mityakov, V. O. Rapoport, and V. Yu. Trakhtengerts, Parametric interaction between electromagnetic radiation and ionospheric plasma, *Radiophys. Quantum Electron. Engl. Transl.*, **20**, 1254-1258, 1977.
- Grach, S. M., A. N. Karashtin, N. A. Mityakov, V. O. Rapoport, and V. Yu. Trakhtengerts, Theory of the thermal parametric instability in an inhomogeneous plasma, *Sov. J. Plasma Phys. Engl. Transl.*, **4**, 737-741, 1978a.
- Grach, S. M., A. N. Karashtin, N. A. Mityakov, V. O. Rapoport, and V. Yu. Trakhtengerts, Thermal parametric instability in an inhomogeneous plasma (nonlinear theory), *Sov. J. Plasma Phys. Engl. Trans.*, **4**, 742-747, 1978b.
- Grach, S. M., N. A. Mityakov, and V. Yu. Trakhtengerts, Electron acceleration in the presence of parametric heating of a bounded layer of plasma, *Radiophys. Quantum Electron. Engl. Transl.*, **27**, 1096-1101, 1984.
- Gurevich, A. V., Ya. S. Dimant, G. M. Milikh, and V. V. Vas'kov, Multiple acceleration of electrons in the regions of high-power radio-wave reflection in the ionosphere, *J. Atm. Terr. Phys.*, **47**, 1057-1070, 1985.
- Hagfors, T., W. Kofman, H. Kopka, P. Stubbe, and T. Äijanen, Observations of enhanced plasma lines by EISCAT during heating experiments, *Radio Sci.*, **18**, 861-866, 1983.



- Hansen, J. D., G. J. Morales, L. M. Duncan, and G. Dimonte, Large-scale HF-induced ionospheric modifications: experiments, *J. Geophys. Res.*, **97**, 113-122, 1992.
- Hanssen, A., Resonance broadening modification of weak plasma turbulence theory, *J. Geophys. Res.*, **96**, 1867-1871, 1991.
- Hanssen, A., E. Mjølhus, D. F. DuBois, and H. A. Rose, Numerical test of the weak turbulence approximation to ionospheric Langmuir turbulence, *J. Geophys. Res.*, **97**, 12073-12091, 1992.
- Hedberg, Å., H. Derblom, G. Hamberg, B. Thidé, H. Kopka, and P. Stubbe, Measurements of HF backscatter cross section for striations created by ionospheric heating at different power levels, *Radio Sci.*, **21**, 117-125, 1986.
- Helmersen, E., and E. Mjølhus, A semikinetic model for ionospheric Langmuir turbulence, *J. Geophys. Res.*, **99**, 17623-17629, 1994.
- Hibbert, F. H., E. Nielsen, P. Stubbe, H. Kopka, and M. T. Rietveld, Production of auroral zone E region irregularities by powerful HF heating, *J. Geophys. Res.*, **88**, 6347-6351, 1983.
- Hibbert, F. H., E. Nielsen, P. Stubbe, H. Kopka, and M. T. Rietveld, Correction to "Production of auroral zone E region irregularities by powerful HF heating," *J. Geophys. Res.*, **89**, 11061, 1984.
- Høeg, P., Directional changes in the irregularity drift during artificial generation of striations, *Physica Scr.*, **33**, 469-474, 1986.
- Høeg, P., E. Nielsen, P. Stubbe, and H. Kopka, Heater induced 1-meter irregularities, *J. Geophys. Res.*, **91**, 11309-11320, 1986.
- Inhester, B., Thermal modulation of the plasma density in ionospheric heating experiments, *J. Atmos. Terr. Phys.*, **44**, 1049-1059, 1982.
- Inhester, B., A. C. Das, and J. A. Fejer, Generation of small-scale field aligned irregularities in ionospheric heating experiments, *J. Geophys. Res.*, **86**, 9101-9106, 1981.
- Isham, B., and T. Hagfors, Observations of the temporal and spatial development of induced and natural plasma lines during HF modification experiments at Arecibo using chirped incoherent scatter radar, *J. Geophys. Res.*, **98**, 13605-13625, 1993.
- Isham, B., W. Birkmeyer, T. Hagfors, and W. Kofman, Observations of small-scale plasma depletions in Arecibo heating experiments, *J. Geophys. Res.*, **92**, 4629-4637, 1987.
- Isham, B., W. Kofman, T. Hagfors, J. Nordling, B. Thidé, C. LaHoz, and P. Stubbe, New phenomena observed by EISCAT during an RF ionospheric modification experiment, *Radio Sci.*, **25**, 251-262, 1990.
- Isham, B., and T. Hagfors, Observations of the temporal and spatial development of induced and natural plasma lines during HF modification experiments at Arecibo using chirped incoherent scatter radar, *J. Geophys. Res.*, **98**, 13605-13625, 1993.
- Jones, T. B., T. Robinson, P. Stubbe, and H. Kopka, A hysteresis effect in the generation of field-aligned irregularities by a high-power radio wave, *Radio Sci.*, **18**, 835-839, 1983.



- Kantor, I. J., High frequency induced enhancements of the incoherent scatter spectrum at Arecibo, 2, *J. Geophys. Res.*, 79, 199-208, 1974.
- Kelley, M. C., T. L. Arce, J. Salowey, T. Armstrong, M. Carter, and L. M. Duncan, Density depletions at the ten-meter scale induced by the Arecibo heater, *J. Geophys. Res.*, 100, 17367-17376, 1995.
- Kofman, W., J.-P. St-Maurice, and A. P. van Eyken, Heat flow effect on the plasma line frequency, *J. Geophys. Res.*, 98, 6,079-6,085, 1993.
- Kohl, H., H. Kopka, C. LaHoz, and P. Stubbe, Propagation of artificially excited Langmuir waves in the ionosphere, *Radio Sci.*, 22, 655-661, 1987.
- Kohl, H., H. Kopka, P. Stubbe, and C. LaHoz, EISCAT VHF-observations of artificially excited parametric decay instabilities, presented at the 27th Plenary Meeting of the Committee on Space Research, Espoo, Finland, 18 - 29 July, 1988.
- Kolesnik, A. G., Perturbation of the ionospheric *F*-region with high-power radiowaves, *Radiophys. Quantum Electron. Engl. Transl.*, 25, 87-91, 1982.
- Kuo, S. P., and M. C. Lee, Temporal evolution of HF-Enhanced plasma lines, *Geophys. Res. Lett.*, 17, 2209-2212, 1990.
- Kuo, S. P., and M. C. Lee, A source mechanism producing HF-induced plasma lines (HFPLS) with up-shifted frequencies, *Geophys. Res. Lett.*, 19, 249-252, 1992.
- Kuo, S. P., B. R. Cheo, and M. C. Lee, The role of parametric decay instabilities in generating ionospheric irregularities, *J. Geophys. Res.*, 88, 417-423, 1983.
- Kuo, S. P., M. C. Lee, and F. T. Djuth, A new interpretation of plasma-line overshoot phenomena, *Geophys. Res. Lett.*, 14, 961-964, 1987.
- Kuo, S. P., J. Huang, and M. C. Lee, On the altitude of the HF-enhanced plasma lines, *J. Geophys. Res.*, 98, 11671-11676, 1993.
- Lee, M. C., and J. A. Fejer, Theory of short-scale field aligned density striations due to ionospheric heating, *Radio Sci.*, 13, 893-899, 1978.
- Lee, M. C., and S. P. Kuo, Excitation of upper hybrid waves by a thermal parametric instability, *J. Plasma Phys.*, 30, 463-478, 1983.
- Leyser, T. B., B. Thidé, S. Goodman, M. Waldenvik, E. Veszelei, S. M. Grach, A. N. Karashtin, G. P. Komrakov, and D. S. Kotik, Narrow cyclotron harmonic absorption resonances of stimulated electromagnetic emission in the ionosphere, *Phys. Rev. Lett.*, 68, 3299-3302, 1992.
- Lobachevsky, L. A., Yu. V. Gruzdev, V. Yu. Kim, G. A. Mikhaylova, V. A. Panchenko, V. P. Polimatidi, V. A. Puchkov, V. V. Vaskov, P. Stubbe, and H. Kopka, Observations of ionospheric modification by the Tromsø heating facility with the mobile diagnostic equipment of IZMIRAN, *J. Atm. Terr. Phys.*, 54, 75-85, 1992.
- Mantas, G. P., H. C. Carlson, Jr., and C. M. LaHoz, Thermal response of the *F* region ionosphere in artificial modification experiments by HF radio waves, *J. Geophys. Res.*, 86, 561-574, 1981.



- Mantas, G. P., Large 6300-Å airglow intensity enhancements observed in ionospheric heating experiments are excited by thermal electrons, *J. Geophys. Res.*, **99**, 8993-9002, 1994.
- Minkoff, J., and R. Kreppel, Spectral analysis and step response of radio frequency scattering from a heated ionospheric volume, *J. Geophys. Res.*, **81**, 2844-2856, 1976.
- Minkoff, J., P. Kugelman, and I. Weissman, Radio frequency scattering from a heated ionospheric volume, 1, VHF/UHF field-aligned and plasma-line backscatter measurements, *Radio Sci.*, **9**, 941-955, 1974.
- Mjølhus, E., On linear conversion in a magnetized plasma, *Radio Sci.*, **25**, 1321-1339, 1990.
- Mjølhus, E., On reflexion and trapping of upper-hybrid waves, *J. Plasma Phys.*, **29**, 195-215, 1983.
- Mjølhus, E., Anomalous absorption and reflection in ionospheric radio modification experiments, *J. Geophys. Res.*, **90**, 4269-4279, 1985.
- Morales, G. J., A. Y. Wong, J. Santoru, and L. Wang, Dependence of plasma line enhancement on HF pulse length and ionosphere preconditioning, *Radio Sci.*, **17**, 1313-1320, 1982.
- Muldrew, D. B., The role of field-aligned ionization irregularities in the generation of the HF-induced plasma line at Arecibo, *J. Geophys. Res.*, **83**, 2552-2560, 1978.
- Muldrew, D. B., Frequency asymmetry in the upshifted and downshifted plasma lines induced by an HF wave at Arecibo, *J. Geophys. Res.*, **84**, 2705-2714, 1979.
- Muldrew, D. B., An ionization duct explanation of some plasma line observations with a 46.8-MHz radar and with a 430-MHz radar, *J. Geophys. Res.*, **90**, 6662-6666, 1985.
- Muldrew, D. B., Duct model explanation of the plasma line overshoot observed at Arecibo, *J. Geophys. Res.*, **93**, 7598-7604, 1988.
- Muldrew, D. B., Duct-model explanation of the broad component of plasma-line spectra observed at Arecibo, *Geophys. Res. Lett.*, **18**, 2289-2292, 1991.
- Muldrew, D. B., Initial duct growth determined from cold-start plasma-line data recorded at Arecibo, *Geophys. Res. Lett.*, **19**, 65-68, 1992.
- Muldrew, D. B., and R. L. Showen, Height of the HF-enhanced plasma line at Arecibo, *J. Geophys. Res.*, **82**, 4793-4804, 1977.
- Newman, A. L., H. C. Carlson, G. P. Mantas, and F. T. Djuth, Thermal response of the F-region ionosphere for conditions of large HF-induced electron-temperature enhancements, *Geophys. Res. Lett.*, **15**, 311-314, 1988.
- Nicholson, D. R., and M. V. Goldman, Cascade and collapse of Langmuir waves in two dimensions, *Phys. Fluids*, **21**, 1766-1776, 1978.
- Nicholson, D. R., G. L. Payne, R. M. Downie, and J. P. Sheerin, Soliton versus parametric instabilities during ionospheric heating, *Phys. Rev. Lett.*, **52**, 2152-2155, 1984.
- Noble, S. T., F. T. Djuth, R. J. Jost, W. E. Gordon, Å. Hedberg, B. Thidé, H. Derblom, R. Boström, E. Nielsen, P. Stubbe, , and H. Kopka, Multiple frequency radar observations of high-latitude E region irregularities in the HF modified ionosphere, *J. Geophys. Res.*, **92**, 13613-13627, 1987.



- Noble, S. T., and F. T. Djuth, Simultaneous measurements of HF-enhanced plasma waves and artificial field-aligned irregularities at Arecibo, *J. Geophys. Res.*, 95, 15195-15207, 1990.
- Nordling, J. A., Å. Hedberg, G. Wannberg, T. B. Leyser, H. Derblom, H. J. Opgenoorth, H. Kopka, H. Kohl, P. Stubbe, M. T. Rietveld, and C. LaHoz, Simultaneous bistatic European Incoherent Scatter UHF, 145-MHz radar and stimulated electromagnetic emission observations during HF ionospheric modification, *Radio Sci.*, 23, 809-819, 1988.
- Payne, G. L., D. R. Nicholson, R. M. Downie, and J. P. Sheerin, Modulational instability and soliton formation during ionospheric heating, *J. Geophys. Res.*, 89, 10921-10928, 1984.
- Payne, G. L., D. R. Nicholson, and M-M. Shen, Numerical test of weak turbulence theory, *Phys. Fluids B*, 9, 1797-1804, 1989.
- Perkins, F. W., A theoretical model for short-scale field-aligned plasma density striations, *Radio Sci.*, 9, 1065-1070, 1974.
- Richards, P. G., and D. G. Torr, A factor of 2 reduction in theoretical F2 peak electron density due to enhanced vibrational excitation of N<sub>2</sub> in summer at solar maximum, *J. Geophys. Res.*, 91, 11,331-11,336, 1986.
- Russell, D., D. F. DuBois, and H. A. Rose, Collapsing caviton turbulence in one dimension, *Phys. Rev. Lett.*, 56, 838-842, 1986.
- Russell, D., D. F. DuBois, and H. A. Rose, Nucleation in two-dimensional Langmuir turbulence, *Phys. Rev. Lett.*, 60, 581-584, 1988.
- Schlegel, K., M. Rietveld, and A. Maul, A modification event of the auroral E region as studied with EISCAT and other diagnostics, *Radio Sci.*, 22, 1063-1072, 1987.
- Sheerin, J. P., J. C. Weatherall, D. R. Nicholson, G. L. Payne, M. V. Goldman, and P. J. Hanson, Solitons and ionospheric modification, *J. Atmos. Terr. Phys.*, 44, 1043-1048, 1982.
- Showen, R. L., and D. M. Kim, Time variations of HF-induced plasma waves, *J. Geophys. Res.*, 83, 623-628, 1978.
- Sprague, R. A., and J. A. Fejer, Simultaneous excitation of parametric decay cascades and of the OTSI in 1D numerical simulations based on Zakharov's equations, *J. Geophys. Res.*, 100, 23959-23972, 1995.
- Stocker, A. J., T. R. Robinson, and T. B. Jones, Observations of the effects of ionospheric heating on the amplitude of low-power diagnostic radio waves at Arecibo, *J. Geophys. Res.*, 97, 6315-6322, 1992.
- Stubbe, P., and H. Kopka, Stimulated electromagnetic emission in a magnetized plasma: a new symmetric spectral feature, *Phys. Rev. Lett.*, 65, 183-186, 1990.
- Stubbe, P., H. Kopka, B. Thidé, and H. Derblom, Stimulated electromagnetic emission: A new technique to study the parametric decay instability in the ionosphere, *J. Geophys. Res.*, 89, 7523 - 7536, 1984.



- Stubbe, P. H. Kopka, M. T. Rietveld, A. Frey, P. Hoeg, H. Kohl, E. Nielsen, G. Rose, C. LaHoz, R. Barr, H. Derblom, A. Hedberg, B. Thide, T. B. Jones, T. Robinson, A. Brekke, T. Hansen, and O. Holt, Ionospheric modification experiments with the Tromsø Heating Facility, *J. Atm. Terr. Phys.*, **47**, 1151-1163, 1985.
- Stubbe, P., H. Kohl, and M. T. Rietveld, Langmuir turbulence and ionospheric modification, *J. Geophys. Res.*, **97**, 6285-6297, 1992a.
- Stubbe, P., H. Kohl, and M. T. Rietveld, Reply to "Comment on 'Langmuir Turbulence and Ionospheric Modification' by P. Stubbe, H. Kohl, and M. T. Rietveld" by D. F. DuBois, A. Hanssen, and H. A. Rose, *J. Geophys. Res.*, **97**, 15067-15071, 1992b.
- Sulzer, M. P., A radar technique for high range resolution incoherent scatter autocorrelation function measurements utilizing the full average power of klystron radars, *Radio Sci.*, **21**, 1033-1040, 1986.
- Sulzer, M. P., and J. A. Fejer, Simultaneous observations of 46.8-MHz and 430-MHz radar backscatter from HF-induced ionospheric Langmuir turbulence, *J. Geophys. Res.*, **96**, 17891-17895, 1991.
- Sulzer, M. P., and J. A. Fejer, Radar spectral observations of HF-induced ionospheric Langmuir turbulence with improved range and time resolution, *J. Geophys. Res.*, **99**, 15035-15050, 1994.
- Sulzer, M. P., H. M. Ierick, J. A. Fejer, and R. L. Showen, HF-induced ion and plasma line spectra with two pumps, *J. Geophys. Res.*, **89**, 6804, 1984.
- Sulzer, M. P., H. M. Ierick, and J. A. Fejer, Observational limitations on the role of Langmuir cavitons in ionospheric modification experiments at Arecibo, *J. Geophys. Res.*, **94**, 6841-6854, 1989.
- Thidé, B., Stimulated scattering of large amplitude waves in the ionosphere: experimental results, *Phys. Scripta*, **T30**, 170-180, 1990.
- Thidé, B., and B. Lundborg, Structure of HF pump in ionospheric modification experiments: Linear treatment, *Phys. Scr.*, **33**, 475-479, 1986.
- Thidé, B., H. Kopka, and P. Stubbe, Observations of stimulated scattering of a strong high frequency radio wave in the ionosphere, *Phys. Rev. Lett.*, **49**, 1561-1564, 1982.
- Thidé, B., H. Derblom, Å. Hedberg, H. Kopka, and P. Stubbe, Observations of stimulated electromagnetic emissions in ionospheric heating experiments, *Radio Sci.*, **18**, 851-859, 1983.
- Thidé, B., Å. Hedberg, J. A. Fejer, and M. P. Sulzer, First observations of stimulated electromagnetic emission at Arecibo, *Geophys. Res. Lett.*, **5**, 369-372, 1989.
- Thidé, B., F. T. Djuth, H. M. Ierick, and T. B. Leyser, Evolution of Langmuir turbulence and stimulated electromagnetic emissions excited with a 3-MHz pump wave at Arecibo, *J. Geophys. Res.*, **100**, 23887-23899, 1995.
- Utlaut, W. F., E. J. Violette, and A. K. Paul, Some ionosonde observations of ionosphere modification by very high power, high frequency ground-based transmissions, *J. Geophys. Res.*, **75**, 6429-6435, 1970.



- Vas'kov, V. V., Multiple acceleration of plasma resonance electrons in the presence of a magnetic field, *Geomag. Aeronomy*, 23, 604-608, 1983.
- Vas'kov, V. V., and A. V. Gurevich, Nonlinear resonant instability of a plasma in the field of an ordinary electromagnetic wave, *Sov. Phys. JETP Engl. Transl.*, 42, 91-97, 1975.
- Vas'kov, V. V., and A. V. Gurevich, Resonance instability of small-scale plasma perturbations, *Sov. Phys. JETP Engl. Transl.*, 46, 487-494, 1977.
- Vas'kov, V. V., and G. M. Milikh, Artificial luminescence and additional ionization of the upper ionosphere in the field of a powerful radio wave, *Geomag. Aeronomy*, 23, 157-161, 1983.
- Weatherall, J. C., J. P. Sheerin, D. R. Nicholson, G. L. Payne, M. V. Goldman, and P. J. Hansen, Solitons and ionospheric heating, *J. Geophys. Res.*, 87, 823-832, 1982.
- Weinstock, J., and B. Bezzerides, Theory of electron acceleration during parametric instabilities, *Phys. Rev. Lett.*, 32, 754, 1974.
- Weinstock, J., Theory of enhanced airglow during ionospheric modifications *J. Geophys. Res.*, 80, 4331, 1975.
- Wong, A. Y., and R. J. Taylor, Parametric excitation in the ionosphere, *Phys. Rev. Lett.*, 27, 644-647, 1971.